

A Study of P-type Zinc Oxide Thin Films

by

Yang, Hung-Pao

**Department of Electrical & Computer Engineering
McGill University
Montreal, Canada
August, 2006**

A thesis submitted to the Faculty of Graduate Studies and Research in partial fulfillment of the requirements for the degree of Master of Engineering

© 2006 Yang, Hung-Pao



Library and
Archives Canada

Bibliothèque et
Archives Canada

Published Heritage
Branch

Direction du
Patrimoine de l'édition

395 Wellington Street
Ottawa ON K1A 0N4
Canada

395, rue Wellington
Ottawa ON K1A 0N4
Canada

Your file *Votre référence*
ISBN: 978-0-494-28634-0
Our file *Notre référence*
ISBN: 978-0-494-28634-0

NOTICE:

The author has granted a non-exclusive license allowing Library and Archives Canada to reproduce, publish, archive, preserve, conserve, communicate to the public by telecommunication or on the Internet, loan, distribute and sell theses worldwide, for commercial or non-commercial purposes, in microform, paper, electronic and/or any other formats.

The author retains copyright ownership and moral rights in this thesis. Neither the thesis nor substantial extracts from it may be printed or otherwise reproduced without the author's permission.

AVIS:

L'auteur a accordé une licence non exclusive permettant à la Bibliothèque et Archives Canada de reproduire, publier, archiver, sauvegarder, conserver, transmettre au public par télécommunication ou par l'Internet, prêter, distribuer et vendre des thèses partout dans le monde, à des fins commerciales ou autres, sur support microforme, papier, électronique et/ou autres formats.

L'auteur conserve la propriété du droit d'auteur et des droits moraux qui protègent cette thèse. Ni la thèse ni des extraits substantiels de celle-ci ne doivent être imprimés ou autrement reproduits sans son autorisation.

In compliance with the Canadian Privacy Act some supporting forms may have been removed from this thesis.

Conformément à la loi canadienne sur la protection de la vie privée, quelques formulaires secondaires ont été enlevés de cette thèse.

While these forms may be included in the document page count, their removal does not represent any loss of content from the thesis.

Bien que ces formulaires aient inclus dans la pagination, il n'y aura aucun contenu manquant.


Canada

Abstract

In the past decade, p-type ZnO material has been investigated extensively. Its properties offer the potential for broad applications including the development of ultraviolet light emitting devices. Although n-type ZnO material is well known and studied for decades, the fabrication method and properties of p-type ZnO material are still to date not clearly understood.

In this report, reproducible p-type ZnO thin films sputtered on glass substrates are reported. On the same substrate, p-type ZnO film is local and surrounded by n-type ZnO regions. The thickness of the films is typically three microns after several hours of deposition by radio-frequency magnetron sputtering technique. Both p-type ZnO and n-type thin films are characterized by optical and electrical measurements at room temperature.

The crystal structure of p-type ZnO is examined by X-ray diffraction patterns. The X-ray diffraction patterns show that the material is polycrystalline and has (100) and (101) preferred orientation. Photoluminescence spectra of ZnO help to identify the energy levels in the material and spectra analysis reveals the presence of defects and dopants in the material. For p-type ZnO, the resistivity, the hole concentration and hole mobility are found to be 148.8 Ω -cm, $4.34 \times 10^{18}/\text{cm}^3$ and $1.72 \times 10^{-2} \text{ cm}^2/\text{V-sec}$ respectively.

Résumé

Durant la décennie passée, le matériau ZnO de type p a été l'objet d'une recherche intense. Ses propriétés sont à l'origine de nombreuses applications dont le développement de dispositifs électroluminescents ultraviolets. Contrairement au matériau ZnO de type n qui a été étudié depuis longtemps et dont on connaît parfaitement ses propriétés, la méthode de fabrication du matériau ZnO de type p ainsi que ses propriétés ne sont pas encore clairement éludées.

Durant ce stage, de minces couches ZnO de type p ont été déposées sur des substrats de verre. Sur chaque substrat, le film ZnO de type p reste dans une zone localisée et est entouré par le matériau ZnO de type n. L'épaisseur finale du film est typiquement de trois microns après plusieurs heures de dépôt élaboré par pulvérisation magnétron RadioFréquence. Les films ZnO de type p et de type n ont été ensuite étudiés en effectuant des mesures optiques et électriques à température ambiante.

La structure en cristal de ZnO de type p a été étudiée en déterminant son diagramme de diffraction par rayon Z ainsi que son spectre de photoluminescence. Ainsi, la diffraction par rayon X a montré que le matériau est poly cristallin dont l'orientation est majoritairement (100) et (101). Son spectre de photoluminescence a permis d'identifier les différents niveaux d'énergie du matériau ; par ailleurs, l'analyse spectrale a indiqué la présence de dopants et de défauts. Les mesures expérimentales ont montré que pour le matériau ZnO de type p, la résistivité, la concentration et la mobilité des trous valent respectivement $148.8 \Omega\text{-cm}$, $4.34 \times 10^{18}/\text{cm}^3$ et $1.72 \times 10^{-2} \text{ cm}^2/\text{V}\text{-sec}$.

Acknowledgements

The author would like to express his uttermost gratitude to his supervisor, Dr. Ishiang Shih for his guidance and patience throughout this study. His persuasive teaching approach has helped the author to build superior confidence.

The author would like to express his appreciation to Dr. Clifford Champness for the insightful discussion on the project and Hall effect measurements. The author would like to thank to Dr. Steven Xiao for allowing sample measurements using photoluminescence equipment at Organic Vision Inc.

The author is sincerely grateful to his family and friends for their inspiration, encouragement, and support during the studies.

Table of Contents

ABSTRACT	I
RESUME.....	II
ACKNOWLEDGEMENTS	III
TABLE OF CONTENTS.....	IV
CHAPTER 1 INTRODUCTION	1
CHAPTER 2 A LITERATURE SURVEY ON P-TYPE ZNO AND FILM DEPOSITION CONDITION USED IN THE LABORATORY	5
2.1 Introduction to ZnO	5
2.1.1 Difficulty in fabrication of p-type ZnO	5
2.1.2 Literature survey on p-type ZnO.....	6
2.1.3 Theoretical predictions of p-type ZnO doping.....	7
2.1.3.1 N-doped ZnO	7
2.1.3.2 Co-doping method	7
2.2 ZnO film deposition condition used in the laboratory	17
2.2.1 Strategy for p-type ZnO fabrication.....	17
2.2.2 Substrate preparation	17
2.2.3 Targets preparation	18
2.2.4 ZnO deposition conditions.....	19
CHAPTER 3 EQUIPMENT AND MEASUREMENT METHODS.....	23
3.1 Introduction.....	23
3.2 Vacuum System	23
3.2.1 The Need for Vacuum in Thin Film Depositions	24
3.2.2 High Vacuum Evacuation Procedure.....	24
3.2.3 Operation of diffusion pump.....	25
3.2.4 Pressure Gauges	26
3.3 Deposition Techniques.....	30
3.3.1 Principle of sputtering.....	30
3.3.2 Magnetron Sputtering	31
3.3.3 DC Sputtering	31
3.3.4 RF Sputtering.....	32
3.3.5 Metal Evaporation.....	32
3.4 Vacuum Equipments Used.....	33
3.5 Measurement Techniques	39
3.5.1 Electrical measurements	39
3.5.2 Optical measurement	46

CHAPTER 4 RESULTS AND DISCUSSION	50
4.1 Introduction.....	50
4.2 Photoluminescence spectra of ZnO films	51
4.2.1 Photoluminescence spectra of ZnO films (Single deposition).....	52
4.2.2 Photoluminescence spectra of ZnO films (Multiple deposition).....	56
4.3 Optical transmission of the ZnO film after eight depositions.....	61
4.4 Mapping of limited p-type ZnO film areas after eight depositions	77
4.4.1 Identification of limited p-type ZnO film area	77
4.4.2 Explanation for formation of non-uniform sputtered films	77
4.5 Electrical properties of ZnO films	82
4.5.1 Metal contacts to ZnO films	82
4.5.2 Stabilization of contacts/material.....	83
4.5.3 Contact resistance measurements	84
4.5.4 Hall effect measurements.....	84
4.5.5 Discussion of results	86
4.6 Crystal structure of ZnO by X-ray diffraction analysis	98
 CHAPTER 5 CONCLUSIONS.....	 102
5.1 Summary of the study	102
5.2 Main contribution of this work	106
5.3 Future work.....	107
 REFERENCES	 108

CHAPTER 1 INTRODUCTION

An amazing technological breakthrough was marked by the invention of the light emitting diode (LED) a few decades ago. In 1907, Henry Joseph Round reported the first working LED of which the active material was SiC (silicon carbide) [1.1]. Since then, LEDs have been improved and lead to the invention of many other devices used vastly nowadays. A LED is basically a PN junction that can emit light under specific voltage biasing conditions. The evolution of the LED is being characterized by constant effort in making LED operate in shorter wavelength range. In the 1960's, GaAsP (gallium arsenic phosphorous) based devices were fabricated and emitted red light at around 655 nm [1.1]. The leap in technology has allowed the fabrication of various devices emitting orange, yellow, green, and even blue colours over the years. Figure 1.1 shows the visible light region of the electromagnetic spectrum. Nowadays, LEDs made of GaN (gallium nitride) or SiC (silicon carbide), that can emit light with wavelength below 400 nm, are commercially available.

GaN is currently a very popular material for fabricating short wavelength LED devices because they can emit a strong blue light efficiently, (which is one of the primary colours). The primary colours are red, yellow and blue and the associated wavelengths are approximately 700, 585, and 470 nm respectively. The main advantage of short wavelength devices over long wavelength counterparts is their potential to effectively operate in small critical dimensions. The application of short wavelength devices is very broad. For example, some recent DVD/CD read head uses GaN based devices. Other applications may require advanced photolithography techniques at short wavelength light.

Finding alternative materials is also part of the evolution of LED devices. The LED industry has continuously been looking for alternative semiconductor materials for making efficient and yet cost effective devices. Zinc oxide (ZnO) is one of the extensively studied materials due to its potential applications in creating active devices such as laser diodes (LD's) and light emitting devices (LED's). ZnO has several advantages, for example, it is neither toxic nor expensive and it is a wide band gap energy semiconductor. ZnO is not only a candidate for laser systems, but can also offer a broad range of applications in other fields, namely ultraviolet (UV) resistive coatings, gas sensors, solar cells, and many more [1.2].

ZnO films have unique characteristics, which push scientists and researchers to study further its intriguing properties. First of all, ZnO is a direct band gap semiconductor and an excellent material for short wavelength light-emitting diodes and lasers due to its wide band gap energy of 3.37 eV at room temperature. Moreover, ZnO and GaN have similar properties at room temperature, which are shown in the Table 1.1.

In Table 1.1, it is seen that the crystal structure, lattice parameters, and band gap energy of ZnO are very similar to the one's of GaN. Therefore, ZnO is believed to be an alternative material for GaN. Several research groups around the world are working intensively in the fabrication of ZnO LEDs. One of their intentions is to successfully make ZnO PN homojunctions. The deposition methods and conditions for n-type ZnO films are well known by scientists and engineers. However, the fabrication of p-type ZnO

films and PN homojunctions is still uncertain. The literature survey shows several groups claimed successfully making p-type ZnO films and PN homojunctions, but their work is often irreproducible by other researchers.

The main objective of this thesis is to summarize past work and present findings for investigating the deposition conditions and dopants for p-type ZnO films. The structure of the thesis is described as follows. In chapter 2, the literature survey of the reported p-type ZnO films of the selected work will be presented. The chapter will also include a section devoted to material preparation and deposition conditions used in this work. In chapter 3, measurement techniques for the films and the equipment used will be described. The equipments used in this work are r.f. (radio frequency) sputtering, metal evaporation, and photoluminescence system. The techniques include Hall effect, hot-point probe, four-point probe and photoluminescence spectra measurements. In chapter 4, the results and analysis of measurements will be described in details. Photoluminescence spectra analysis will identify the energy levels of excitons, dopants and defects of ZnO. Furthermore, the electrical properties such as concentration, sheet resistance and Hall mobility will be given. X-ray diffraction patterns of ZnO samples will identify the preferred orientation of the crystal structure. In chapter 5, the conclusions of the thesis will summarize the current finding. A detailed listing about each section in a chapter is available in the table of contents.

Table 1.1 Properties of ZnO and GaN at room temperature

Material	Crystal structure	Lattice parameters		Bandgap energy (eV)	Exciton binding energy (meV)	Melting point (K)
		a (Å)	c (Å)			
ZnO [1.3]	Wurtzite	3.250	5.207	3.37	60	2248
GaN [1.4]	Wurtzite	3.189	5.186	3.39	21	1073

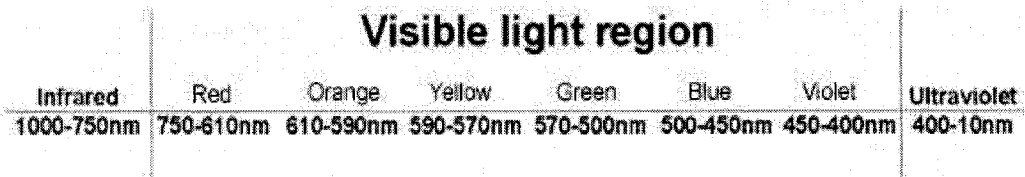


Figure 1.1 Visible light region of the electromagnetic spectrum

CHAPTER 2 A LITERATURE SURVEY ON P-TYPE ZnO AND FILM DEPOSITION CONDITION USED IN THE LABORATORY

2.1 Introduction to ZnO

Zinc oxide is a direct bandgap II-VI semiconductor. The bandgap is 3.37 eV and the electron affinity is 4.35 eV [2.1]. The crystal structure of ZnO is wurtzite and shown in Figure 2.1 with the following lattice parameters: $a = 3.250 \text{ \AA}$ and $c = 5.207 \text{ \AA}$. Intrinsic ZnO is naturally n-type due to high concentration of native defects, which include zinc interstitial and oxygen vacancy. Zinc interstitial and oxygen vacancies could also act as compensating centers, and the concentration could be as high as $2 \times 10^{16} \text{ cm}^{-3}$ and $3 \times 10^{17} \text{ cm}^{-3}$ respectively [2.2]. The defect levels of ZnO are shown in Figure 2.4. Among all the defects in ZnO, zinc interstitial is considered the most mobile defects in ZnO. In other words, the current flow in n-type ZnO is mostly due to this defect [2.32]. Assuming all electrons with energy higher than the bandgap can generate photons, the conservation of energy states ($E_g = hc/\lambda$) that light emission in the neighborhood of 368 nm is possible.

2.1.1 Difficulty in fabrication of p-type ZnO

The difficulties in making p-type ZnO films are due to native defects in the material. The fabrication of p-type ZnO films has always been a challenge due to low solubility of the dopant and high self-compensating process on doping [2.3]. As described before, ZnO is naturally n-type because of its high concentration of zinc interstitial and oxygen vacancy that could prevent the incorporation of group V element dopants in the material. Nevertheless, theoreticians have tried to predict the electrical properties of

various dopants and their roles in ZnO material. They come to agreement that group-V nitrogen (N) is the best-suited dopant element for replacing oxygen (O) due to their small difference in ionic radii [2.8]. Typical dopants for p-type ZnO films are nitrogen (N), arsenic (As) and phosphorous (P) elements as the primary dopant. The differences in empirical ionic radii are listed in Table 2.1. The notation N_o means that O is substituted by N in ZnO material.

2.1.2 Literature survey on p-type ZnO

Various ZnO fabrication methods are used for the deposition of p-type ZnO films. The methods are direct current (DC) and radio frequency (RF) sputtering, pyrolysis, molecular beam epitaxy, electron cyclotron resonance, pulsed laser deposition, ion implantation, and chemical vapour deposition. The reported p-type ZnO films often have low carrier concentration, low mobility, and high resistivity. Moreover, reproducibility is a recurring issue in the fabrication of p-type ZnO [2.10, 2.11].

Results of a literature survey have shown that most p-type ZnO films is based on DC/RF sputtering and pyrolysis deposition techniques. Table 2.4 lists the deposition techniques, choice of dopants, dopant sources and substrate types of selected reports. Tables 2.5 and 2.6 contain the experimental conditions and electrical properties of ZnO of the selected reports. Table 2.7 gives photoluminescence peaks of p-type ZnO of the selected reviews whenever available.

2.1.3 Theoretical predictions of p-type ZnO doping

2.1.3.1 N-doped ZnO

Theoreticians predicted that group-V elements such as N, P and As can substitute for O in ZnO films. Substitutional group-V elements such as P and As are deep acceptors compared to N [2.27]. Furthermore, it was suggested earlier that nitrogen element are good substitute for oxygen element due to their similarity in ionic radius shown in Table 2.1. Therefore, N is a better candidate as dopant in obtaining p-type ZnO. Figure 2.2 is a stick model of the chemical bonds showing the intended impurity incorporation in the hexagonal wurtzite structure.

Typical dopant sources reported in literature are N_2 , NH_3 , N_2O , CH_3COONH_4 and $(Zn(CH_3COO)_2 \cdot 2H_2O)$. It is noted that several reports listed in Table 2.4 used two dopants for making p-type films. Theoreticians also predicted that co-doping could have beneficial effects on the fabrication of good quality p-type ZnO [2.29, 2.30]. In particular, Yamamoto's co-doping theory on N-In co-dopant pair is going to be discussed in the next section. Figure 2.3 shows a model of the hexagonal wurtzite structure of N-In co-doped ZnO.

2.1.3.2 Co-doping method

The creation of Zn-O bonds is easier than Zn-N bonds because the formation enthalpy of $-348.28KJ/mol$ for ZnO is much larger than $-20KJ/mol$ for Zn_3N_2 [2.30]. As a result, N has a low-solubility in ZnO due to low tendency of Zn_3N_2 creation.

Yamamoto [2.29, 2.30] suggests that co-doping of donor (D) with acceptor (A) can enhance the incorporation of acceptor in ZnO films due to a decrease in lattice energy and decrease in binding energy of acceptor impurities. The donor is a reactive co-dopant because it can activate acceptors.

Yamamoto's model is based on A-D-A configuration, which can stabilize ionic charges, reduce the repulsive interactions between the acceptors, and enhance strong attractions between the donor and acceptor. Furthermore, the acceptor binding energy of the acceptors can be reduced and the binding energy of the donors can be raised. As a result, shallower acceptor energy levels can be obtained and ameliorate the electrical characteristics of co-doped p-type ZnO films. Figure 2.4 shows the energy band levels for Yamamoto's A-D-A model.

Yamamoto expected that N-In to be one of the best co-dopants for making p-type ZnO. The atomic radii dimension comparison shown in Table 2.3 illustrates that the N and In are good candidates in replacing O and Zn respectively. In summary, co-doping method would enhance the introduction of group V dopants in ZnO and reduce its bandgap energy. The energy band diagram of co-doped ZnO is shown in Figure 2.7.

Table 2.1 Empirical ionic radii of O, N_o, P_o, and As_o [2.9]

Element	Ionic radii (pm)
Oxygen	60
Nitrogen	65
Phosphorous	100
Arsenic	115

Table 2.2 Empirical ionic radii of Zn, Li_{Zn}, Na_{Zn}, and K_{Zn} [2.9]

Element	Ionic radii (pm)
Zinc	135
Lithium	145
Sodium	180
Potassium	220

Table 2.3 Co-dopants: empirical ionic radii of O, N_o, Zn, Al_{Zn}, In_{Zn}, and Ga_{Zn} [2.9]

Element	Ionic radii (pm)
Oxygen	60
Nitrogen	65
Zinc	135
Gallium	130
Aluminum	143
Indium	155

Table 2.4 Deposition techniques, dopants, dopant sources and substrate types reported in selected reports

Ref.	Technique(s)	Dopant(s)	Dopant source(s)	Substrate(s)
DC1 [2.12]	DC magnetron sputtering	N	N ₂	Amorphous quartz
DC2 [2.13]	DC magnetron sputtering	N	NH ₃	α -Al ₂ O ₃ (0001)
DC3 [2.14]	DC magnetron sputtering	N	NH ₃	α -Al ₂ O ₃ (0001)
DC4 [2.15]	DC magnetron sputtering	-	-	Si (100) and Si (111)
DC5 [2.16]	DC magnetron sputtering	N	NH ₃	Si (100) and Sapphire
RF1 [2.17], [2.18]	RF sputtering	P	P ₂ O ₅	Sapphire c plane
RF2 [2.19]	RF magnetron sputtering	P	Zn ₃ P ₂	p-InP
RF3 [2.20]	RF magnetron sputtering	As	GaAs	GaAs
RF4 [2.21]	RF diode sputtering	Ga-N	GaN (4N)	-
PLD1 [2.22]	Pulsed laser deposition	Ga-N	Ga ₂ O ₃ and N ₂ O	Sapphire
PLD2 [2.23]	Pulsed laser deposition	Ga-N	Ga ₂ O ₃ and N ₂ O	Corning #7059 glass
PLD3 [2.24]	Pulsed laser deposition	Ga-N	Ga ₂ O ₃ and N ₂	Sapphire
ION1 [2.25]	Ion implantation	N	N	Si ₃ N ₄
Pyrolysis1 [2.26]	Pyrolysis	N-In	CH ₃ COONH ₄ and In(NO ₃) ₃	n-type Si(100)
Pyrolysis2 [2.27]	Pyrolysis	N-In	CH ₃ COONH ₄ and In(NO ₃) ₃	n-type Si(100)
Pyrolysis3 [2.28]	Pyrolysis	N	(Zn(CH ₃ COO) ₂ ·2H ₂ O)	Glass slide

Table 2.5 Experimental conditions and electrical properties of p-type ZnO reported in selected reports

Ref.	Experimental Conditions								Electrical properties		
	Substrate	Target	Working gas (x:y)	x to y ratio	Total pressure (chamber)	Substrate temperature	Power and time	Annealing	Resistivity (Ω -cm)	Mobility ($\text{cm}^2/\text{V-s}$)	Hole concentration (cm^{-3})
DC1 [2.12]	Amorphous quartz	Pure zinc	Ar-N ₂	3:1	7.0×10^{-1} Pa	$150 \pm 0.5^\circ\text{C}$	70 W for 3 mins	In air, 350-550°C for 3 h	83.2	1.34	1.22×10^{17}
DC2 [2.13]	α -Al ₂ O ₃ (0001)	Zinc (4N)	NH ₃ -O ₂	1:3, 1:1, 3:1	~5 Pa	500°C	32 W for 30 mins	-	31	1.3	7.3×10^{17}
DC3 [2.14]	α -Al ₂ O ₃ (0001)	Zinc (4N)	NH ₃ -O ₂	0:1, 1:4, 1:2, 1:1, 2:1	~5 Pa	400-550°C	32 W for 30 mins	-	35	1.8	3.2×10^{17}
DC4 [2.15]	Si (100) and (111)	Zinc (4N)	Ar-O ₂	0.17:0.83	3×10^{-2} Torr	350°C	20 W for 3 mins	750°C for 30 mins (~10 ⁻⁶ torr)	30	130	2×10^{15}
DC5 [2.16]	Si (100) and Sapphire	Zinc (4N)	NH ₃ -O ₂	0:1, 3:2	~5 Pa	300-550°C	32 W for 30 mins	-	~35	~2.47	~10 ¹⁷
RF1 [2.17], [2.18]	Sapphire c plane coated with undoped ZnO (1 μ m)	Zinc mixed 1 wt% P ₂ O ₅	-	-	-	350-750°C	-	1-3 mins at 600-950°C in N ₂	0.59-2.4	2.5	1.75×10^{19}
RF2 [2.19]	p-InP (initial doping concentration: $3 \times 10^{18} \text{cm}^{-3}$)	Zinc (5N) + presputtering	Ar	-	-	400°C	150 W	60 mins at 495°C in Zn ₃ N ₂	-	-	10 ¹⁶
RF3 [2.20]	GaAs (001)	Zinc (5N) + presputtering	Ar-O ₂	1:1	-	400°C	150 W	60 mins at 600°C in vacuum ampoule	-	-	10 ¹⁹
RF4 [2.21]	-	GaN (4N) + presputtering	N ₂ -O ₂	1:0 to 1:3	-	-	-	-	11.7	64	9×10^{16}
PLD1 [2.22]	Sapphire	ZnO mixed 0.1 wt% Ga ₂ O ₃	N ₂ O (ECR on)	-	-	400°C	10 Å/min	12 h at 1000°C (Ga doping)	5.8×10^{-3}	0.96	1.1×10^{21}
PLD2 [2.23]	Corning #7059 glass	ZnO mixed 0.1 wt% Ga ₂ O ₃	N ₂ O (ECR on)	-	-	400°C	-	12 h at 1000°C (Ga doping)	2.0	0.07	4×10^{19}
PLD3 [2.24]	Sapphire	ZnO mixed 5.0 wt% Ga ₂ O ₃	Ar-N ₂ (ECR on)	4:6	0.2 Pa	550°C	-	30 mins at 850°C in N ₂	All n-type ZnO films	All n-type ZnO films	All n-type ZnO films
ION1 [2.25]	Si ₃ N ₄	ZnO	N with (80kev)	Dose: 5×10^{12} - $5 \times 10^{15} \text{cm}^{-2}$	-	-	-	20 mins at 850°C in N ₂	~12	~4.0	~10 ¹⁷

Table 2.6 Experimental conditions and electrical properties of p-type ZnO reported in selected reports

Ref.	Experimental Conditions						Electrical properties		
	Substrate	Zinc	Nitrogen	Indium	N-In codoped film	Substrate temperature	Resistivity ($\Omega\text{-cm}$)	Mobility ($\text{cm}^2/\text{V-s}$)	Hole concentration (cm^{-3})
Pyrolysis1 [2.26]	[15] n-type Si(100) wafers ($\rho=0.0015 \Omega \cdot \text{cm}$)	$\text{Zn}(\text{CH}_3\text{COO})_2 \cdot 2\text{H}_2\text{O}$ (AR, 0.5 mol/l)	$\text{CH}_3\text{COONH}_4$ (AR, 2.5 mol/l)	$\text{In}(\text{NO}_3)_3$ (AR, 0.5mol/l)	Zn/N/In is 1:2:0.15	450°C	1.7×10^{-2}	155	2.44×10^{18}
Pyrolysis2 [2.27]	[16] n-type Si(100) wafers ($\rho=0.0015 \Omega \cdot \text{cm}$)	$\text{Zn}(\text{CH}_3\text{COO})_2 \cdot 2\text{H}_2\text{O}$ (AR, 0.5 mol/l)	$\text{CH}_3\text{COONH}_4$ (AR, 2.5 mol/l)	$\text{In}(\text{NO}_3)_3$ (AR, 0.5mol/l)	Zn/N/In is 1:3:0.05	450°C	5.04×10^{-3}	33.5	3.69×10^{19}
Pyrolysis3 [2.28]	Microscope glass slide	99% AR grade ($\text{Zn}(\text{CH}_3\text{COO})_2 \cdot 2\text{H}_2\text{O}$)	Ammonia	-	-	-	1.11×10^2	0.22	2.5×10^{17}

Table 2.7 Photoluminescence of reported p-type ZnO films

Ref.	Photoluminescence			
	Excitation wavelength (nm)	Peak response (nm)	Peak response (eV)	Dominant color
DC1 [2.12]	-	-	-	-
DC2 [2.13]	-	-	-	-
DC3 [2.14]	-	-	-	-
DC4 [2.15]	273	379	3.27	Ultraviolet
DC5 [2.16]	-	-	-	-
RF1 [2.17], [2.18]	325	370	3.35	Ultraviolet
RF2 [2.19]	-	-	-	-
RF3 [2.20]	-	382	3.24	Ultraviolet
RF4 [2.21]	-	-	-	-
PLD1 [2.22]	-	375	3.30	Ultraviolet
PLD2 [2.23]	-	-	-	-
PLD3 [2.24]	-	382	3.24	Ultraviolet
ION1 [2.25]	-	375	3.30	Ultraviolet
Pyrolysis1 [2.26]	-	-	-	-
Pyrolysis2 [2.27]	-	-	-	-
Pyrolysis3 [2.28]	-	-	-	-

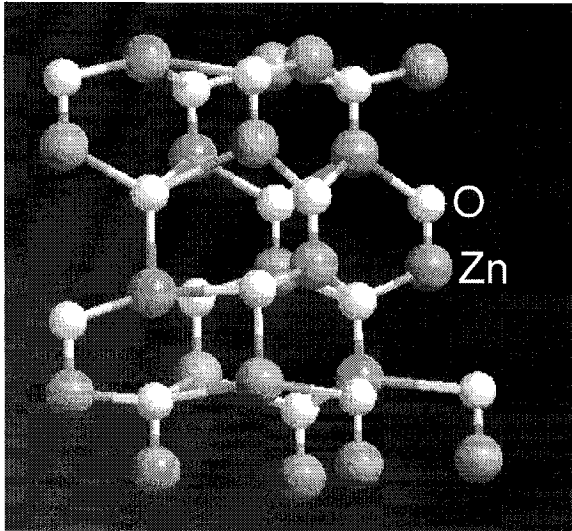


Figure 2.1 Hexagonal wurtzite structure

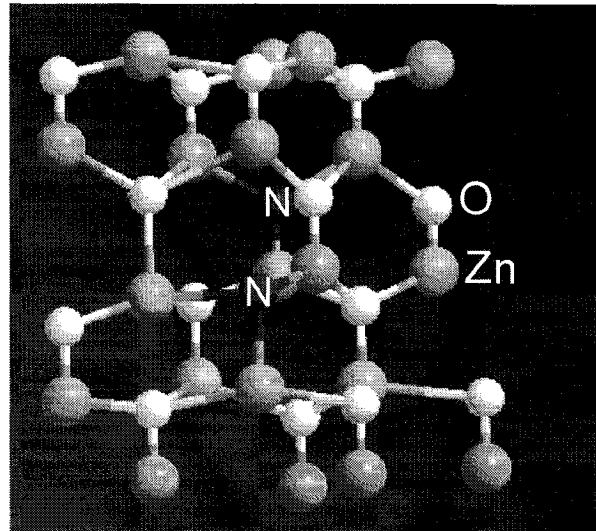


Figure 2.2 Hexagonal wurtzite structure (N replacing O)

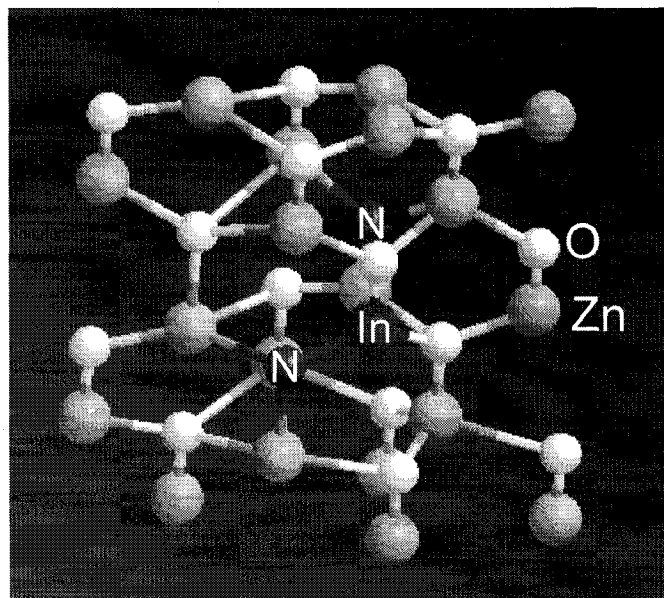


Figure 2.3 Hexagonal wurtzite structure (N-In co-dopants)

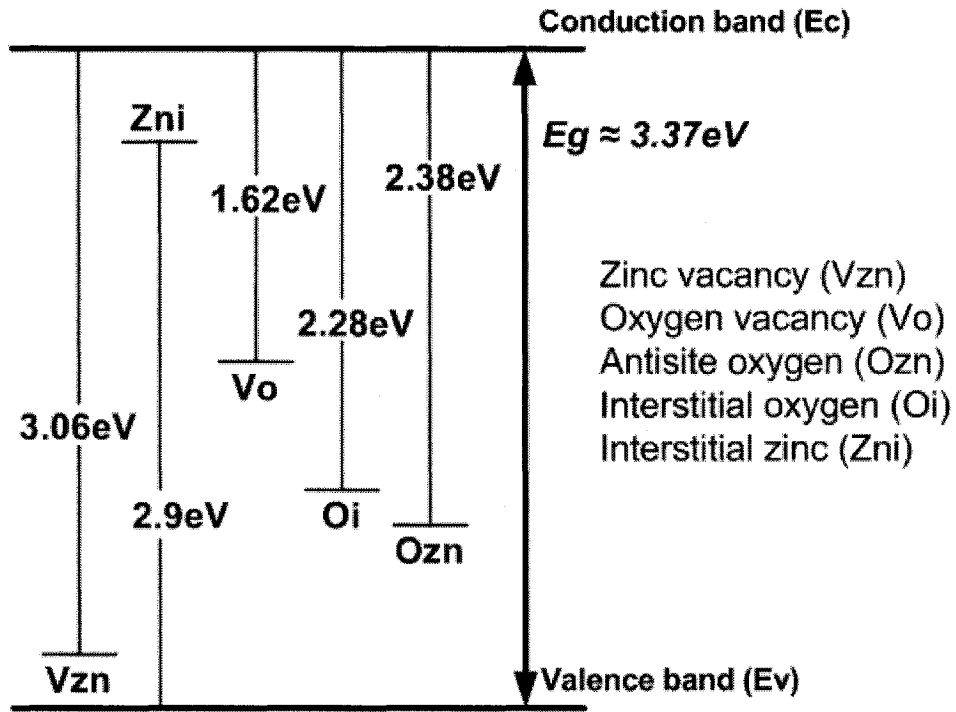


Figure 2.4 Calculated defect levels in ZnO [2.31]

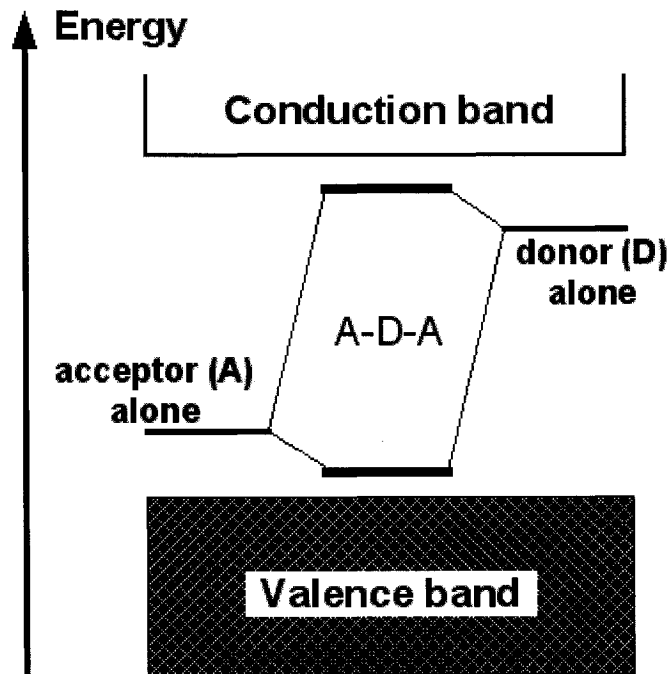


Figure 2.5 Energy band levels of a p-type semiconductor using A-D-A model [2.29]

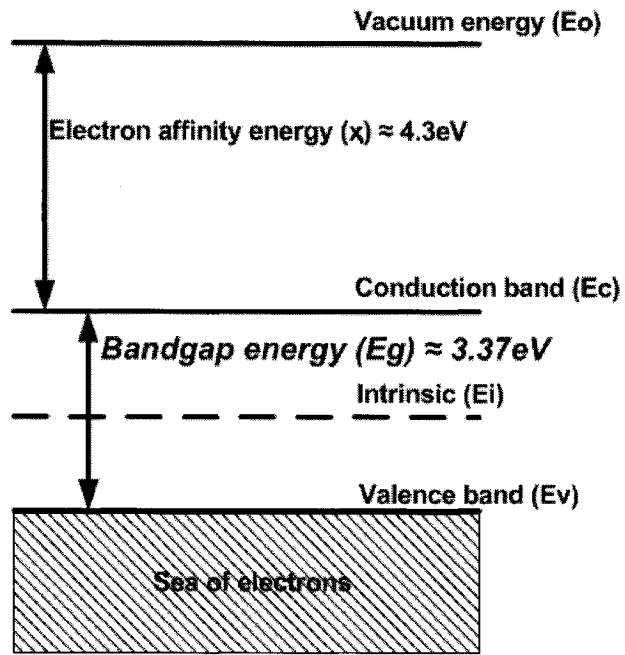


Figure 2.6 Energy band diagrams of ZnO in an ideal case

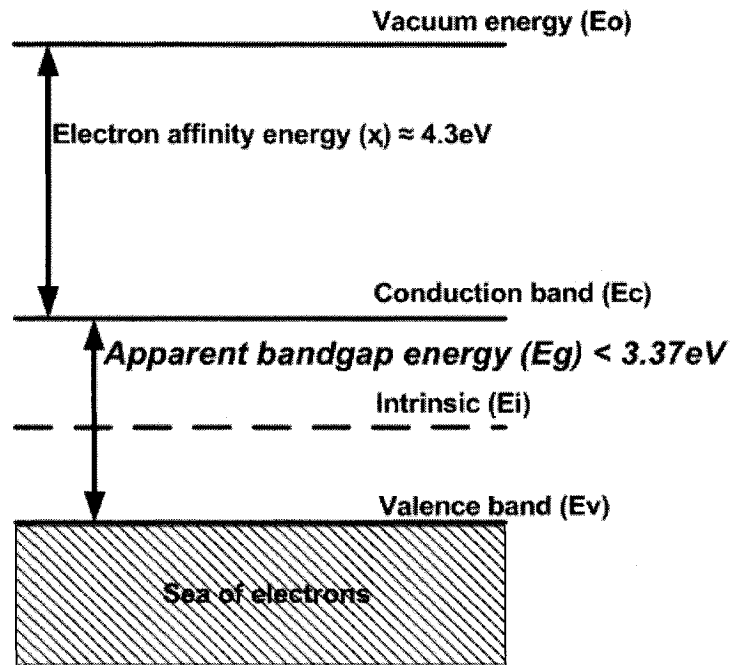


Figure 2.7 Energy band diagrams of ZnO adapted to A-D-A concept

2.2 ZnO film deposition condition used in the laboratory

2.2.1 Strategy for p-type ZnO fabrication

The objective is to minimize fabrication cost as much as possible. As a result, ZnO films are sputtered by RF magnetron on transparent glass substrate. The dopants are nitrogen and indium and are introduced in two ways. The nitrogen dopant is introduced as a working gas making the total pressure in the chamber a combination of the partial pressure from N₂ and Ar. The indium dopant comes from In₂O₃ powder, which is mixed in the ZnO powder target. For achieving better crystal structure, the thickness should be large and in the order of micrometer, thus there is a need to increase the deposition time. A thick intrinsic ZnO buffer layer shall be deposited first for minimizing the compensation effect. On the thick buffer layer, co-doped ZnO films shall be deposited.

2.2.2 Substrate preparation

The literature survey reveals that one of the most popular substrates used for p-type ZnO fabrication is (0001) orientated sapphire α -Al₂O₃ due to lattice matching near the interface. One way to work around the need for sapphire substrate is to increase the deposition time of the films deposited on glass substrate.

The glass substrates are pre-cleaned microscope slides from Fisher Scientific (Catalog No. 12-550A). The dimensions of a glass slide are 75 mm long, 25 mm wide, and 1mm thick. The glass slides are immersed in tap water containing SparkKleen (Fisher Scientific Catalog No. 04-320-4) and thoroughly washed with cotton cloth. Afterwards,

the glass slides are thoroughly rinsed with de-ionized (DI) water, spin-dry at 3000rpm for 20 seconds and then baked in oven at 90°C for 10 mins.

For studying photoluminescence spectra of ZnO films, two inches (111) n-type silicon wafers with phosphorous doping concentration about 10^{15} cm^{-3} are selected as the substrates. The silicon substrates are first immersed in acetone and introduced in ultrasonic bath for about 3 mins. Afterwards, they are immersed in buffered HF solution for 30 seconds and then thoroughly rinsed under DI water. Finally they are spin-dried at 3000 rpm for 20 seconds and then baked in oven at 90°C for 10 mins.

2.2.3 Targets preparation

High purity white ZnO powder (99.999%) is used for preparing two ZnO targets. One of the targets contains undoped ZnO powder and the other contains impurities. Undoped ZnO powder is spread evenly on a circular aluminum disk with 7.0 cm diameter and its groove is about 0.3 mm deep able to contain ZnO powder. Once ZnO powder is spread evenly on the disk, the powder is pressed for achieving visible uniformity.

The doped target is prepared as follows. The amount of In_2O_3 must be small enough to be just a by-player for enhancing the incorporation of nitrogen in ZnO films due to the donor nature of In_2O_3 in ZnO. Initially, 99.8 wt% ZnO and 0.2 wt% of In_2O_3 are prepared, which corresponds to 7.05 g of high purity white ZnO powder and 0.01383 g of high purity In_2O_3 . The powders are mixed thoroughly for at least 10 mins in a clean

beaker before putting the mixture on an aluminum disk with the same dimensions described earlier.

After a few depositions, the In_2O_3 weight percentage is increased to 0.5 and the weight percentage of ZnO is reduced to 99.5. The additional amount needed is calculated as follows:

Total weight of ZnO and In_2O_3 after 3 depositions: 6.9395 g
99.8 wt% of ZnO: 6.926 g
0.2 wt% of In_2O_3 : 0.0135 g

$$\frac{0.0135 + X}{0.5} = \frac{6.926}{99.5}$$
$$X = 0.0213 \text{ g}$$

Therefore, 0.0213 g of In_2O_3 is then added to the original target and thoroughly mixed for at least 10 mins. Notice that the remixed target is used for p-type ZnO deposition.

The targets of undoped and doped ZnO powder after several depositions are shown in Figures 2.8 and 2.9, respectively. The targets are not remixed before the next deposition. Notice that the color of the doped target becomes more and more dark brownish with each deposition. The undoped white ZnO target becomes yellowish with additional depositions.

2.2.4 ZnO deposition conditions

The total thickness of ZnO films is expected to be in the order of micrometer. There are a total of eight depositions needed for making p-type ZnO. The first four

depositions are intended to create a buffer layer, thus undoped ZnO target is used and the working gases are argon and oxygen. The following four depositions are planned for doping ZnO films. Therefore, doped ZnO target is needed and the working gases are argon and nitrogen. No substrate heating is required for all depositions. Following each deposition, the samples are cooled in vacuum for about 30 mins and stored in vacuum before the next deposition. In the case of doped ZnO deposition condition, the chamber pressure is initially 10 mtorr for 30 mins and then reduced to 5 mtorr for 7:30 hrs. Table 2.8 summarizes the deposition conditions.

Figure 2.10 shows a Scanning Electron Microscope (SEM) picture of the cross-section of a typical multi-layer ZnO film. The thickness of ZnO differs at different location of substrate with respect to the target, which will be discussed in Chapter 4. The picture is taken at an angle of 8 degrees with respect to the horizontal plane. The total thickness of the ZnO sample after the eighth deposition is approximately 5 μm .

Table 2.8 Deposition conditions for p-type ZnO

Deposition count	Target	Working gas (x:y)	Power	Total chamber pressure	Time
1	Undoped ZnO	Ar:O ₂ 0.75:0.25	50 W	10 mTorr	8 hrs
2	Undoped ZnO	Ar:O ₂ 0.75:0.25	50 W	10 mTorr	8 hrs
3	Undoped ZnO	Ar:O ₂ 0.75:0.25	50 W	10 mTorr	8 hrs
4	Undoped ZnO	Ar:O ₂ 0.75:0.25	50 W	10 mTorr	8 hrs
5	Doped ZnO	Ar:N ₂ 0.75:0.25	50 W	10 mTorr 5 mTorr	30 mins 7:30 hrs
6	Doped ZnO	Ar:N ₂ 0.75:0.25	50 W	10 mTorr 5 mTorr	30 mins 7:30 hrs
7	Doped ZnO	Ar:N ₂ 0.75:0.25	50 W	10 mTorr 5 mTorr	30 mins 7:30 hrs
8	Doped ZnO	Ar:N ₂ 0.75:0.25	50 W	10 mTorr 5 mTorr	30 mins 7:30 hrs

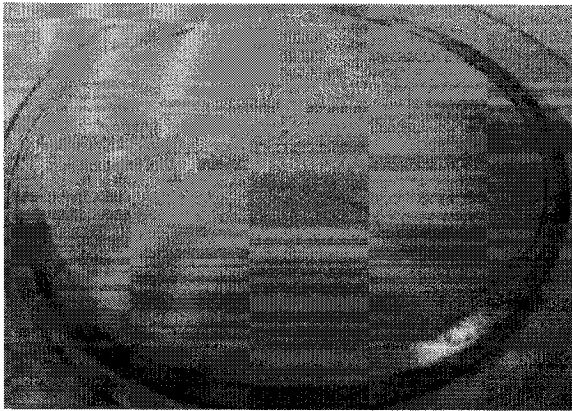


Figure 2.8 Undoped ZnO target after several depositions

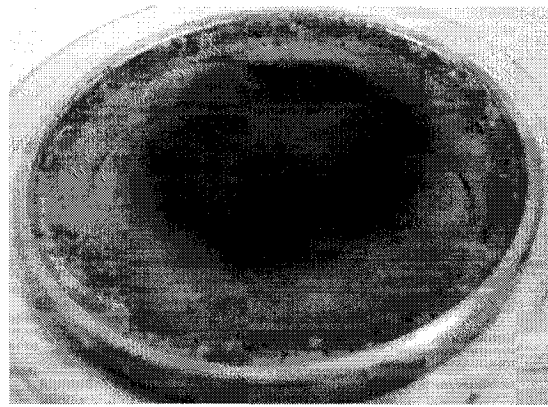


Figure 2.9 Doped ZnO target after several depositions

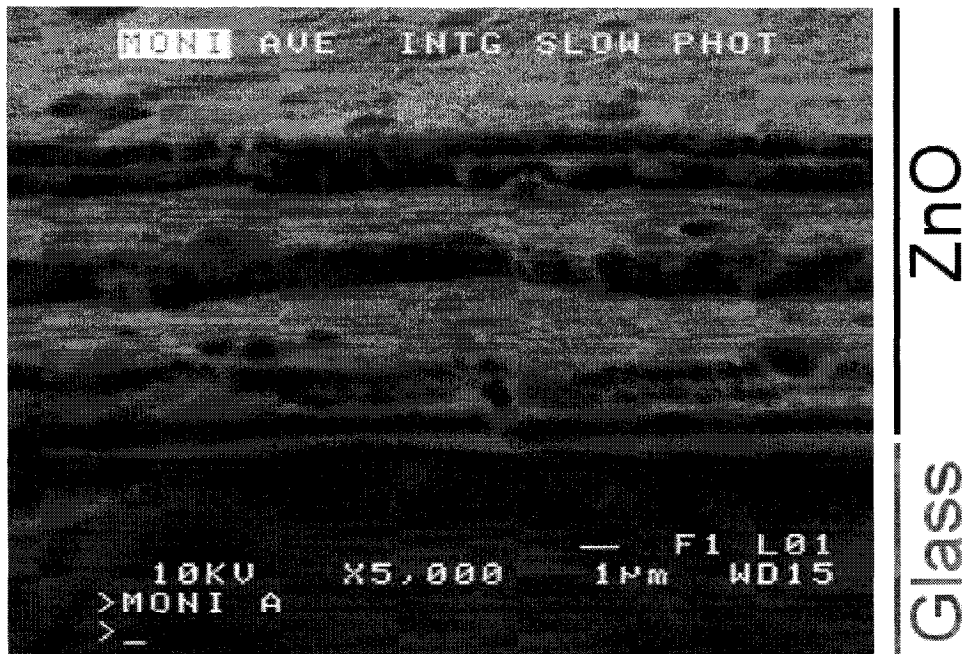


Figure 2.10 Cross-section of ZnO films after the eighth deposition

CHAPTER 3 EQUIPMENT AND MEASUREMENT METHODS

3.1 Introduction

Vacuum system is nowadays widely used in laboratories and industries for thin film deposition. Different deposition methods are used in the laboratories for obtaining thin films. In our laboratories, ZnO films are primarily deposited using RF magnetron sputtering and metal film depositions are done using evaporation. In this chapter, the principle of vacuum system will be explained. Furthermore, three deposition methods namely, DC sputtering, RF sputtering and evaporation will be discussed.

Electrical characterization methods such as four-point-probe and Hall effect measurements are used for characterizing thin films. In addition, optical transmission and photoluminescence measurements are also discussed. The principle of the measurement methods is first explained, followed by the descriptions of equipments and setups used in the lab.

3.2 Vacuum System

A vacuum system is a chamber interconnected to a pumping system through pipes and can withstand a wide range of pressure depending on its application. A typical pumping system consists of two pumps and several valves as shown in Figure 3.1. In the laboratories, high vacuum is the preferred category for thin film deposition and its operating pressure is between 10^{-3} - 10^{-8} torr. Other possible pressure ranges are shown in Table 3.1. The standard international (SI) unit of pressure is Pascal (Pa); however, most

gauges in a vacuum system use other units such as bar and torr and the existing relationship between the units is 100 Pa is equivalent to 1 mbar or 0.76 torr.

3.2.1 The Need for Vacuum in Thin Film Depositions

Film depositions are done in vacuum because as the pressure decreases, the unwanted impurities contained in chamber diminish. Thus, depositions done in vacuum will allow the deposited films to be as pure as possible. Moreover, the *mean-free-path* increases dramatically at low pressure. The mean free path is defined as the average distance traveled by a molecule or atom before colliding with another one. Therefore, it would require that mean-free-path to be much greater than the dimensions of the vacuum chamber in order to achieve films with high uniformity. The expression, mean-free-path = $0.007/p$, relates the mean-free-path in cm to pressure in mbar [3.4]. If a chamber were pumped down to 10^{-7} torr, the mean-free-path would be about 100 m.

3.2.2 High Vacuum Evacuation Procedure

The pumping system for high vacuum evacuation is complex because there are pumps interconnected and opened/closed valves to control the gas flow path. The pumping system of a high vacuum chamber is shown in Figure 3.1. The mechanical pump, also called rotary pump, and the diffusion pump permit the chamber to be evacuated in different pressure ranges. Typical operation for evacuating is described as follows. The evacuation process starts with the mechanical pump “ON” and all valves closed except for the roughing valve. Depending on the type and size of the mechanical pump, it could evacuate to an ultimate pressure of 5×10^{-3} torr in about 20 minutes [3.2].

The diffusion pump needs to warm up for about 20 minutes and is turned “ON” while the mechanical pump is functioning. The next step would be to close the roughing valve and open the backing valve in order to let the diffusion pump evacuate the system. Notice that in this case the mechanical pump is pumping out the gas evacuated by the diffusion pump. Due to the initial high viscosity of the air at atmospheric pressure, it is preferable to start the evacuation using the mechanical pump rather than the diffusion pump. Depending on the size and type of diffusion pump, it could reach the ultimate pressure of 10^{-8} torr after 30 minutes of evacuation [3.3]. The main valve is then gradually opened and adjusted to the desired pressure for thin film deposition. The vent valve can be opened when all the valves are closed because it allows air to flow into the chamber so that the pressure inside the chamber could return to 1 atm. Notice that improper evacuation procedure could lead to breakdown of vacuum system.

3.2.3 Operation of diffusion pump

Diffusion pumps can be used for achieving lower pressure than mechanical pumps. The principle behind diffusion pump is that high energetic fluid (often hydrocarbon oil, also known as diffusion oil) pushes down unwanted gas molecules to the bottom and then to the exhaust. The heater on the bottom boils diffusion oil and vapour is created. The pump is surrounded with flowing water-cooling system. In order to recollect high energetic oil, the exhaust pipe is made in “U” shape and surrounded with cooling water so that the oil would be cooled down and return in liquid phase after an evacuation cycle. Figure 3.2 shows the schematic of a diffusion pump. The deviation plates inside

the diffusion pump force the energetic oil molecules to travel downwards, which in turn push the unwanted gas molecules to the exhaust.

3.2.4 Pressure Gauges

Pressure, measured in force per unit area, in a pumping system is measured using two different kinds of gauge, namely Pirani and Penning gauges. Depending of the gas in the Pirani and the Penning gauges, they could detect pressure down to 10^{-3} torr and 10^{-3} - 10^{-6} torr respectively.

3.2.4.1 Principle of a Pirani gauge

Pirani gauge is thermal conductive meaning that the gauge is able to sense an increase in thermal resistivity of a heated wire as the pressure is reduced. As the wire heats up, the electrical resistance increases. This type of gauge is composed of a hot wire centrally placed in a vessel in which the surrounding, i.e cover, remains at room temperature. At high pressure, gas molecules could hit the cover and then hit the wire filament to cool it down because the temperature of the molecules hitting the wire would be approximately the same as of the cover [3.5]. At low pressure, the number of molecules would be dramatically reduced and they will not be able to cool the heated wire as efficiently as in the high pressure case. The heat loss from the current-carrying wire is related to the pressure. Furthermore, the temperature change of the wire is proportional to the resistance change of the wire.

3.2.4.2 Principle of a Penning Gauge

The Penning gauge is a cold cathode gauge. One advantage of cold cathode gauge over hot cathode gauge counterpart is that the filament could not be burnout. The Penning gauge is composed of a cylindrical anode at high voltage about +2 kV and on the two extremities there are two flat-disc cathodes connected to ground. Furthermore, there is a permanent magnet providing $\frac{1}{2}$ kilogauss placed in between the two poles [3.6].

As the pressure decreases, a discharge happens at about 10^{-2} torr. The current would decrease because it is composed of positive ions that have reached the cathodes. The electrical discharge is enhanced by the presence of an external magnet, since the electrons are constrained by the magnetic field to move in spiral paths between the two cathodes.

Table 3.1 Pressure range [3.1]

Category	Bar	Pascal	Torr
Low vacuum	Atmospheric pressure to 1 mbar	Atmospheric pressure to 100 Pa	Atmospheric pressure to 0.76 torr
Medium vacuum	1 mbar to 10^{-3} mbar	100 Pa to 0.1 Pa	0.76 torr to 0.76×10^{-3} torr
High vacuum	10^{-3} mbar to 10^{-8} mbar	0.1 Pa to 10^{-6} Pa	0.76×10^{-3} torr to 0.76×10^{-8} torr
Ultra-high vacuum	10^{-8} mbar to 10^{-12} mbar	10^{-6} Pa to 10^{-10} Pa	0.76×10^{-8} torr to 0.76×10^{-12} torr
Extreme high vacuum	$< 10^{-12}$ mbar	$< 10^{-10}$ Pa	$< 0.76 \times 10^{-12}$ torr

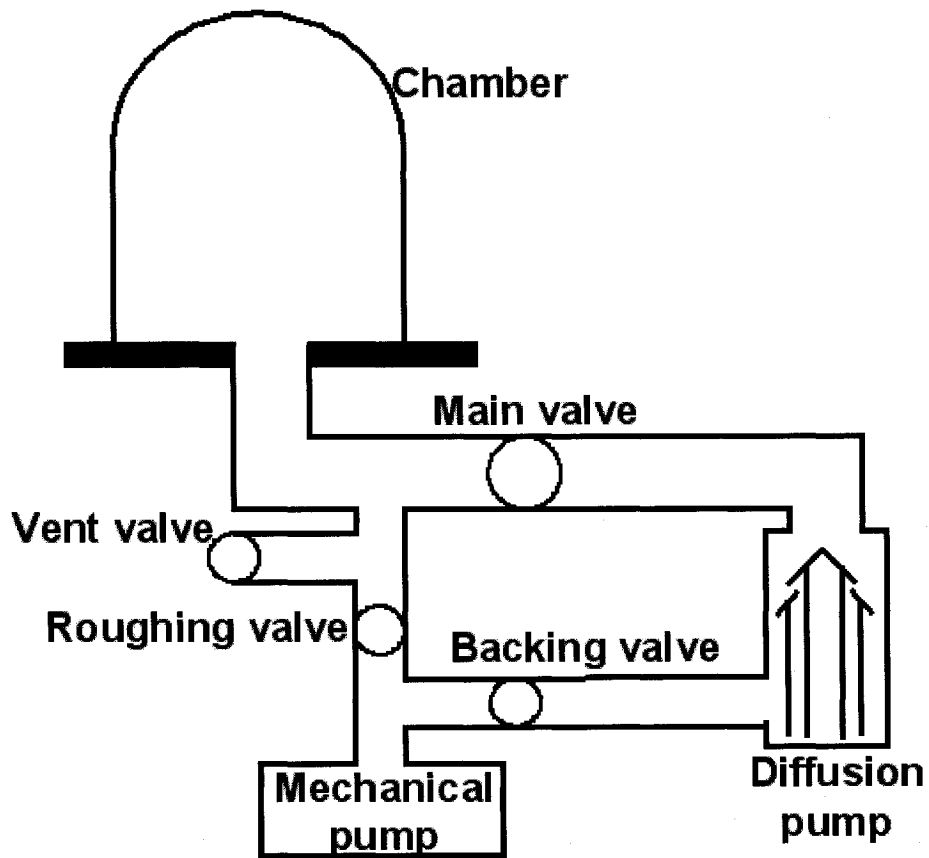


Figure 3.1 A schematic diagram of a vacuum system

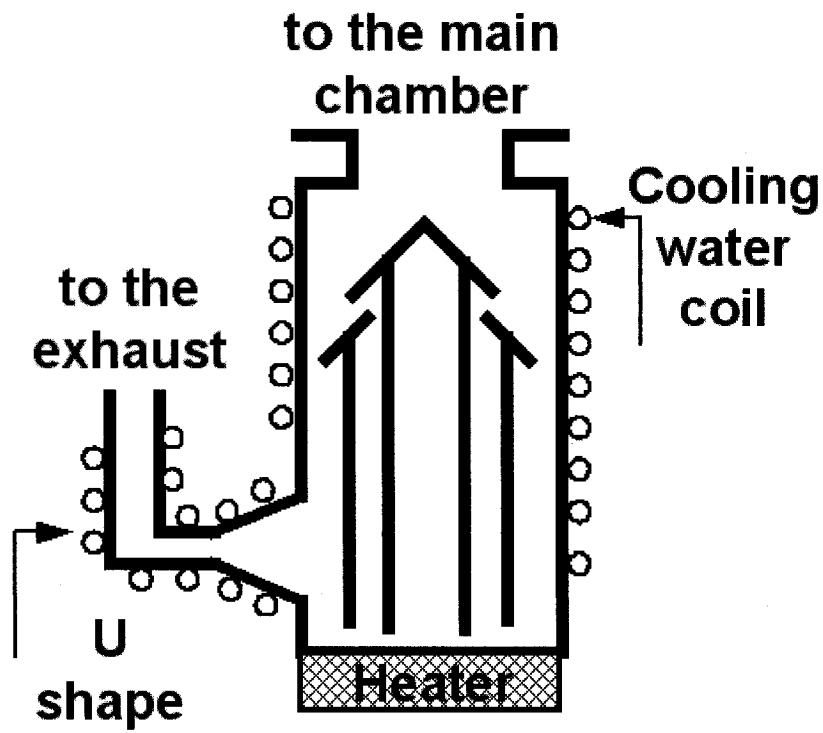


Figure 3.2 A schematic diagram of diffusion pump

3.3 Deposition Techniques

Three deposition techniques, namely direct current (DC) sputtering, radio frequency (RF) sputtering and evaporation, operating at low pressure are used in the laboratory. DC sputtering technique is primarily used for depositing metallic films. RF sputtering method can be used for depositing both metallic and non-metallic films. Metal evaporation is principally for contact or thick layer deposition. The main advantages of sputtering over evaporation are the capability to control the thickness of the deposited films and the uniformity of the films is better. Varying the deposition time while other deposition conditions are kept constant can control film thickness. Uniformity is better because sputtering consists of monolayer deposition. The following section will discuss about the principle of the deposition techniques.

3.3.1 Principle of sputtering

Sputtering deposition technique is based on a mechanism where particles having high momentum and energy collide with atoms on a surface. The atoms from the surface are ejected and will travel until reaching a surface. This process is destructive because the ions bombardment will disintegrate the target surface. The principle of sputtering deposition is illustrated in Figure 3.4.

Inert gases are preferred in sputtering deposition because they are most unlikely to react with the sputtered atoms at the target surface. One of the most popular inert gases is argon (Ar). Not only is it considered as a heavy gas but also because it has low ionization energy. In order to form an Ar ion, an energetic electron collides with an Ar atom, which

ejects another electron (secondary electron) and itself. The Ar atom becomes ionized and positively charged because it loses an electron; as a result, this ion can be attracted to the negatively charged surface (target). Notice that the glow discharge, which is the formation of plasma in Ar gas due to high voltage applied, can be observed at $10^{-1} - 10^{-2}$ torr.

In order for sputter deposition to occur, the accelerated ions must exceed threshold energy. The ions exceeding the threshold energy are subject to sputtering yield, which is defined as the number of atoms ejected per ion. As the energy of ions increases, the sputtering yield increases as shown in Figure 3.3 [3.6].

3.3.2 Magnetron Sputtering

Magnetron sputtering increases the deposition rate and could be used in both DC and RF sputtering. A magnetic field is present to gather electrons near the target by forcing them to move responding to the magnetic field lines. Therefore, if electrons were concentrated near the target, the inert gas entering that region would have a greater probability to be ionized. Therefore, the sputtering rate would increase dramatically than the one for diode sputtering.

3.3.3 DC Sputtering

Direct current (DC) sputtering is also called cathode sputtering and it is primarily used for metal deposition. It is composed of an anode and cathode in which the negative potential is increased up to a few hundred volts. In DC sputtering, the DC source acts as

an electrical energy source because when an ion hits the target, the ion gains an electron, thus it becomes neutralized and turns into an atom. DC sputtering can be used to sputter conductive materials, but it cannot be used for nonconductive material due to charging effect.

3.3.4 RF Sputtering

Radio frequency (RF) sputtering is preferred over DC sputtering because the target could be an insulator or a metal. As more and more ions hit the target, the accumulated charge may increase to a point where they will repel each other. Therefore, in order for neutralization to occur, the polarity of the target must be reversed so that there would be sufficient discharge to eliminate the surface charge. In doing so, there is a need for AC source at high frequency and the International Communication Authorities have set the standard frequency at 13.56 MHz so that it does not interfere with other radio frequency signals.

3.3.5 Metal Evaporation

Metal evaporation is mainly used for contact deposition or thick film deposition. A piece of metal is put on another metal boat where a high current of about 100 A passes through and melts the piece of metal. The boat must have a melting point much higher than the melting point of the metal to be evaporated. In our laboratory, gold is melted in a molybdenum boat.

A neat trick to estimate the mass of the metal required for evaporation will be discussed. Knowing the density of a metal in mass/volume, the thickness (t) of the film required and the distance (d) between the metal and the target, it is possible to find approximately the mass of the metal needed using the equations shown Figure 3.5.

3.4 Vacuum Equipments Used

In our laboratories, RF magnetron sputtering is used for depositing ZnO films. A schematic diagram of the chamber is shown in Figure 3.6. The distance between the target and substrate is about 3.5 cm.

The entire system is composed of Varian vacuum unit and a RF unit. The Varian vacuum unit has a glass chamber with a diameter of 12 inches, a diffusion pump with a diameter about 4 inches and a rotary mechanical pump. The pressure in the pumping system is measured using Pirani and Penning gauges. MKS PDR-D-1 Readout digital meter measures the pressure inside the chamber. The substrate holder is connected to Type K thermocouple, which translates the reading in voltage for monitoring the substrate temperature. Flowing tap water cools the system at three locations: the target, diffusion pump and sputtering gun. Two working gases can be introduced in the chamber at a time and they could be oxygen, nitrogen or argon. Figure 3.7 shows how the gas cylinders are connected to the vacuum system.

The RF unit is composed of a sputtering gun, a matching network for matching the load (sputtering gun) and 500 W power supply. The matching network is basically composed of a variable capacitor and inductor connected in parallel. These components are auto adjusted until it matches the sputtering gun, which has an impedance of 50 Ω .

In roughing position, the rotary pump can pump the chamber pressure from 1 atm to ~ 10 mtorr. By following the evacuation procedure described in Section 3.2.2, the diffusion pump can reach $\sim 10^{-6}$ torr after an over-night pumping. Three hours evacuation using the diffusion pump could reach about $\sim 10^{-5}$ torr.

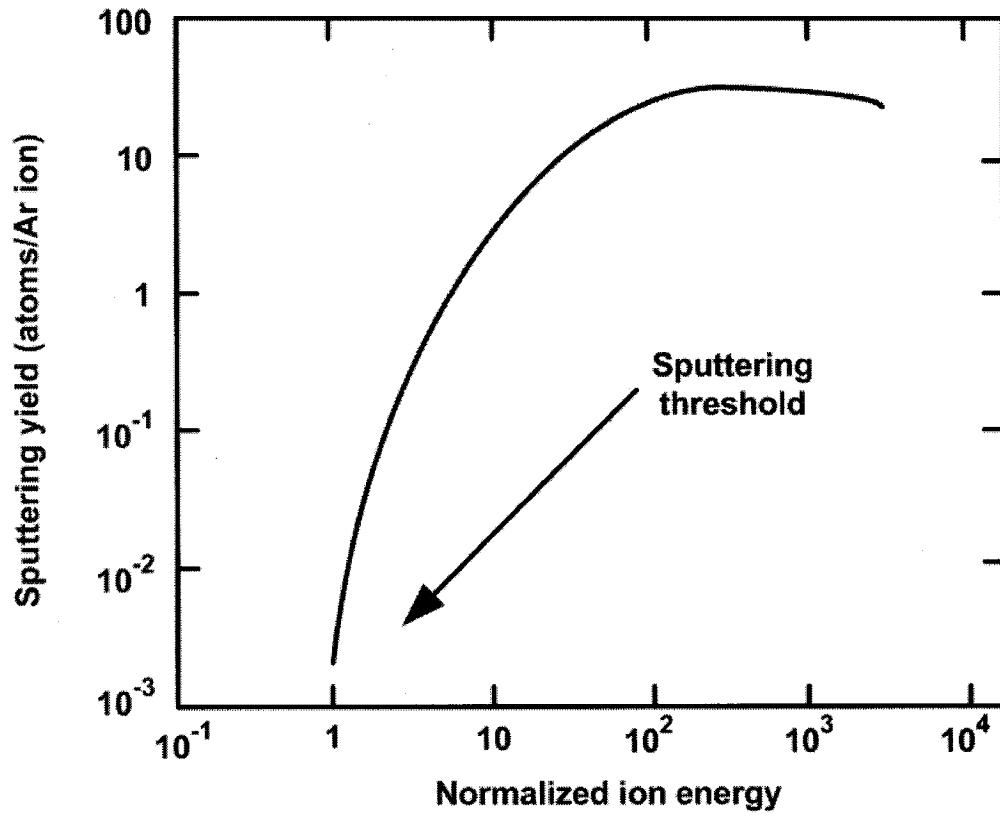


Figure 3.3 Sputtering yield versus ion energy [3.6]

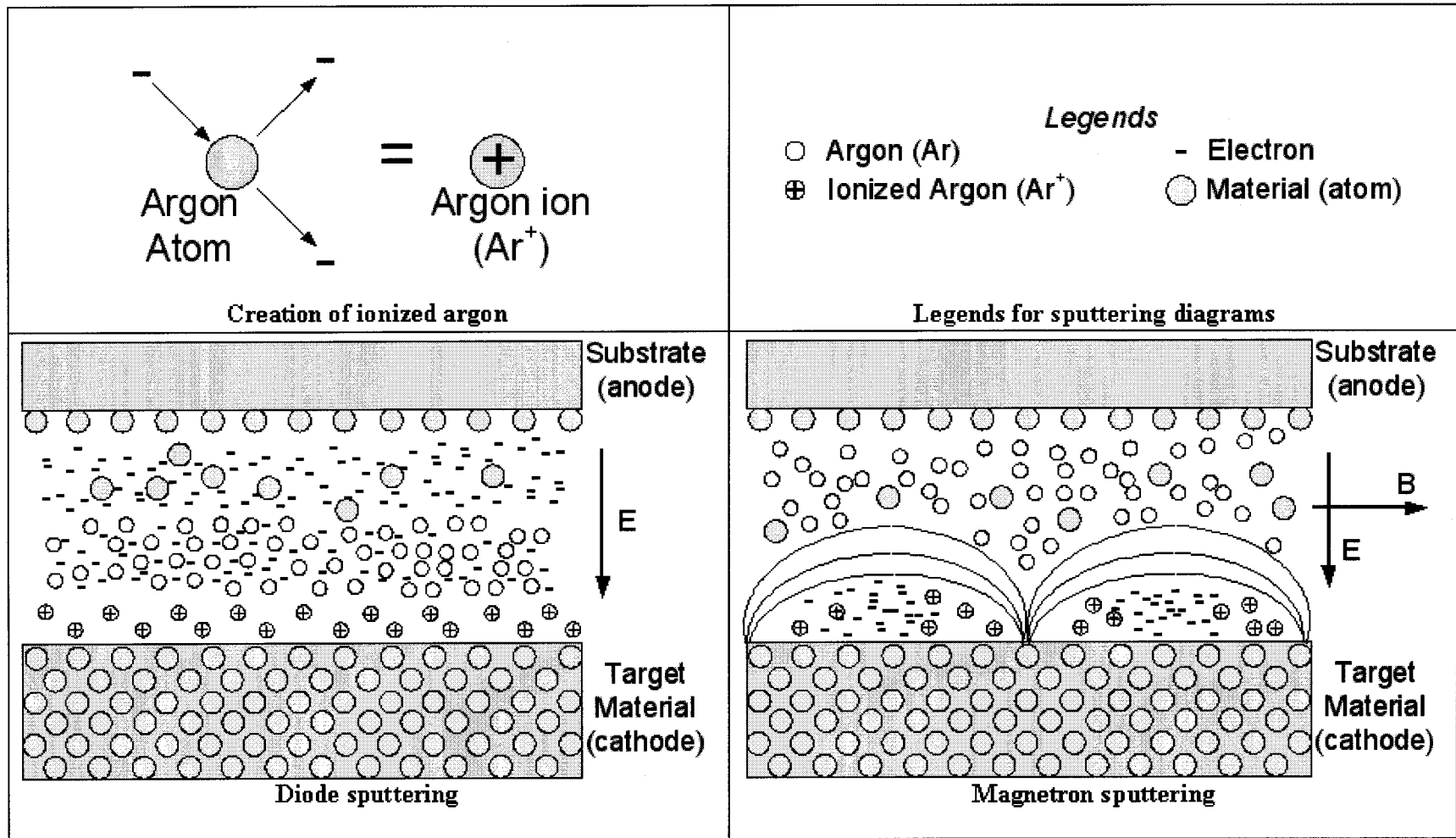


Figure 3.4 Principle of sputtering

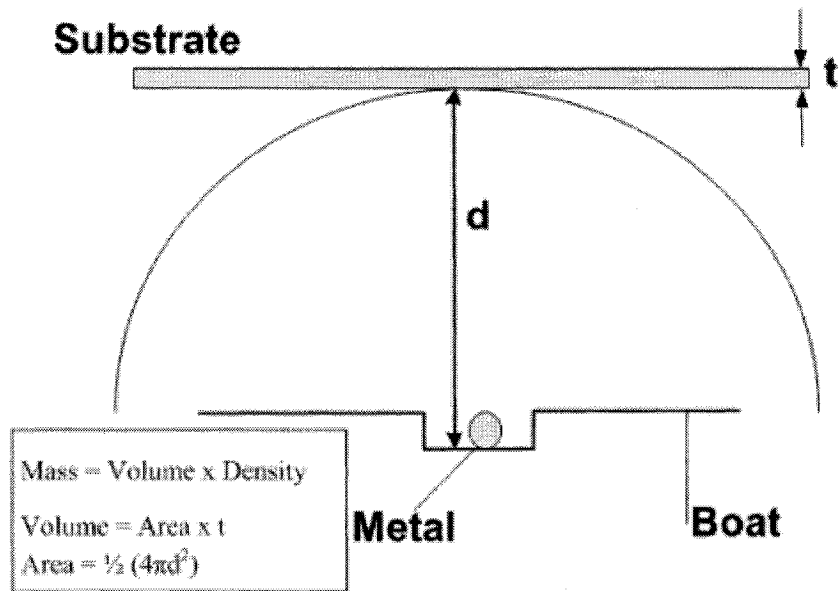


Figure 3.5 Metal evaporation estimation

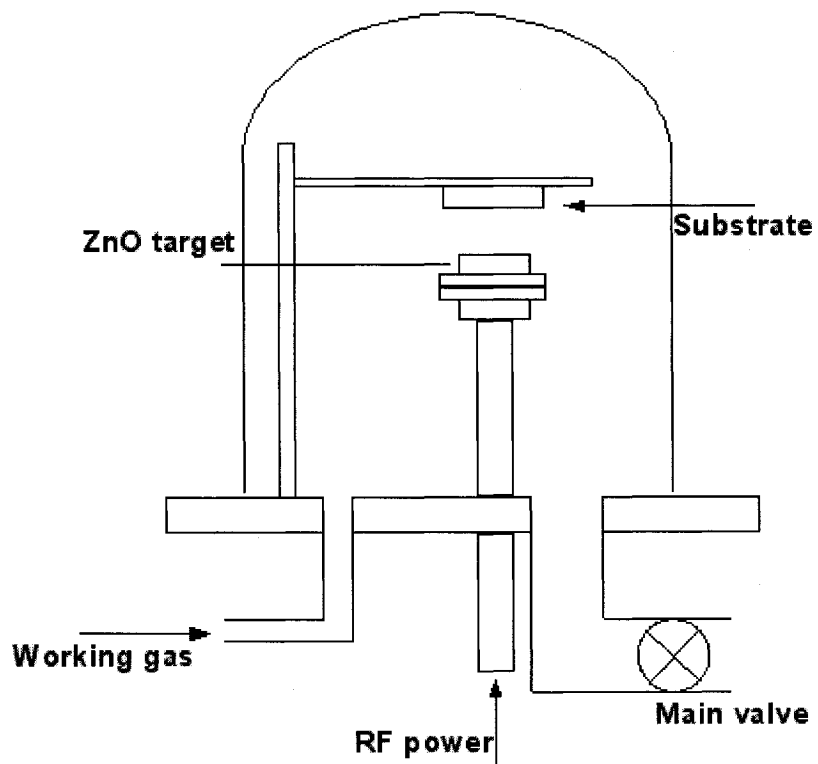


Figure 3.6 A schematic diagram of the RF deposition chamber

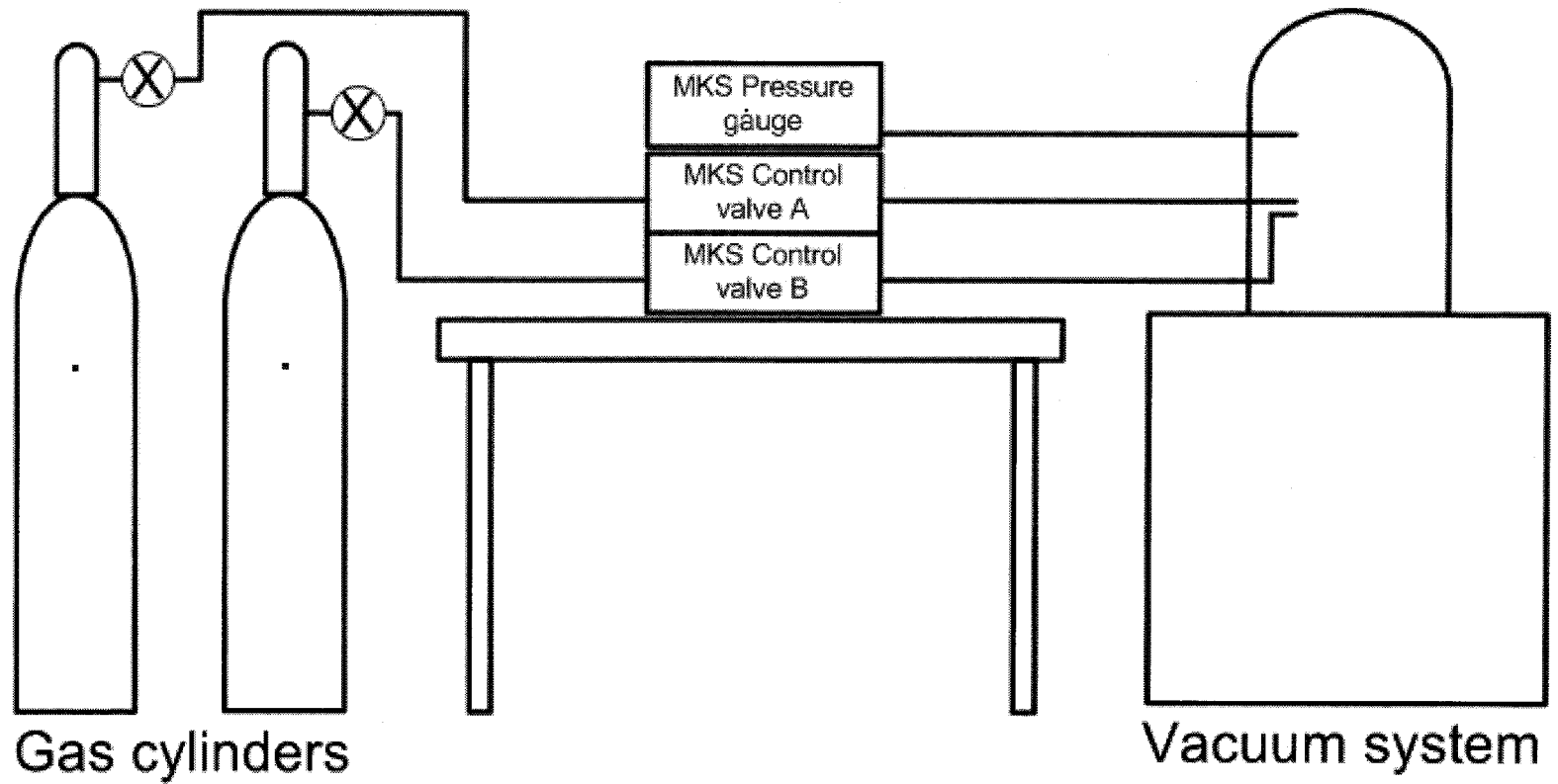


Figure 3.7 Sputtering system setup used in the laboratory

3.5 Measurement Techniques

3.5.1 Electrical measurements

3.5.1.1 Hot-point probe measurement

Hot-point probe measurement is a fast and easy way to determine the conduction type of a semiconductor. The equipment required for this measurement is a hot-point probe, a cold-probe and a voltmeter. The measurement procedure is simple. Letting the hot-point probe to heat up and bringing it in close proximity to the cold-point probe would allow the reading of the voltmeter to be either positive or negative. The hot-point probe in contact with the semiconductor will increase the energy of the majority carrier; as a result, the energized carriers will diffuse in the material creating a deficiency of the majority carrier at the contact as shown in Figure 3.8. The deficiency of the majority carrier at the contact will create a net charge of the opposite conduction, thus allowing reading on the voltmeter. In other words, a p-type material under hot-point probe test would give a negative reading and n-type material would give a positive reading. The spacing between the probes is not critical, meaning that the absolute value given by the voltmeter could change in respect to the spacing between the probes.

In the laboratory, a soldering iron surrounded with copper wire represents the hot-point probe. In order to avoid unwanted junctions created at the contact points, the cold-point probe is connected to a piece of unheated copper wire. Readings are collected using a HP 3478A Multimeter on voltage mode. The setup of hot-point probe is shown in Figure 3.9.

3.5.1.2 Four-point probe measurement

Resistivity (ρ) is an important parameter, which is defined as the resistance of the material to current flow. Four-point probe measurement can be used for determining the resistivity. In the four-point probe setup, there are four probes equally distanced and all contacts make are pressed against the film during measurement. As a result, it causes slight damage to the film where the contacts are made. A DC voltage is applied to the two outer probes and a resistor in series. By measuring the voltage across the resistor and knowing its resistance value, it is possible to find the current passing through the probes. The inner probes are connected to a voltmeter. The setup of four-point probe at the proximity of the contacts is shown in Figure 3.10 and the setup used in the lab is shown in Figure 3.11. The resistivity of the films is calculated using the following approximations [3.6]. Two approximations can be used, (S) is the spacing between two adjacent probes and (t) is the thickness of the sample.

$$\text{For } t \gg S,$$
$$\rho = 2\pi S \frac{V}{I} \text{ (ohm-cm)}$$

$$\text{For } S \gg t,$$
$$\rho = \frac{\pi t}{\ln 2} \frac{V}{I} \text{ (ohm-cm)}$$

Equation 4.1 Equations for resistivity approximation

3.5.1.3 Hall effect measurement

Hall effect measurement is an accurate method for determining the conduction type of semiconductor. Not only it could be used to find the majority carrier type in the semiconductor, but also it can give accurate results of the majority carrier concentration and majority carrier mobility. A schematic diagram showing the Hall effect principle is presented in Figure 3.12.

A voltage V_s is applied with the polarity shown above and the magnetic field B is perpendicular to the vertical surface. Assuming the majority carriers are holes (p-type semiconductor) in the figure above, the force created on a charged particle with velocity v due to magnetic field is given in $\vec{F} = q\vec{v} \times \vec{B}$. As a result, there would be positive charge build-up on the bottom surface and that potential is called the Hall voltage (V_H). The formulas shown in Table 3.2 can be used for determining the majority carrier concentration and mobility [3.7]. The magnitude of the electronic charge is represented by e .

In practical application, different equipotential lines at the contacts are present and there is a need to correct the geometry. The accurate Hall voltage is half of the difference of the collected readings with the same magnetic in and out of the sample at an applied current.

The Hall effect measurement setup used in the laboratory is shown in Figure 3.13. It consists of two type E electromagnets from Newport instrument. The magnetic field is

adjusted through a variac and can be increased up to 0.9 Tesla. The magnitude of the magnetic field is read using a Walker Scientific Gauss meter MG-4D. Flowing tap water cools the system. The apparatus holding the sample is mounted in between the magnets and the surface of the sample is parallel to the flat surface of the magnets. Keithley Programmable current source is carrier injection and data are collected via HP 3147 multimeter.

Table 3.2 Equations for carrier concentration and mobility

	p-type material	n-type material
Carrier concentration	$p = \frac{\vec{I}\vec{B}}{edV_H}$	$n = -\frac{\vec{I}\vec{B}}{edV_H}$
Mobility (independent of dimension)	$\mu_p = \frac{ V_H }{R_s \cdot I \cdot B}$	$\mu_n = \frac{ V_H }{R_s \cdot I \cdot B}$

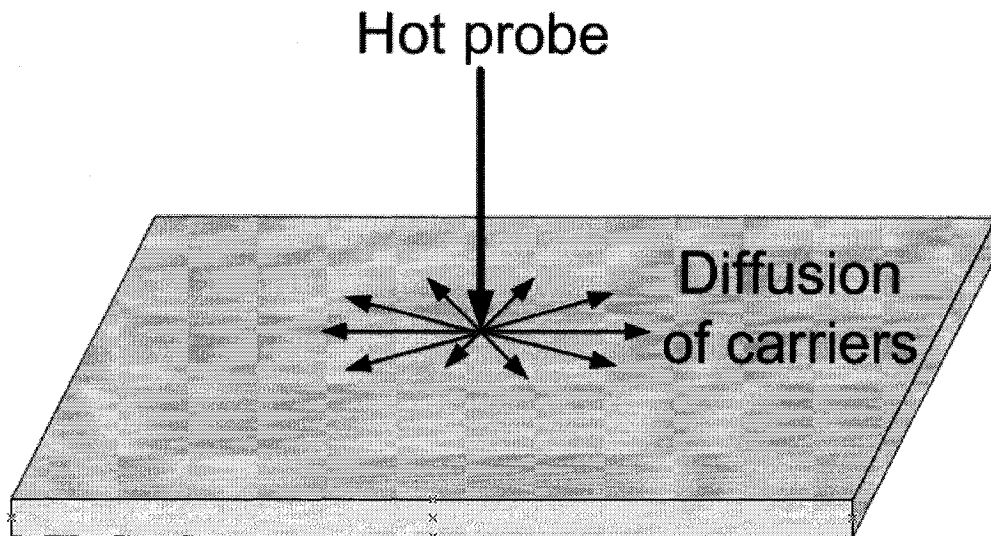


Figure 3.8 Diffusion of carriers in hot-point probe measurement

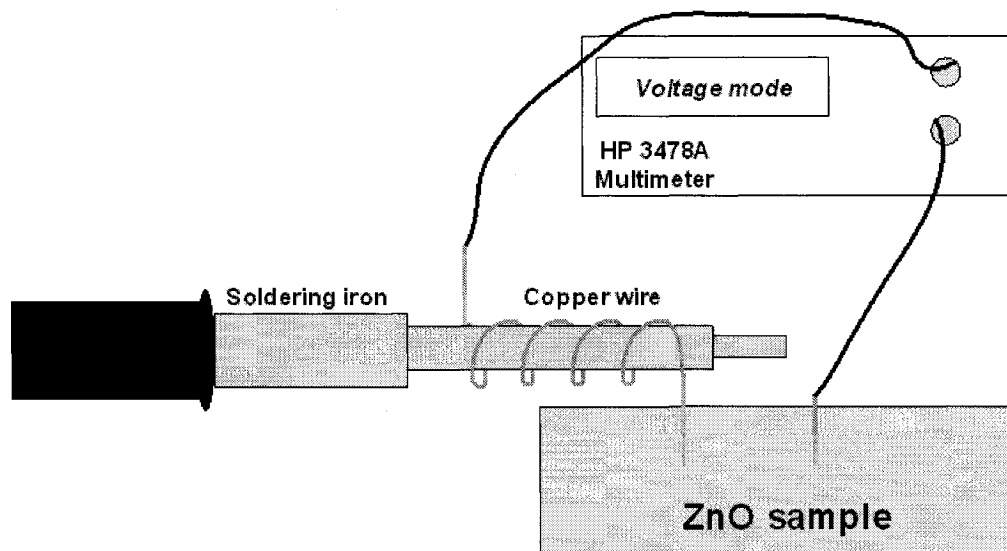
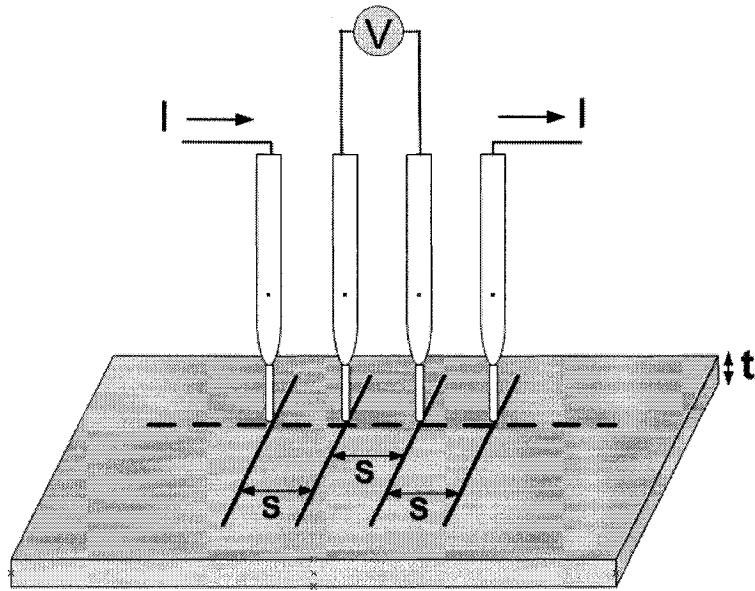


Figure 3.9 Hot-point probe setup used in the laboratory



ZnO sample

Figure 3.10 Four-point probe measurement

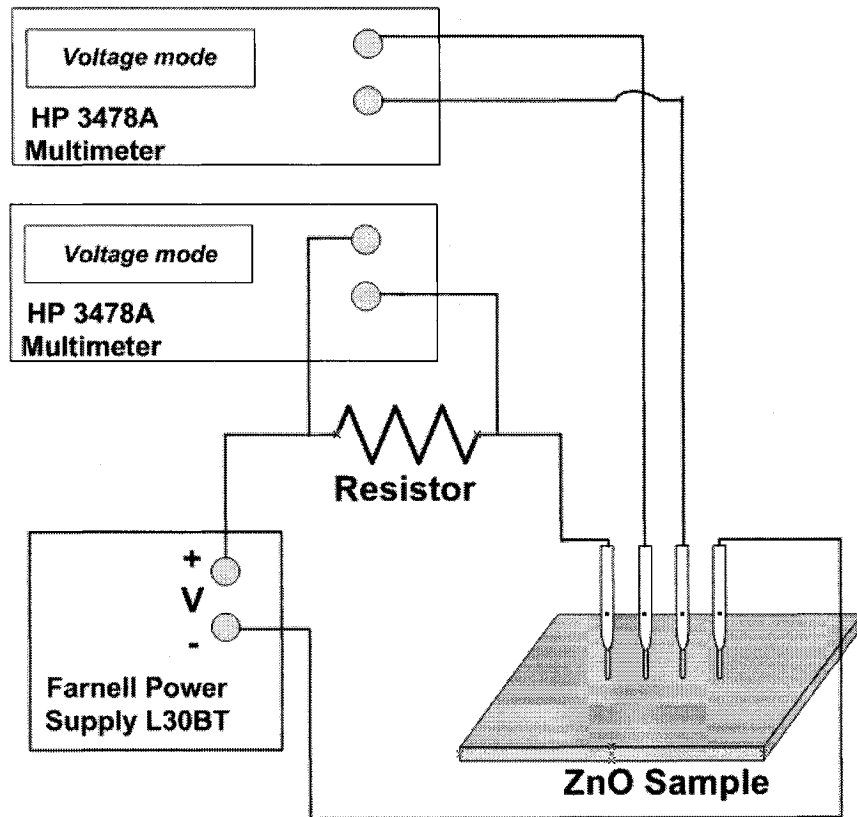


Figure 3.11 Four point-probe setup used in the laboratory

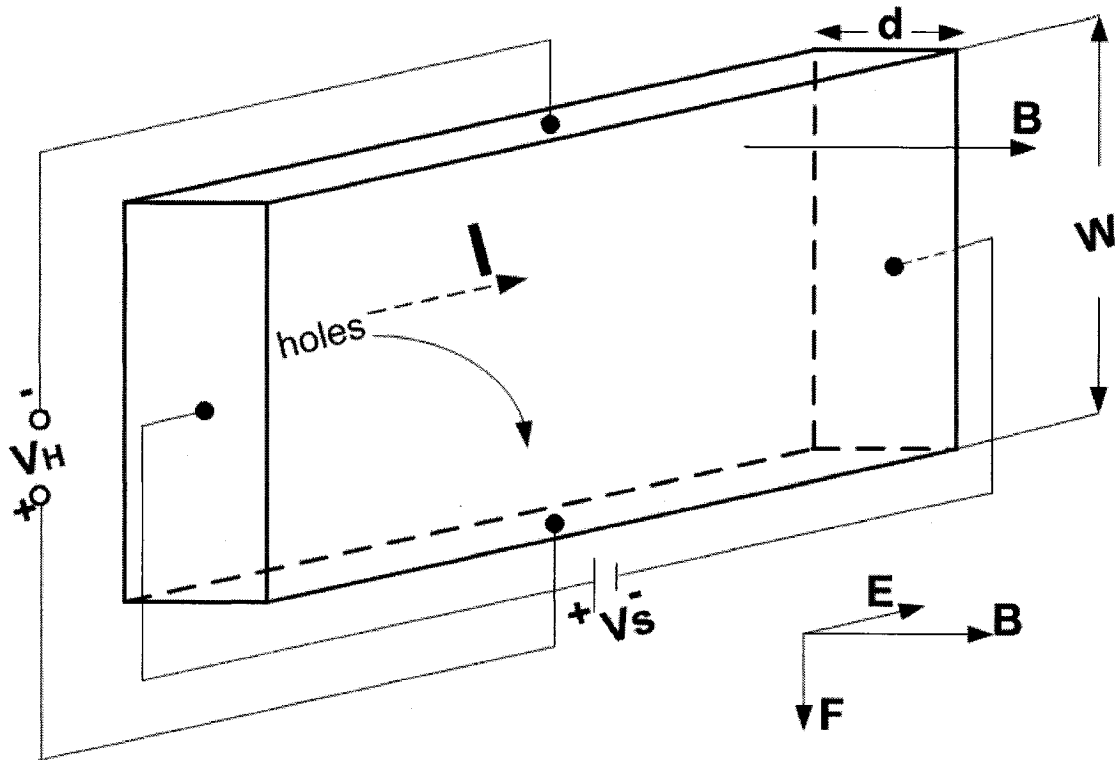


Figure 3.12 Parameters in Hall effect measurement

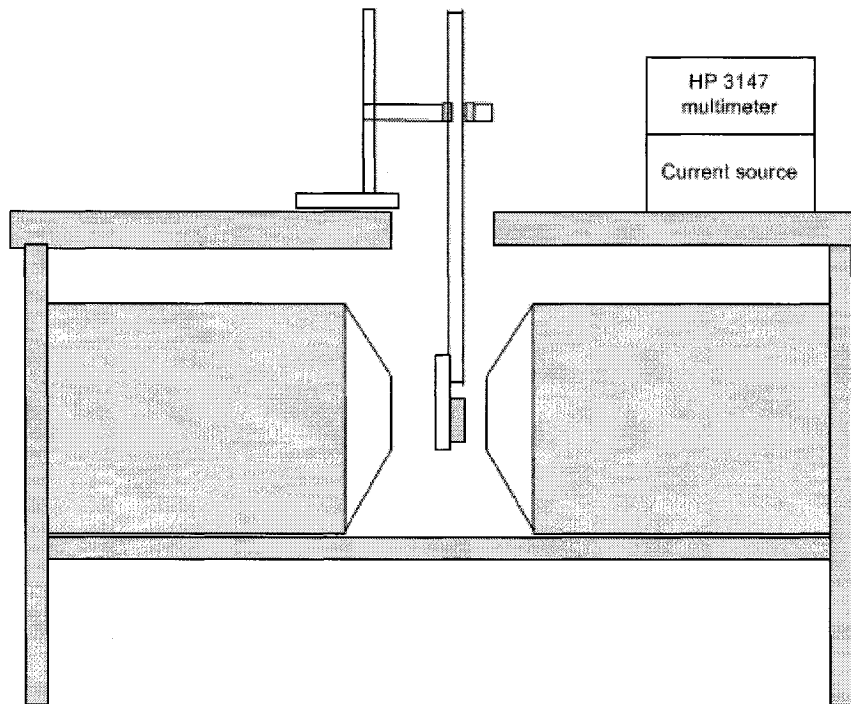


Figure 3.13 Hall effect measurement using electromagnets

3.5.2 Optical measurement

3.5.2.1 Optical transmission measurement

Optical transmission measurement determines the amount of light at different wavelengths passing through a semi-transparent sample. The setup used in the lab is shown in Figure 3.14. Different wavelengths of the tungsten lamp are selected through Beckman Spectrophotometer Model 2400. The sample on glass is mounted between the monochromator and the Si detector. The detector is connected in series with a resistor and biased at -1.5 V during the measurement. The amount of light captured by the detector is converted to voltage drop across the resistor. In this case, ZnO films are deposited on transparent glass substrates; as a result, the transmittance is the ratio of voltage readings of ZnO samples and glass substrate itself.

3.5.2.2 Photoluminescence measurement

Photoluminescence is the light emission at different wavelengths in the electromagnetic spectra by a material through the absorption of a photon. The high-energetic photon excites an electron in the material to a higher energy level, which then returns to a lower energy level and radiates a photon. In the case of a semiconductor, the energy of the radiated photon is associated with the bandgap and other compensating energy levels of the material.

Photon System International (PTI) system is used for obtaining photoluminescence spectra of samples. The schematic diagram of PTI system is shown in Figure 3.15. From an arc lamp, a single wavelength of light is selected by the excitation

monochromator and Xcorr adjusts the horizontal corrected stress. Afterwards, the excitation light travels in the cuvette where the sample under measurement is located. The emitted photons pass through emission monochromator and are captured by photomultiplier detector (PMT). Finally, the data collected is stored in the device.

In order to reduce direct light reflection from the excitation source to the detectors, a homemade jig shown in Figure 3.17 is used for holding the sample under measurement. The plate in the middle holds the sample and the screws on the side are used for tightening the jig to the platform inside the cuvette. Figure 3.16 shows that if the sample is mounted at an angle, direct reflection from the incident light is at an oblique angle not detectable by digital PMT. During measurement, the jig is adjusted at 8° with respect to the incident light. Nevertheless, the emission due to the background, namely the substrate, still needs to be taken into consideration. The difference in intensity of the emission spectra from the sample and the ones due to the background itself is the spectra of the material.

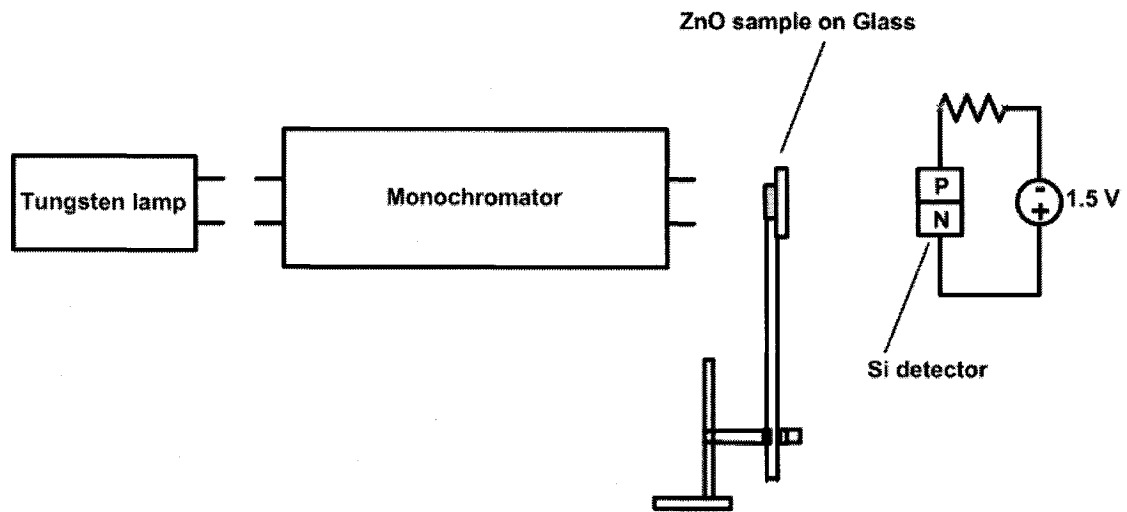


Figure 3.14 Optical transmission setup

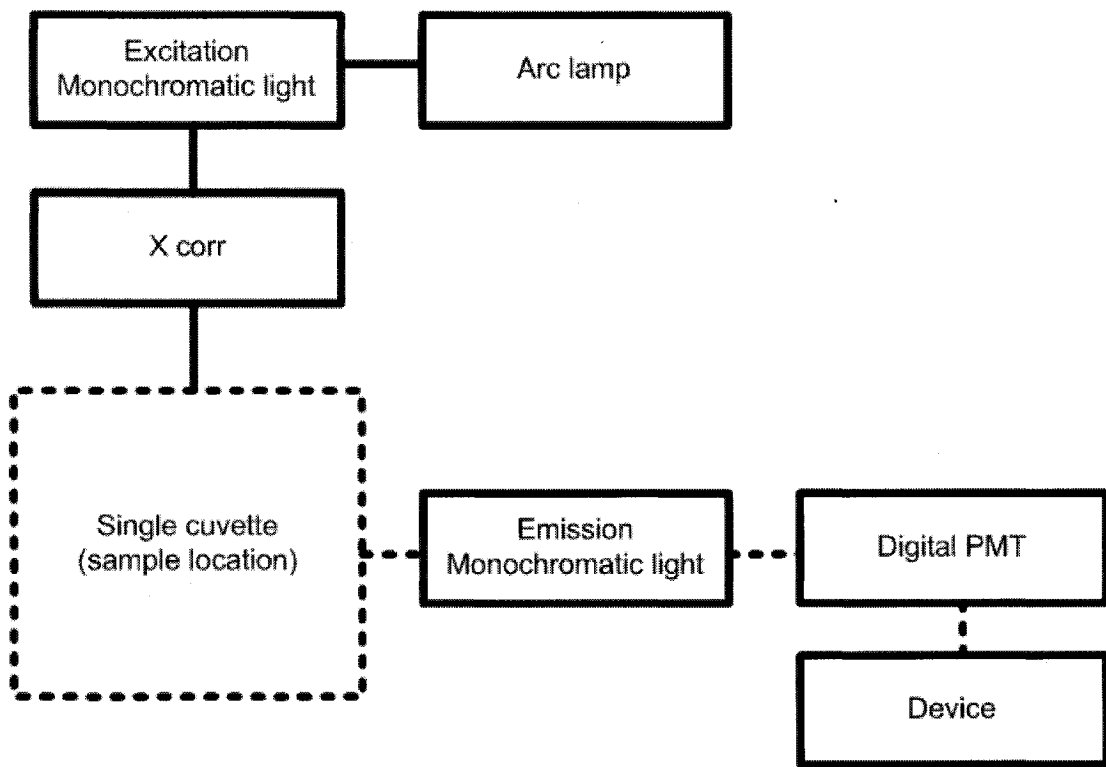


Figure 3.15 A schematic diagram of PTI system

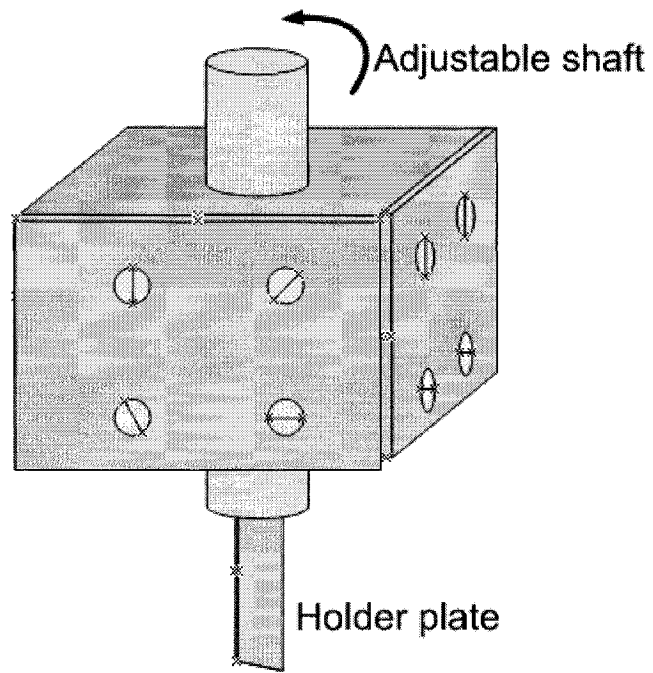


Figure 3.16 Sample holder for photoluminescence measurement

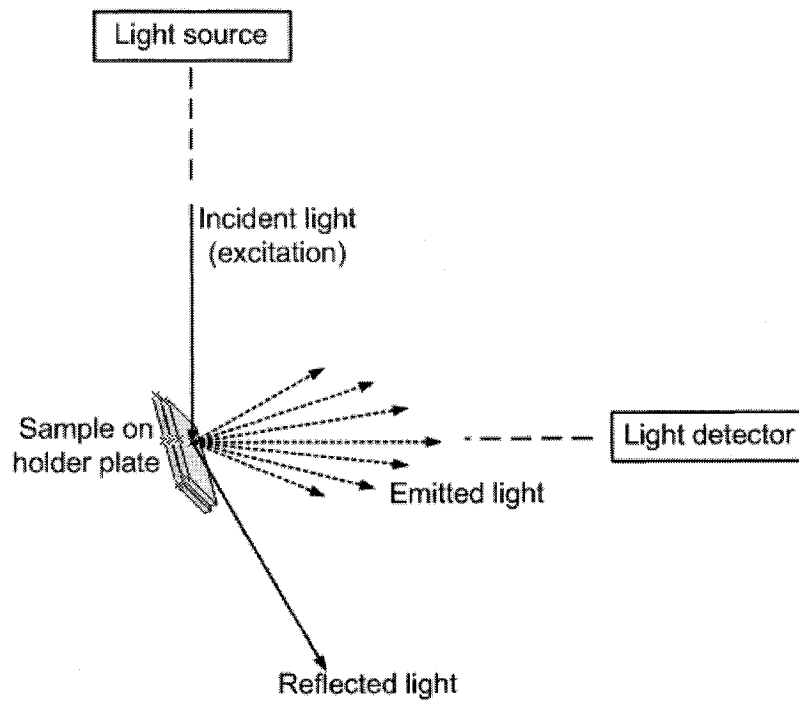


Figure 3.17 Light reflection of a flat surface

CHAPTER 4 RESULTS AND DISCUSSION

4.1 Introduction

During persistent effort in making Metal Insulator Semiconductor (MIS) LED, confined p-type regions of ZnO films on a glass substrate were observed. The MIS device is a “sandwich structure” of Au/i-ZnO/n-Si. The glass substrate served as a shadow mask during sputtering of ZnO material and was subject to several depositions. The performance of the MIS diodes was unstable and randomly showed bright blue, orange and white sparks with high voltage sweeps from 0 to about 100 V. Nevertheless, limited areas showing p-type conduction on the shadow mask were obtained during the experiment. Therefore, two additional runs devoted for reproducing p-type ZnO were carried out and the properties of the films were studied.

The studies of properties of the ZnO films to be described in this chapter are as follows. First of all, results of photoluminescence (PL) of ZnO films deposited on n-type Si and glass substrates will be presented. Analysis of the spectra will help identifying the bandgap energy, the defects levels and the ones due to dopants in ZnO. Once the film has been deposited, hot point probe measurement will be used for identifying the areas with p-type conduction. Afterwards, the optical transmission measurements will be performed at different regions with different conduction types. Hall effect measurements will be done for obtaining the mobility, concentration and sheet resistance at different location on the substrate. Lastly, x-ray diffraction peaks will help the identification of preferred orientation of ZnO crystal at different position. The cross-sections of the ZnO films are examined in SEM for determining the thickness of the samples.

4.2 Photoluminescence spectra of ZnO films

Thin films of ZnO sputtered on either glass or silicon substrates could create a large density of interface states and may have an impact on the crystallinity of ZnO films. Ghosh studied ZnO films grown on Si and glass by x-ray diffractograms and revealed that there are many peaks corresponding to the hexagonal structure [4.9]. Therefore, it is interesting to study photoluminescence spectra at room temperature of ZnO films deposited on glass and Si substrates.

In the present experiments, microscope slides (sodalime glass) and n-type (111) orientated silicon substrates are used. The n-type Si substrates are doped with phosphorous at a nominal concentration of about 10^{15} cm^{-3} . More details about the substrates are available in chapter 2. The main reason to choose silicon substrates is the high melting point, allowing high temperature annealing of the ZnO films. In addition, the bandgap energy of 1.12 eV for Si, which is smaller than ZnO, will allow the photoluminescence spectra of ZnO films to be measured in the short wavelength region without interference from the Si substrate.

The deposition of polycrystalline ZnO films on a low cost substrate such as glass is interesting. However, thin films of good quality can be achieved by increasing the thickness. The first deposited layer often has poor crystallinity and it serves as a buffer layer for subsequent layers. The improvement of crystallinity by increasing the thickness could reduce the recombination centers in the films; therefore, non-radiative

recombination is decreased and radiative recombination is increased [4.10]. It should be pointed out that the PL analysis of ZnO films on transparent glass slides is more difficult because the glass substrate contain various elements, which are photo sensitive and even emissive to UV light. Therefore, PL response of ZnO samples must not contain the background contribution due to substrate. Figure 4.1 shows the PL spectra of clean and uncoated glass substrate.

4.2.1 Photoluminescence spectra of ZnO films (Single deposition)

4.2.1.1 Deposition conditions of ZnO films on silicon

The conditions for the deposition of intrinsic ZnO films are given in Table 4-1. The adoption of sputtering gas containing oxygen makes the deposited ZnO films highly resistive [4.11]. In the present experiments, a two-stage deposition scheme has been adopted: first at 10 mtorr for 30 mins and then at 5 mtorr for another 8.5 hrs without breaking the vacuum. The Si wafers are two inches wide and the target to substrate distance is 3.5 cm. After the deposition, the samples are cut into pieces with dimensions of about 2 x 1 cm.

Table 4.1 Deposition conditions for ZnO film on Si

Substrate(s)	Target	Distance between Subst. - Target	Working gas (x:y)	Power	Substrate heating	Total chamber pressure	Time
Silicon	Undoped ZnO	3.5 cm	Ar : O ₂ 0.73 : 0.27	60 W	No	10 mTorr	30 mins
						5 mTorr	8:30 hours

4.2.1.2 PL spectra of as-deposit ZnO on Si

The excitation wavelength of the incident monochromatic light is set at a wavelength of about 300 nm for the PL experiments. In order to extract the PL spectra due to the ZnO thin films, the PL spectra are first measured on the Si substrate without ZnO and even the sample holder. Figure 4.1 shows PL spectra taken from a Si substrate, a stainless steel sample holder and an as-deposited ZnO films on Si. It is noted that both the Si and stainless holder plate show low PL intensity in the wavelength range from 350 to 550 nm. The PL spectrum of the sample holder plate is measured because excitation light can penetrate glass substrate and reach the sample holder plate.

When excited with a 300 nm incident light, the as-deposited ZnO thin films shows a weak PL response, but with a low intensity. However, weak peaks at about 400, 430 and 475 nm are visible from Figure 4.1 for the as-deposited ZnO. These present results are consistent with the work performed by Maenhout-Van der Vorst and Van Craeynest who also reported weak photoluminescence from as-deposited films grown using white powder ZnO [4.1]. The interface states or dislocations of ZnO lattice created near the surface of Si may have greatly affected the crystal structure of the as-deposited ZnO material. As a result, the crystalline structure of ZnO has to be improved.

4.2.1.3 Thermal annealing of ZnO films on Si

As-deposited ZnO films on silicon were observed to have very weak photoluminescence response and the hexagonal structure of sputtered ZnO may have many orientations as suggested by Ghosh [4.9]. In order to enhance the crystallinity, heat

treatment is performed in a three-zone furnace in our laboratory in an attempt to improve the crystal structure and reduce the defects in ZnO material. However, the glass substrates could not sustain high temperature annealing and only the ZnO films deposited on Si are subject for investigation. The annealing experiments are performed in oxygen and air at an atmospheric pressure with different temperatures for various periods of time. With the excitation wavelength set at 300 nm, the PL spectra of the ZnO films on Si substrates annealed in oxygen and air at 400, 600, 800, 1000 and 1100°C are shown in Figures 4.2 and 4.3. Significant increase in the PL intensity is evident after annealing and is stronger as annealing temperature increases. It is noted that annealing at low temperatures below 400°C has insignificant change in the PL spectra.

In general, ZnO samples annealed in air show lower PL intensity than the ones annealed in oxygen at the same temperature. The highest photoluminescence intensity is observed for the sample annealed at 1100°C for one hour in oxygen as shown Figure 4.2. Figures 4.4 and 4.5 show that the PL spectra of films annealed at 1100°C for slightly different times hour have limited impact on the PL intensity.

4.2.1.4 Analysis of the PL spectra of the annealed ZnO films

The PL of the annealed ZnO samples at 1100°C shows a greater intensity response than the ones heat-treated at lower temperature in both oxygen and air ambient. Figure 4.2 shows the PL spectra for several samples annealed at different temperature. It is seen that no significant increase in PL intensity when treated at 400, 600, and 800°C.

However, the PL intensity increases significantly for those annealed at 1000 and 1100°C. The increase in temperature promotes sharper and more noticeable energy peaks.

As shown in Figure 4.2, the emission spectra of the annealed ZnO have noticeable peaks at about 390, 460 and 500 nm, which corresponds to violet, blue and green luminescence, respectively. These results are consistent with the observation of Kang et al. [4.4], who have reported similar emission peaks for their ZnO films on sapphire (Al_2O_3) substrate. It is noticed that sapphire is a good substrate choice for ZnO due to good lattice matching at the interface, but it is expensive. Although still not understood completely, the peak near 390 nm is believed to be due to the free excitons of ZnO material [4.2]. In other words, PL peak at 390 nm corresponds to the anticipated 3.37 eV bandgap energy of ZnO. The peak near 460 nm is probably due to zinc interstitials, which is one of the native defects in ZnO. The calculated defect level for zinc interstitials is at 2.9 eV [4.3]. Lastly, the peak near 500 nm is believed to be due to oxygen defects. The other defects related to oxygen are vacancies, interstitial and antisite of which the calculated defect levels are at 1.62, 2.28 and 2.38 eV respectively [4.30].

It is observed that the intensity peak due to oxygen defects is more intense in the ZnO sample annealed in air at 1100°C than the one annealed in oxygen. Incorporation of oxygen in ZnO films could have been easier if samples are annealed in oxygen than in air. Therefore, annealing in oxygen could reduce the defects due to oxygen and result in a lower intensity peak near 500 nm.

Figure 4.4 presents PL spectra for the samples annealed 1100°C for different periods of time. In particular, samples annealed for more than 1 hour have reduced PL intensity. Furthermore, in our experiments, the ZnO films showed visible degradations and turned greyish if annealed above 1000°C for one hour. Some pictures shown in Figure 4.6 are taken from the ZnO thin films annealed at different temperatures showing degradations. Pictures 5, 6, 7 and 8 illustrate visible fringes still present in the samples annealed at 1100°C. Picture 9 shows that the annealed film turned completely greyish after four hours at 1100°C. Ko and coworkers observed similar phenomenon and suggested that the ZnO molecules tend to migrate from higher energy surface to more stable energy site during annealing at high temperature [4.5]. Another research group suggested that there was formation of SiO₂ in the ZnO due to interdiffusion of molecules at the interface when annealed at high temperatures [4.8]. In other words, annealing temperature needs to be controlled in order to reduce the migration of molecules when Si substrates are used.

4.2.2 Photoluminescence spectra of ZnO films (Multiple deposition)

4.2.2.1 Annealing of ZnO films on glass substrates

Another approach for improving the crystal structure of sputtered ZnO films is to increase the thickness of the film. The deposition experiments with the increased thickness are done on glass substrates. Furthermore, the influence of positions of the substrates with respect to the target center is specially examined. As mentioned before, the first layer to be deposited would serve as a buffer layer for reducing interface states

and improving the crystallinity of the subsequent ZnO material sputtered. The deposition conditions (deposition 1-4) used in this study have been listed in Table 2.8 in chapter 2.

To investigate the effect of thickness, PL spectra of selected samples are measured after each deposition while the remaining samples are kept in vacuum before the next deposition. After the first and second deposition, no significant PL intensity is detected for the selected ZnO samples on glass substrate. The PL spectra of the selected ZnO films after the third deposition are shown in Figures 4.10 and 4.11 and those after the fourth deposition are shown in Figures 4.12 and 4.13. It is noticed that the PL is more than double in both cases. The substrate holder and the projection of the target and the location of the samples are shown in Figure 4.7. The ZnO sample No. 2 is the one located at a position 2.5 cm from the center of the substrate, whereas the ZnO sample No. 3 is the one located at 5.0 cm from the center of the substrate. From Figure 4.8 a) and Figure 4.9 a), it is seen that the sample No. 2 is more yellowish than sample No. 3 after four depositions. Furthermore, one could observe that the fringes in sample 3 are still visible.

4.2.2.2 PL spectra of the multi-layers ZnO films

For the sample No. 3, the PL spectrum is very weak and not measurable by the equipment after all four depositions. However, in the case of sample No. 2, a spectrum with weak intensity is measured and obtained after third deposition as shown in Figures 4.10 and 4.11. Figures 4.11 and 4.12 show that after the fourth deposition, the intensity peaks become more distinguishable and sharper than the ones after the third deposition. Therefore, it is believed that the crystallinity of ZnO has improved with the increase of

thickness. The dominant peaks are located around 467 and 531 nm, which correspond to zinc and oxygen interstitial, respectively according to the defect energy levels studied by Yang et al. [4.30]. In comparison with Figure 2, the peak at 390 nm is still not detectable. Nevertheless, the films sputtered from undoped ZnO target after four depositions will be the buffer layer for the doped ZnO.

4.2.2.3 Photoluminescence spectra of doped ZnO films

Starting with the samples coated with four intrinsic ZnO depositions, more layers of ZnO are deposited from the doped target for studying the PL spectra. In order to deposit doped ZnO material, doped ZnO targets and N-Ar working gases are used. The deposition conditions (deposition 5-8) are listed in Table 2.8.

After the fifth deposition, both samples No. 2 and No. 3 still do not show detectable emission. One possible reason is degradation of the lattice structure after deposition of the ZnO fifth layer from a different target. In the case of sample No. 3, no detectable luminescence is measured after the fifth, sixth, seventh and eighth deposition even though one can see a thick ZnO film on the substrate as shown in Figure 4.9 b). The PL analysis becomes fairly difficult in the case of sample No. 2 because the film on that sample start peeling off. The peeling off becomes more severe as the deposition layer increases. Photograph of the sample No. 2 after the eighth deposition has been taken and is shown in Figure 4.8 b). Due to the degradation of the film, it is necessary to analyze and study another area located at 2.5 cm from the center of the substrate with no visible damage or degradation. Two more samples are studied after eight depositions, namely

sample No. 1 and No. 1A. Both samples are located at 2.5 cm from the center of the substrate. The PL spectra of both samples are similar and the ones for sample No. 1 are shown in Figures 4.14, 4.15 and 4.16.

4.2.2.4 Analysis of the photoluminescence spectra of the multi-layers doped ZnO films

Sample No. 1 is a piece of doped ZnO film deposited on a buffer layer and located at 2.5 cm from the center of the substrate with no visible damage after the eighth deposition. The analysis of the peaks locations in such a sample will help identify whether the dopants are successfully incorporated in the ZnO film. Figures 4.15 and 4.16 show that the defect peaks at 467 and 531 nm described earlier are still present after eight depositions, but there is another dominant peak located at around 350 nm. This dominant peak is believed to be due to nitrogen dopant, suggesting that the incorporation of nitrogen dopants in the ZnO films is successful. Toumiat et al have reported similar experiments carried out with nitrogen doping [4.6]. They observed that the peak due to excitonic emission of ZnO at 377 nm has shifted to around 350 nm when the film is doped with nitrogen. Although not completely understood, they speculated that there is formation of ZnO nanorods or nanowires, which could have modified the ZnO grain structure and affected the “surface excitons”.

Furthermore, an additional peak around 660 nm is noticed in sample No. 1. This peak is probably due to indium dopant since the doped ZnO target contains a small weight percentage of In_2O_3 (see chapter 2 for more details). Work done by Kumar et al. revealed PL results similar to the ones observed in sample No. 1 [4.7]. Furthermore, they

also suggested that the broad emission spectrum is probably due to phonon-assisted emission.

In summary, it is worthwhile to restate the purpose of having multiple layers. A thick buffer layer for ZnO films is formed on the substrate after four depositions for reducing the lattice mismatch. Furthermore, the crystalline structure of the buffer layer is improved showing the peaks due to excitons and defects. The crystallinity of doped ZnO films deposited on the buffer should be better and make the incorporation of the dopants in the film easier. After eight depositions, the PL spectra of ZnO show the presence of energy peaks attributed to the dopants, which coincides with others' results.

4.3 Optical transmission of the ZnO film after eight depositions

The optical transmittance versus wavelength of ZnO films after eight depositions is shown in Figure 4.17. Measurements are done at room temperature for the ZnO films with no visible damage, namely the ones at 1.0, 2.5 and 5.0 cm away from the center and the sample numbers corresponding to these samples are 5, 1 and 3, respectively. Notice that the transmittance of ZnO films at the center of the target is the same as the ones located at 1.0 cm away from the center. For comparison, optical transmission measurements of films sputtered using doped and undoped ZnO targets after one deposition are also included. The interval of the monochromatic light source is between 400 and 800 nm.

The thickness of ZnO films after eighth deposition is determined by examining the cross-sections of the films in SEM and they are 3.0, 5.0 and 1.5 μm for the films located at 1.0, 2.5 and 5.0 cm from the center of the substrate, respectively. This variation in thickness is due to the difference in magnetic field of the sputtering gun, which has ring shape magnet and the details are presented in the next section. The transmission spectra of a typical p-type film are located at 1.0 and 2.5 cm away from the center. The mapping of p-type and n-type ZnO by hot probe after eight depositions is also shown in the next section.

At 2.5 cm from the center of the substrate, the film is about 5 μm thick and the transmittance for the film is small at short wavelengths as shown in Figure 4.17. Only about 5% of light passes through the film at 400 nm. The transmittance response slowly

increases until 625 nm to 80% and saturates onwards. The conduction of the film at 5.0 cm away from the center of the substrate is n-type and shows higher transmittance through the whole measurement. The difference in the spectra is probably due to the variation in thickness of the films at different position of the substrate. The response obtained at 1.0 cm from the center of the substrate shows that the transmittance at low wavelength is between the “thin” and “thick” ZnO films. At 1.0 cm from the center, the thickness is about 3 μm and some layers of ZnO films peeled off during deposition, which is smaller than 5 μm but bigger than 1.5 μm .

The results obtained from the optical transmission measurements are quite consistent with the theoretical prediction. In chapter 2, Yamamoto’s co-doping model suggests that the bandgap energy of ZnO should decrease if the dopants are successfully incorporated [4.13, 4.14]. The A-D-A model indicates the appearance of the energy levels due to dopants should reduce the bandgap energy. In our measurements, the transmission spectra of the typical p-type film (at 2.5 cm from substrate center) almost completely cut light at 400 nm (~ 3.10 eV). In the case of undoped ZnO film, the cutoff wavelength should be located nearby the bandgap energy of the material [4.12].

Futsuhara et al. carried out zinc oxynitride experiment and observed that the optical bandgap of ZnO could decrease significantly with the increase of nitrogen partial pressure during sputtering [4.23]. They believed that the decrease in bandgap energy is probably caused by decrease of ionicity due to formation of Zn-N bonds.

Furthermore, the films sputtered from undoped ZnO and doped ZnO after only one deposition are also shown in the Figure 4.17 for comparison. Samples No. 6 and 7 are ZnO films sputtered at 2.5 cm from the center of the substrate after one deposition from undoped and doped targets, respectively. The thickness is about 0.3 μm for both films and the hot point probe test showed n-type conduction. Optical transmission measurements show that the transmittance is higher than the ones deposited after eight depositions through almost the entire range.

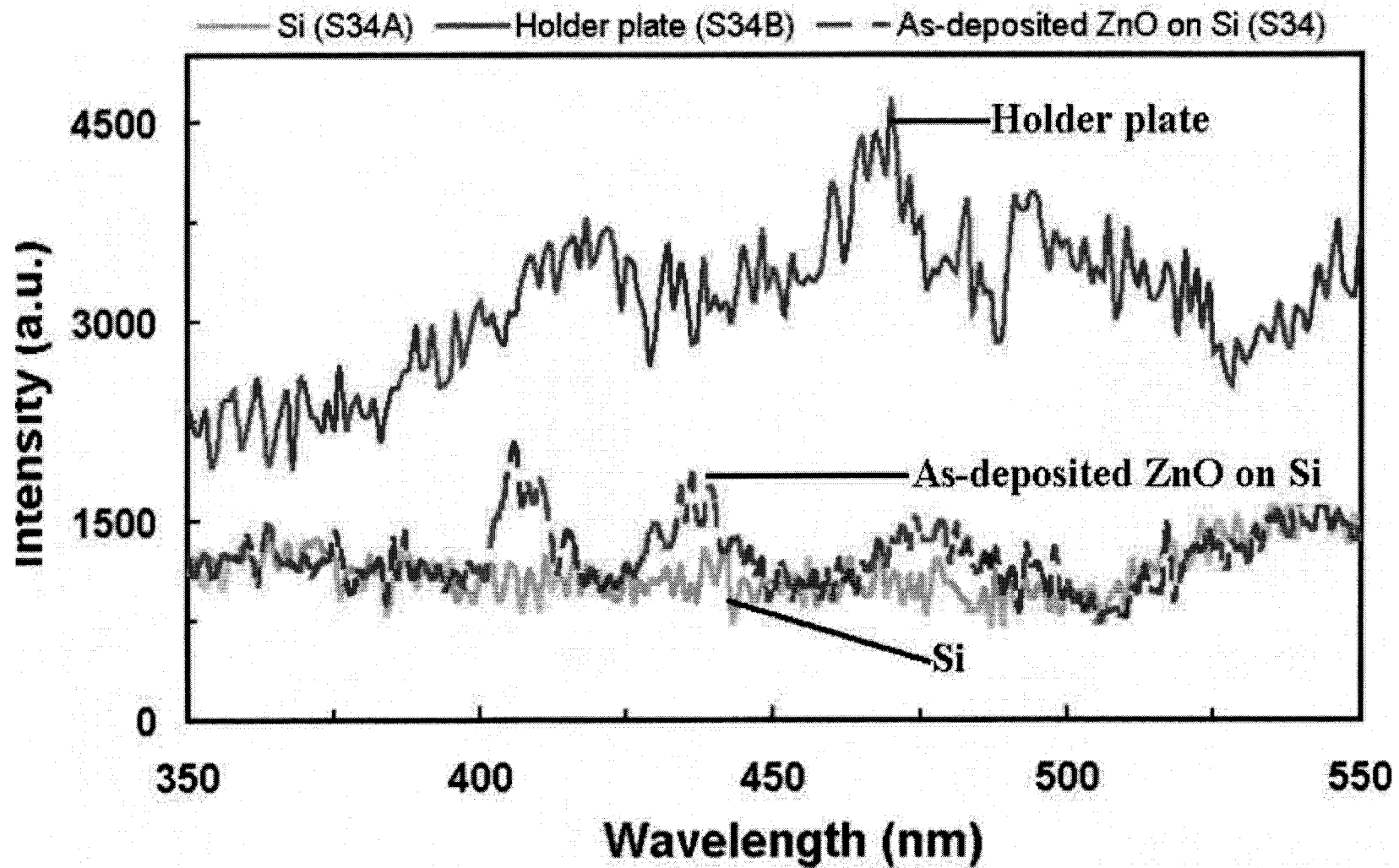


Figure 4.1 Photoluminescence response of silicon, holder plate & as-deposited ZnO film on Si (Excitation wavelength = 300nm)

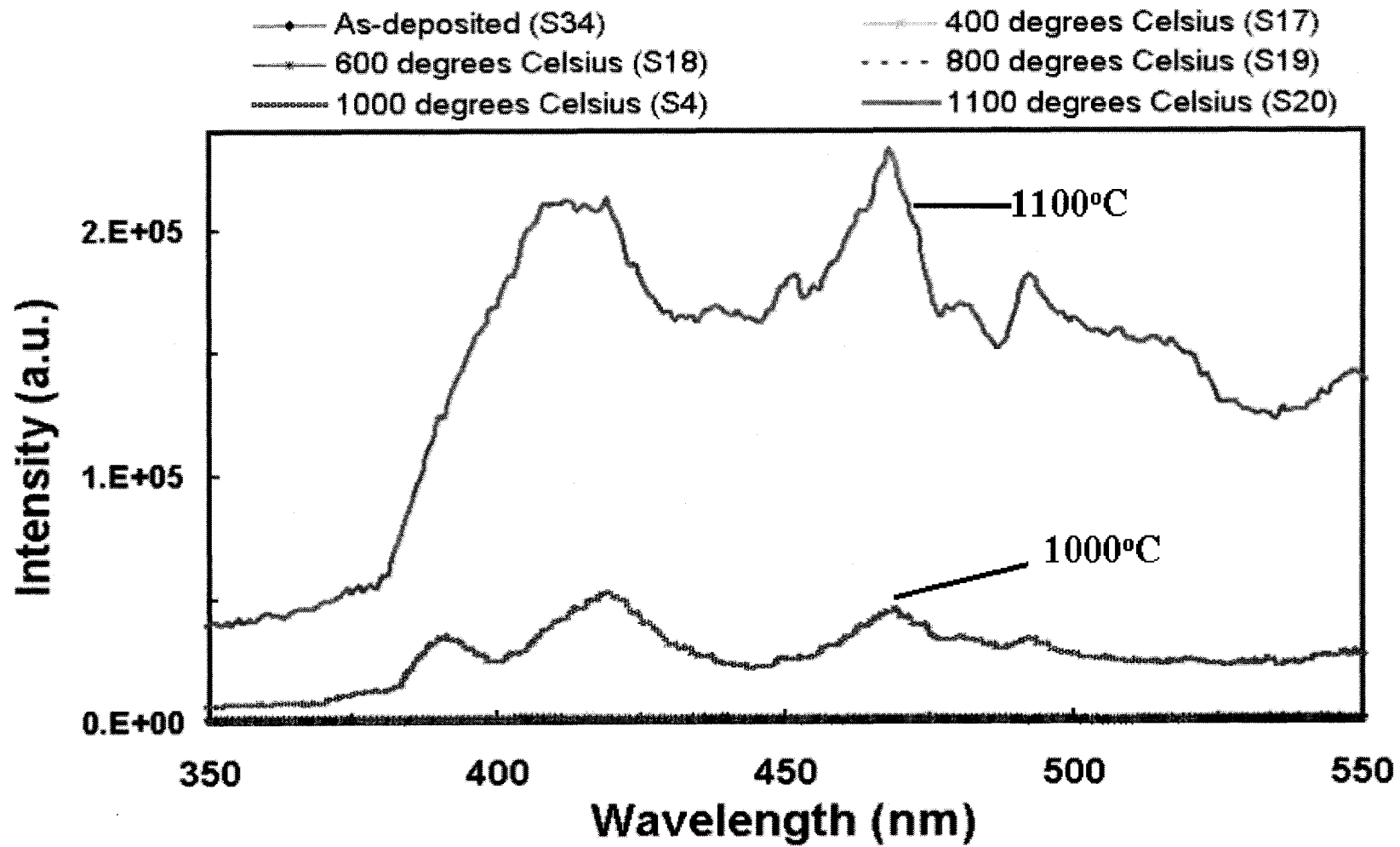


Figure 4.2 Photoluminescence responses of ZnO films on Si annealed for 1 hour in OXYGEN (Excitation wavelength = 300nm)

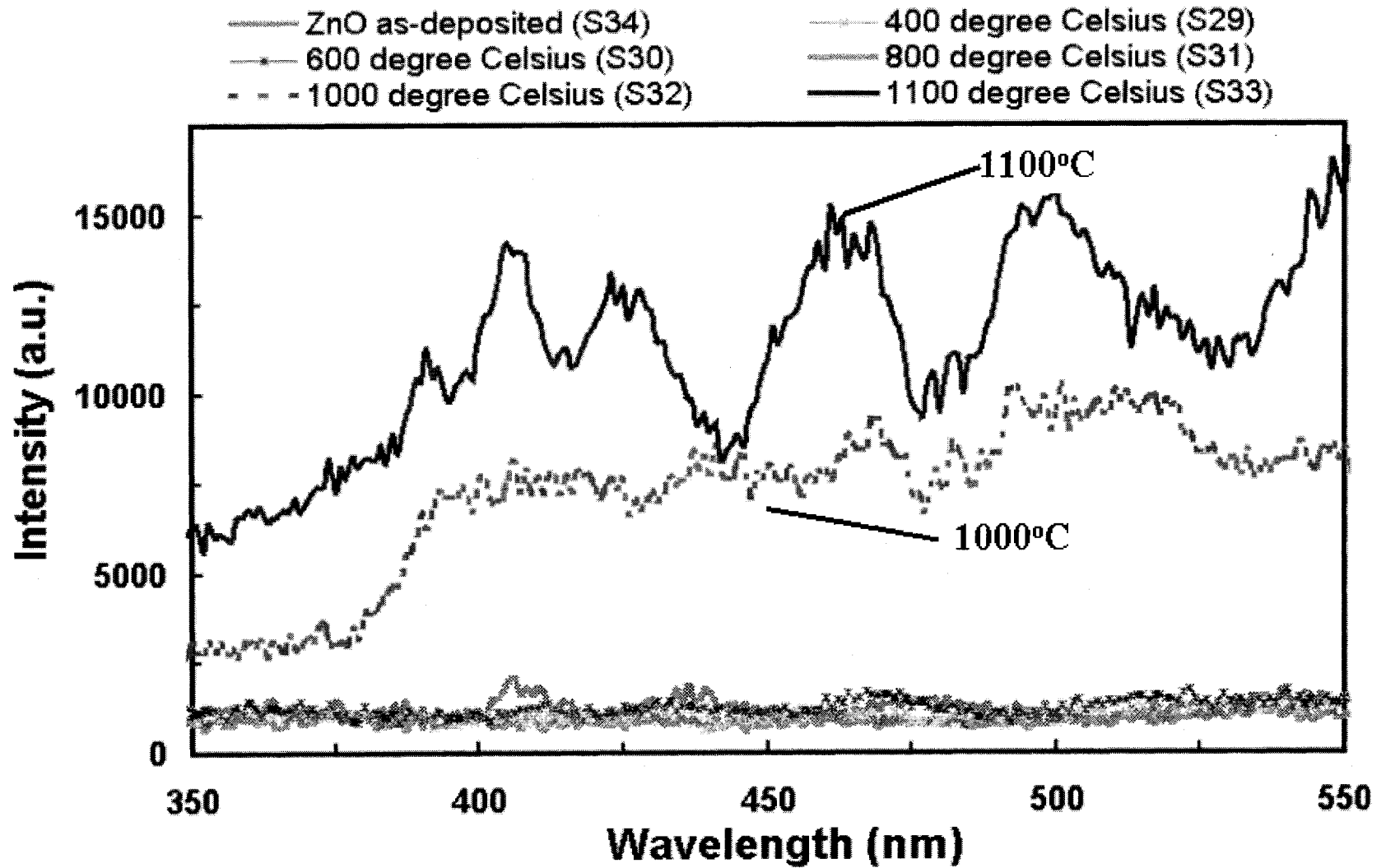


Figure 4.3 Photoluminescence responses of ZnO films on Si annealed for 1 hour in AIR (Excitation wavelength = 300nm)

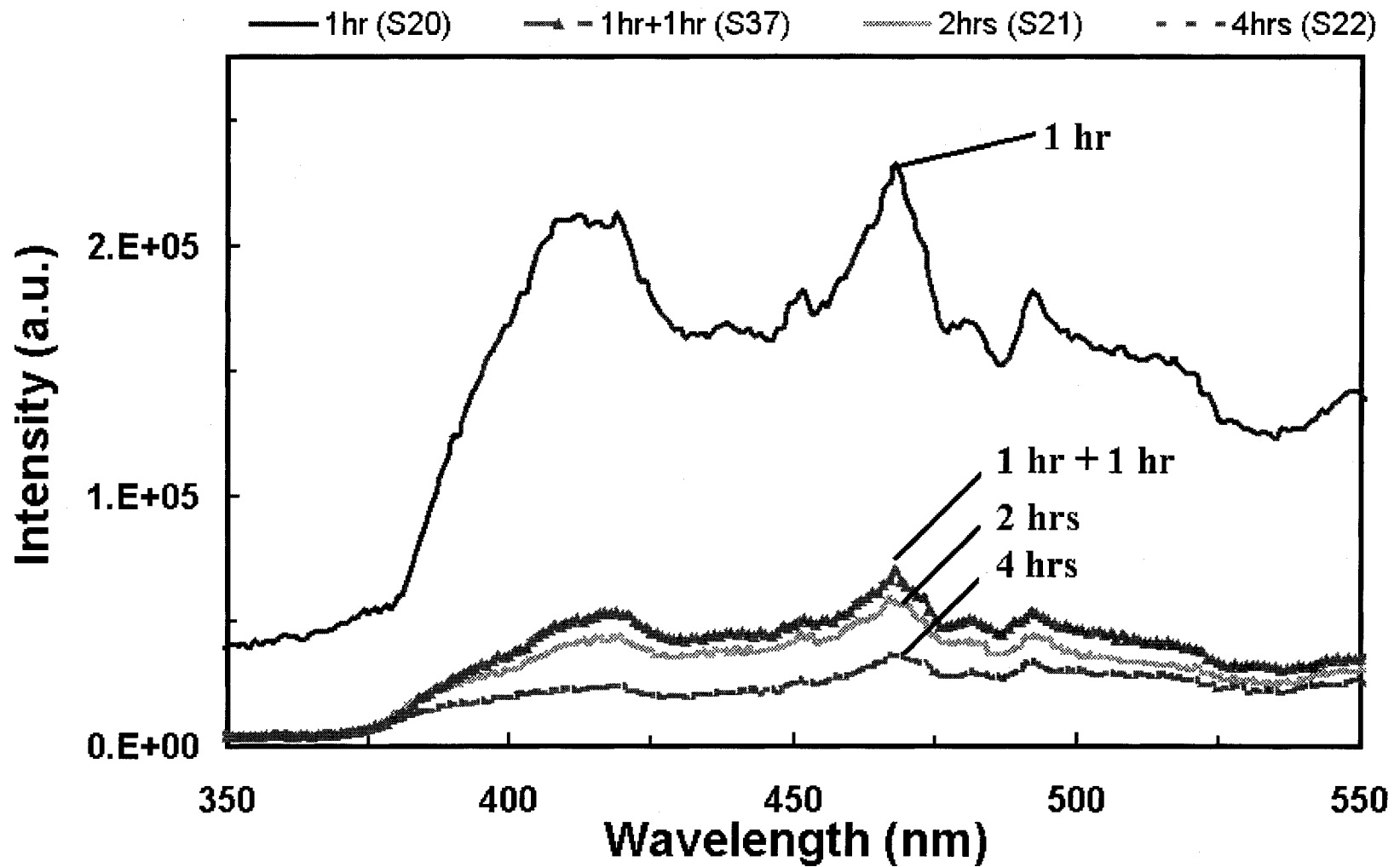


Figure 4.4 Photoluminescence responses of ZnO films annealed at 1100°C for more than 1 hour in OXYGEN (excitation = 300nm) - "1hr + 1hr" indicates that the particular sample is heat-treated two times each for one hour

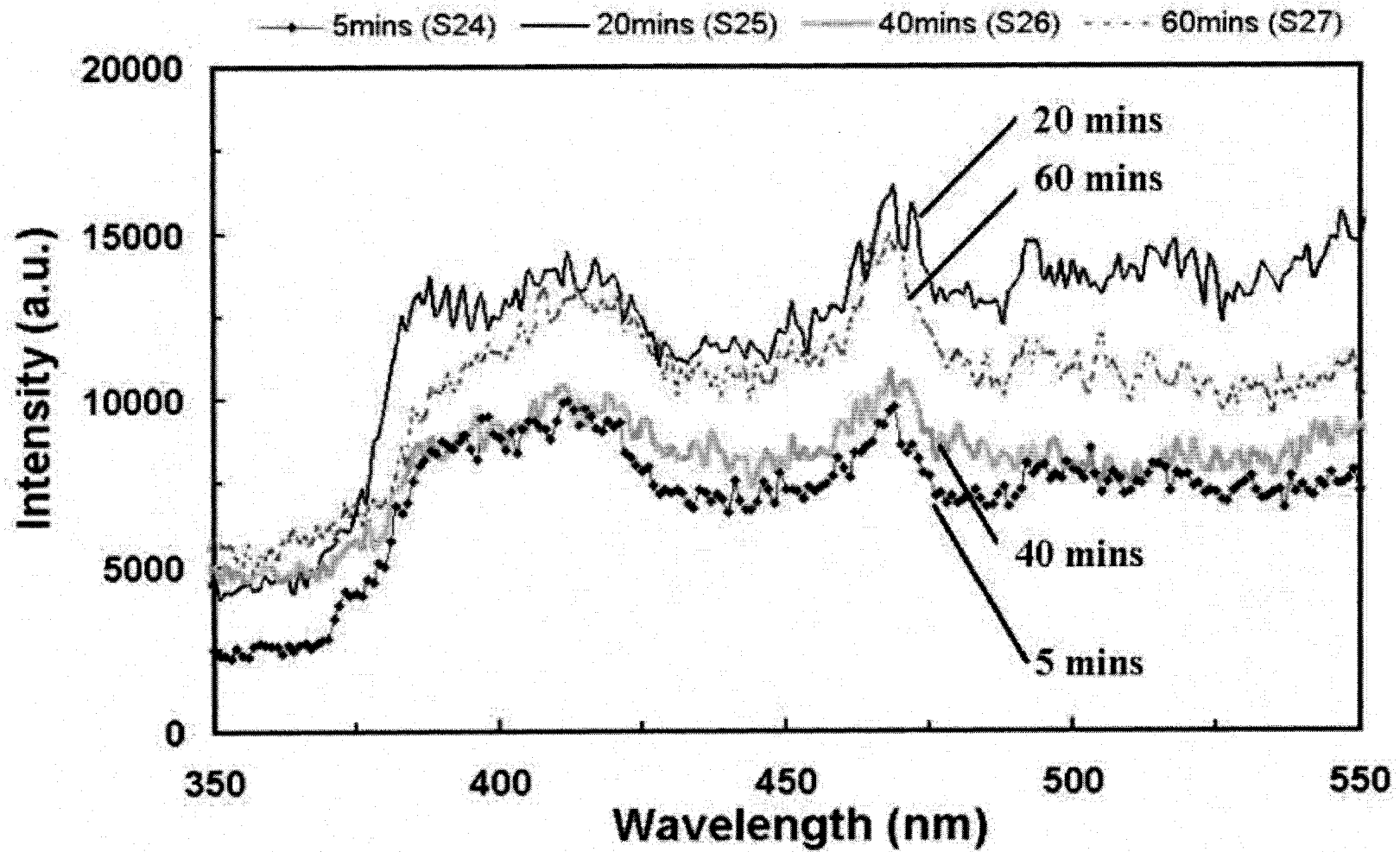


Figure 4.5 Photoluminescence of ZnO films on Si annealed at 1100°C in OXYGEN (excitation = 300nm)

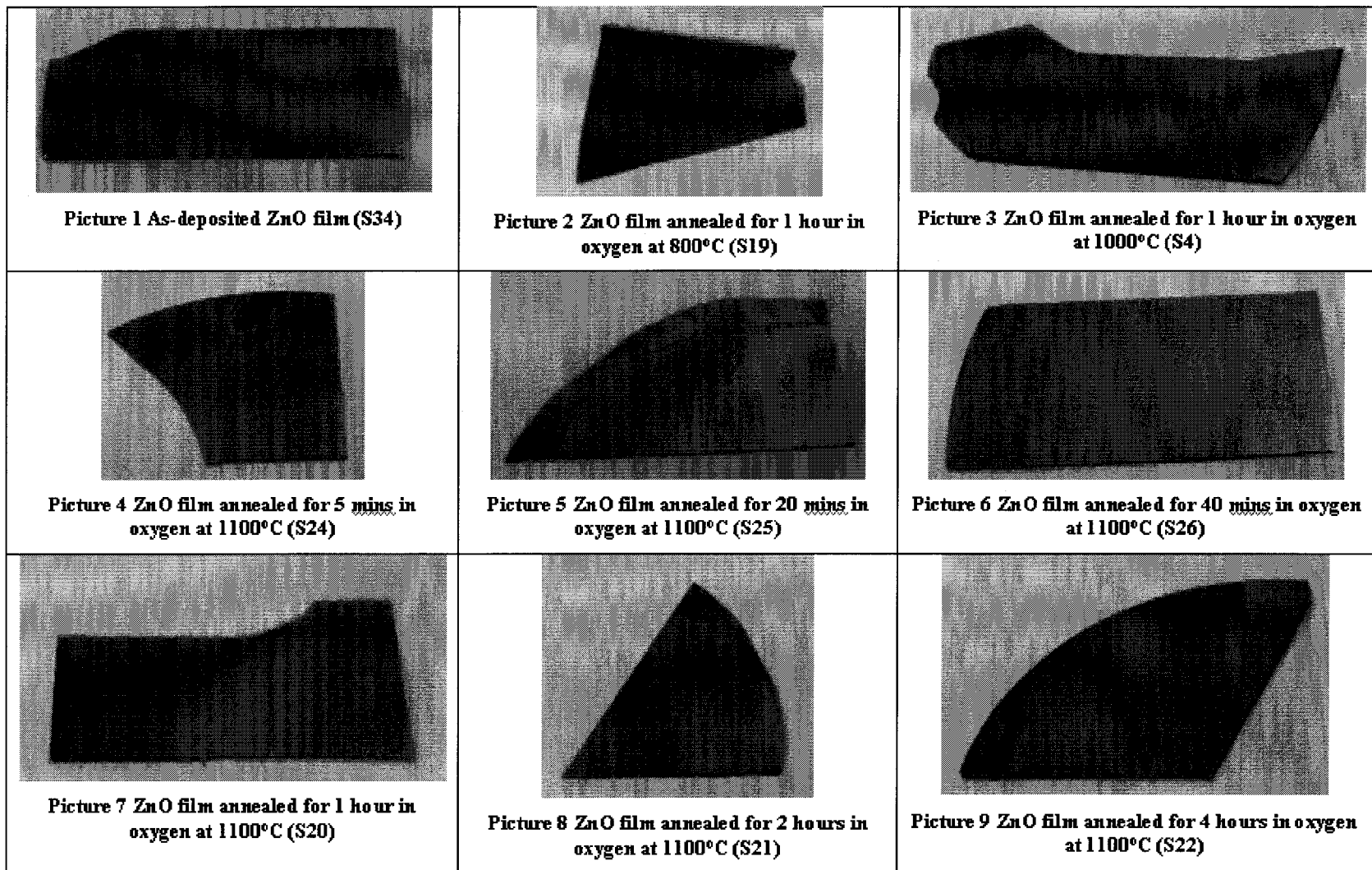


Figure 4.6 ZnO films on Si with different annealing time

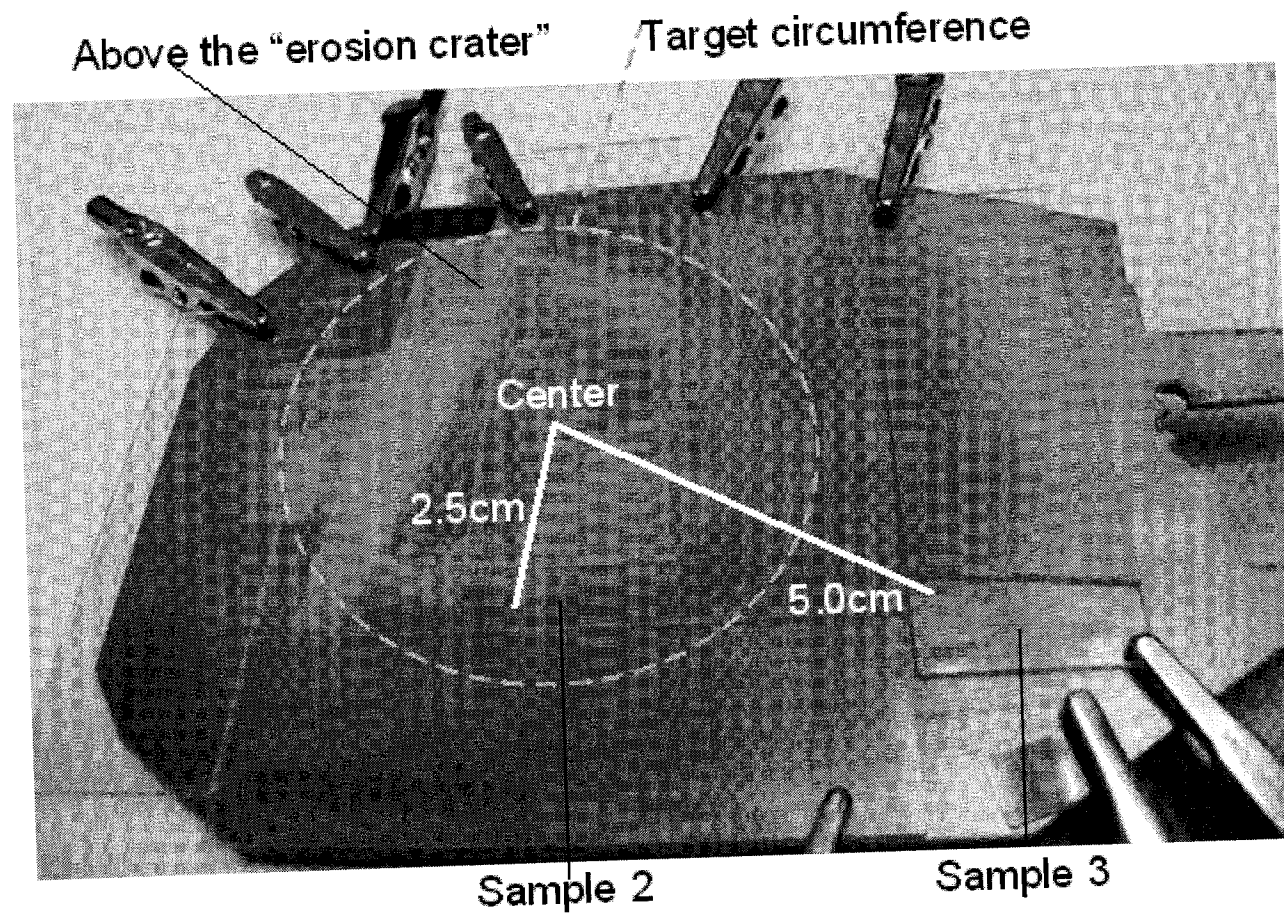


Figure 4.7 ZnO samples on the substrate holder after four depositions

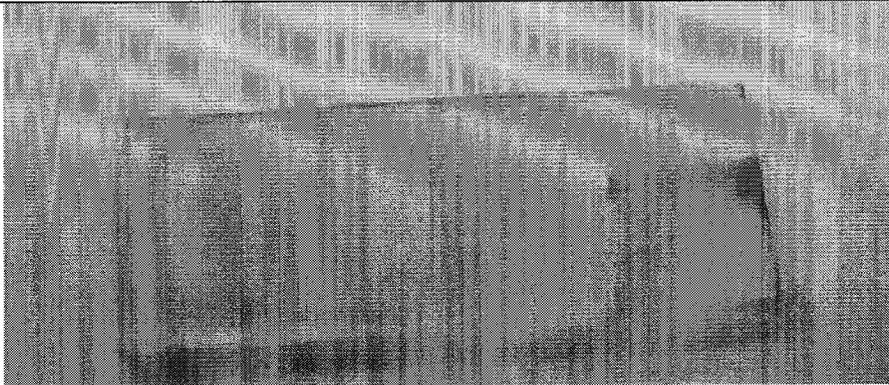


Figure 4.8 a)

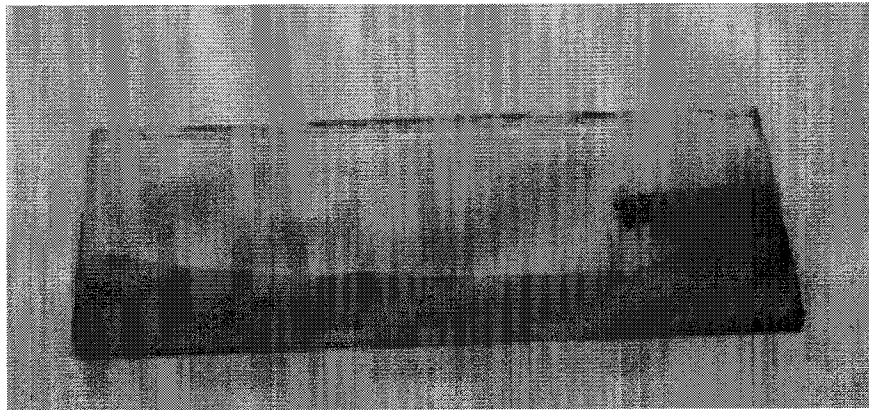


Figure 4.8 b)

Sample 2:

Figure 4.8 a) ZnO sputtered on glass after 4 depositions
Figure 4.8 b) ZnO sputtered on glass after 8 depositions

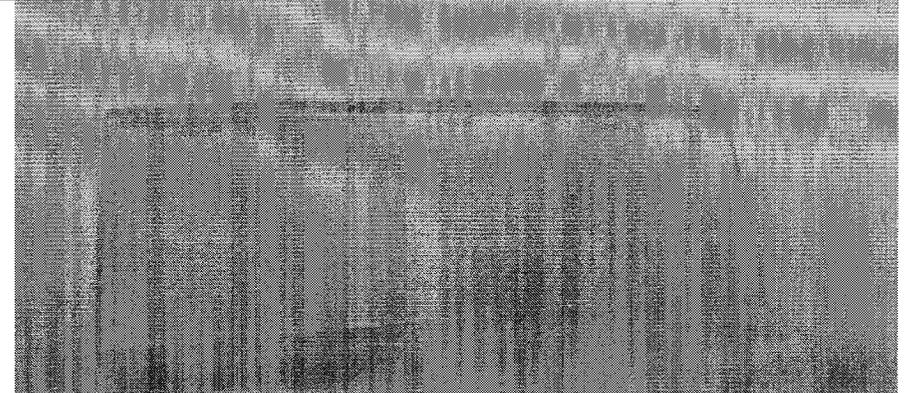


Figure 4.9 a)

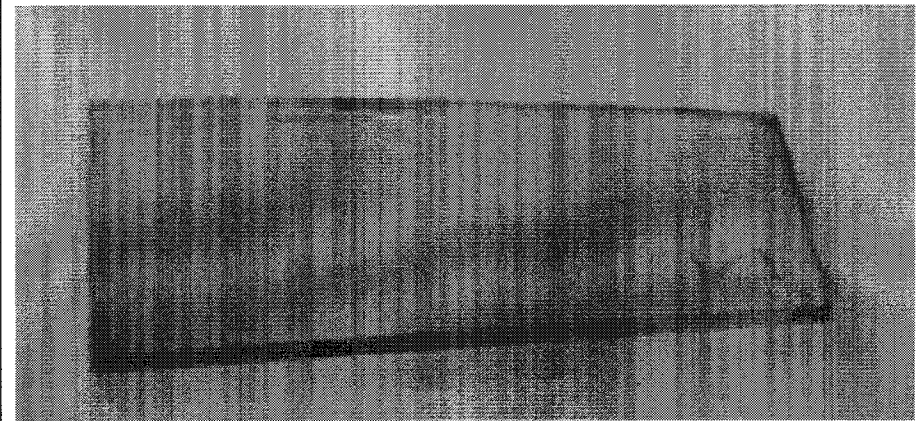


Figure 4.9 b)

Sample 3:

Figure 4.9 a) ZnO sputtered on glass after 4 depositions
Figure 4.9 b) ZnO sputtered on glass after 8 depositions

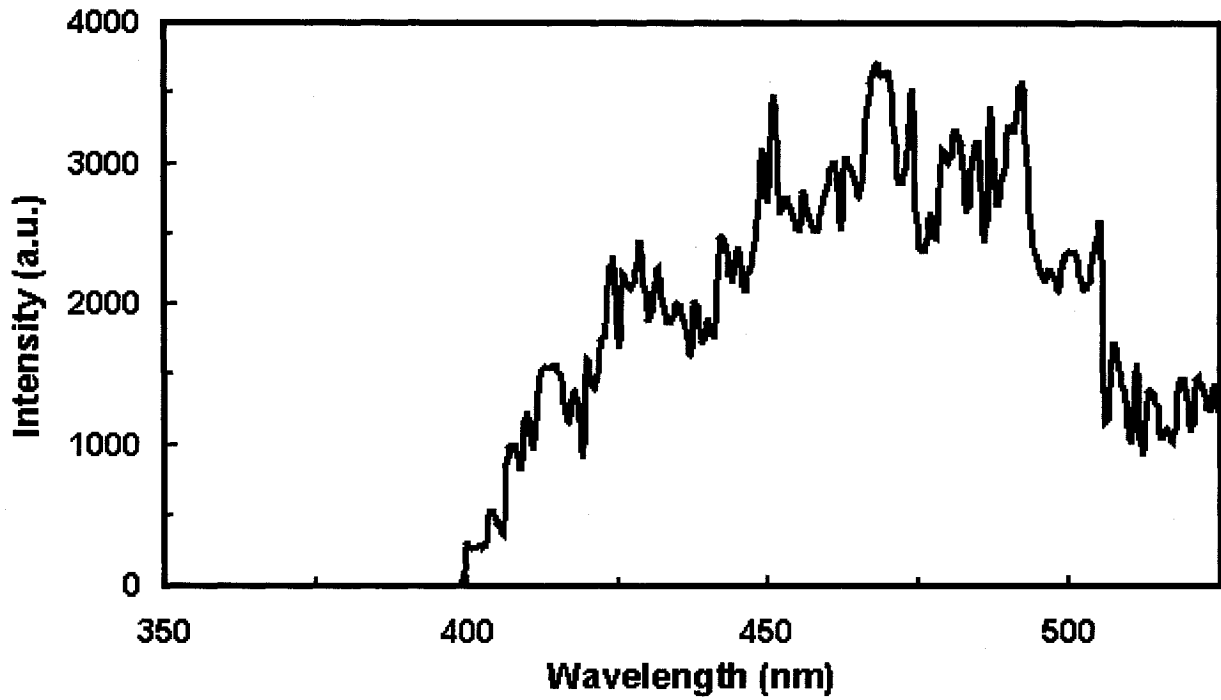


Figure 4.10 PL of sample 2: ZnO on glass - three depositions - Excitation 285 nm

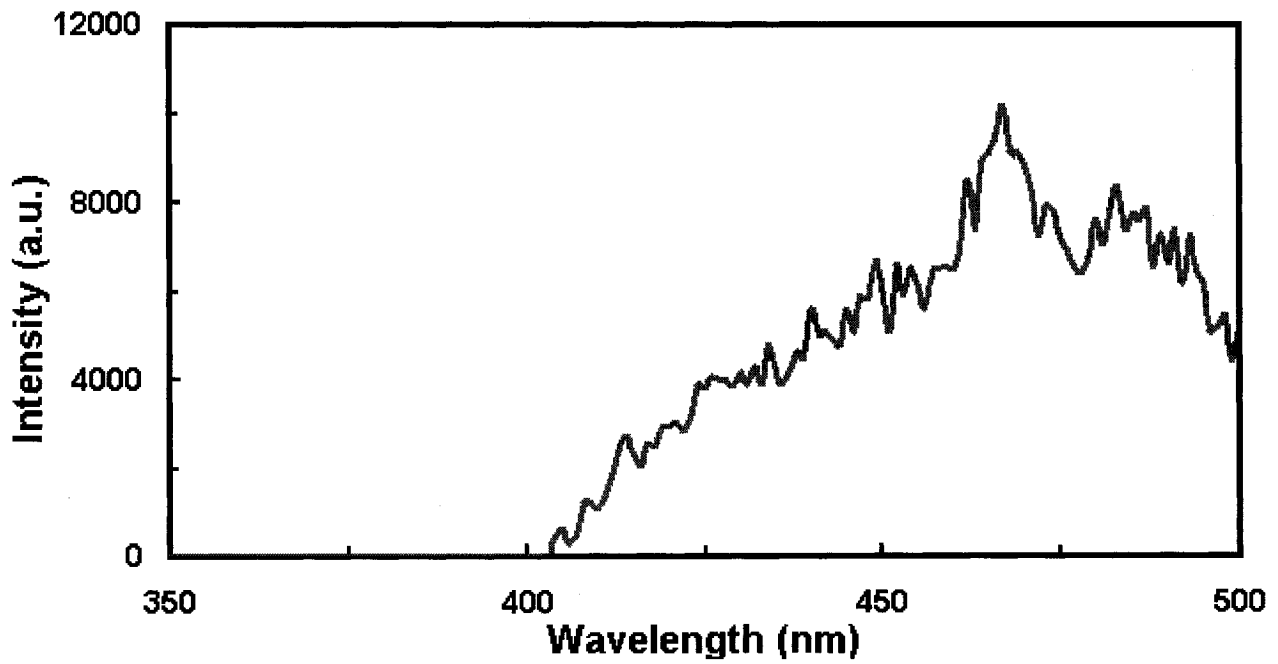


Figure 4.11 PL of sample 2: ZnO on glass - four depositions - Excitation 285 nm

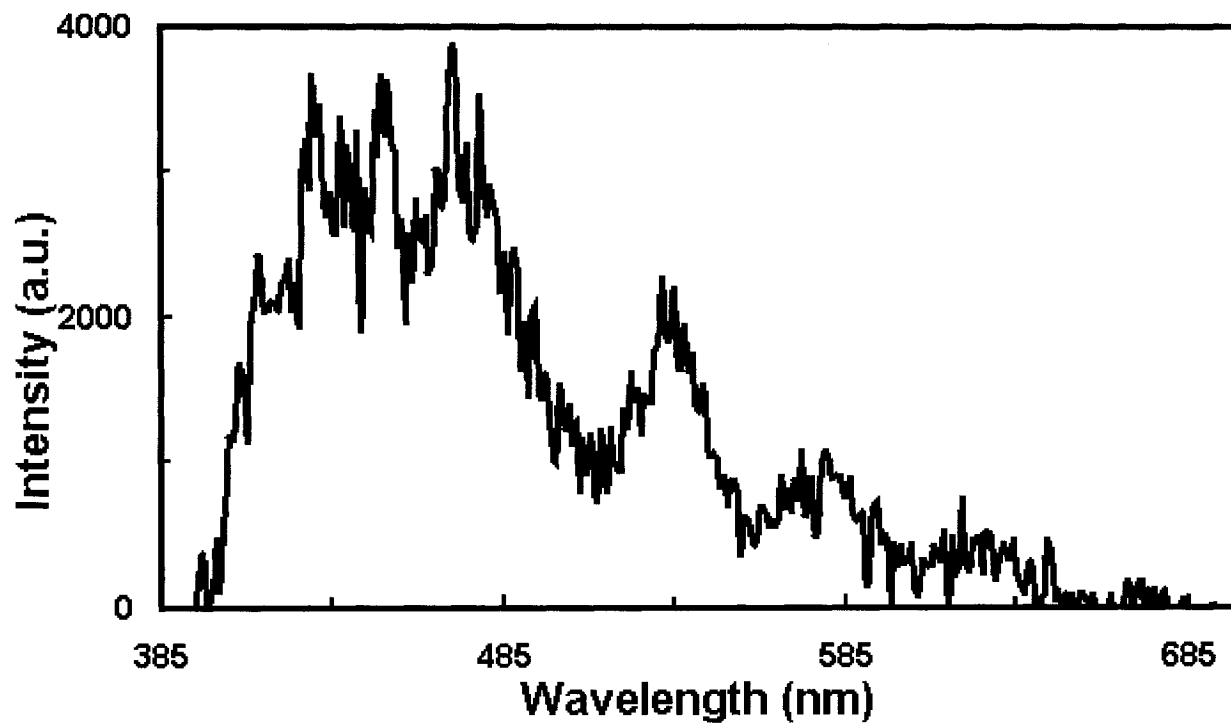


Figure 4.12 PL of sample 2: ZnO on glass - three depositions - Excitation 369 nm

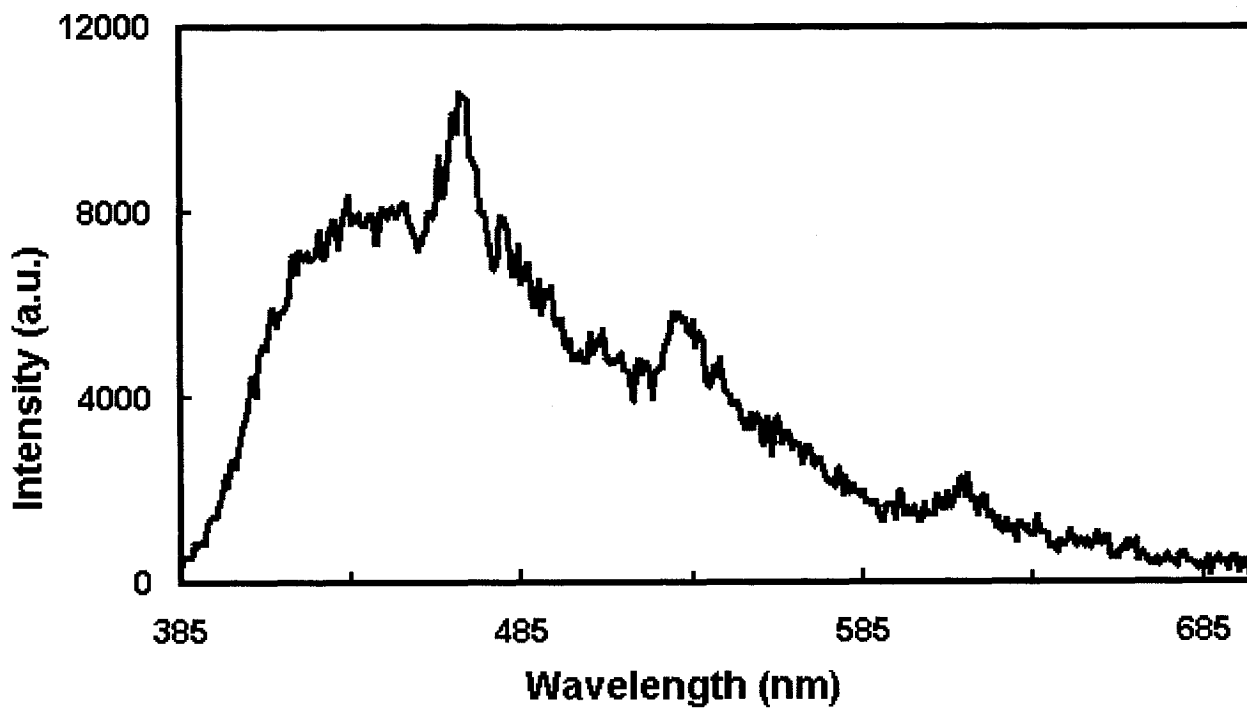


Figure 4.13 PL of sample 2: ZnO on glass - four depositions - Excitation 369 nm

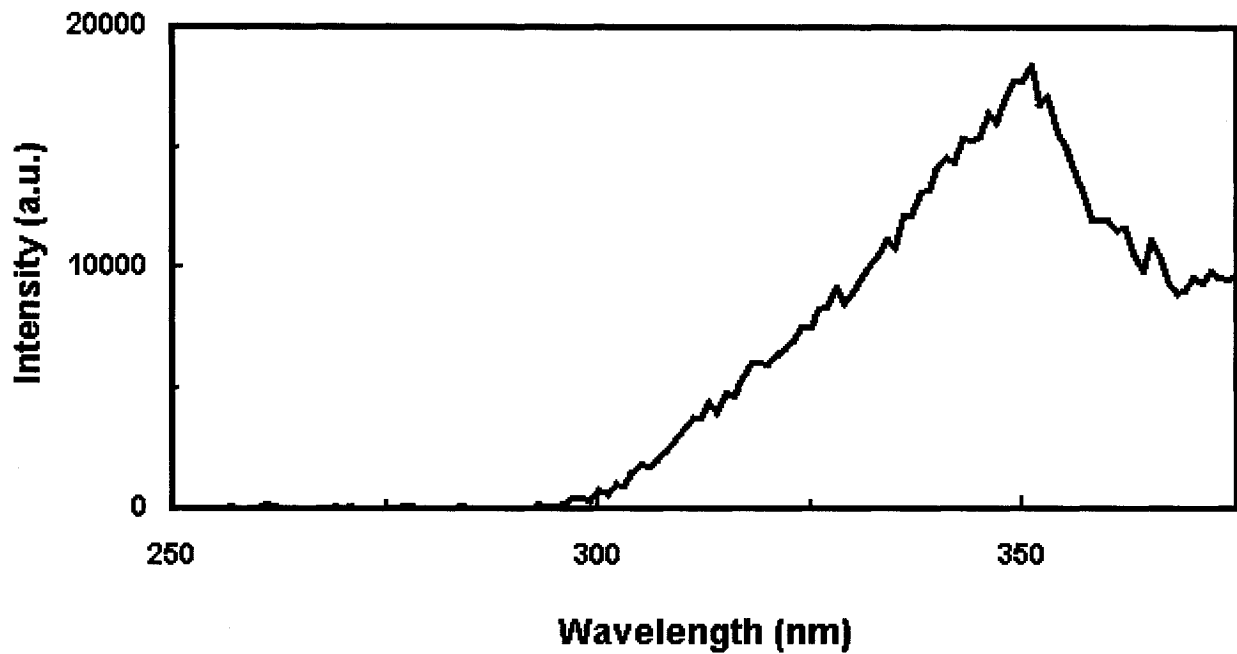


Figure 4.14 PL of sample 1: ZnO on glass - eight depositions - Excitation 200 nm

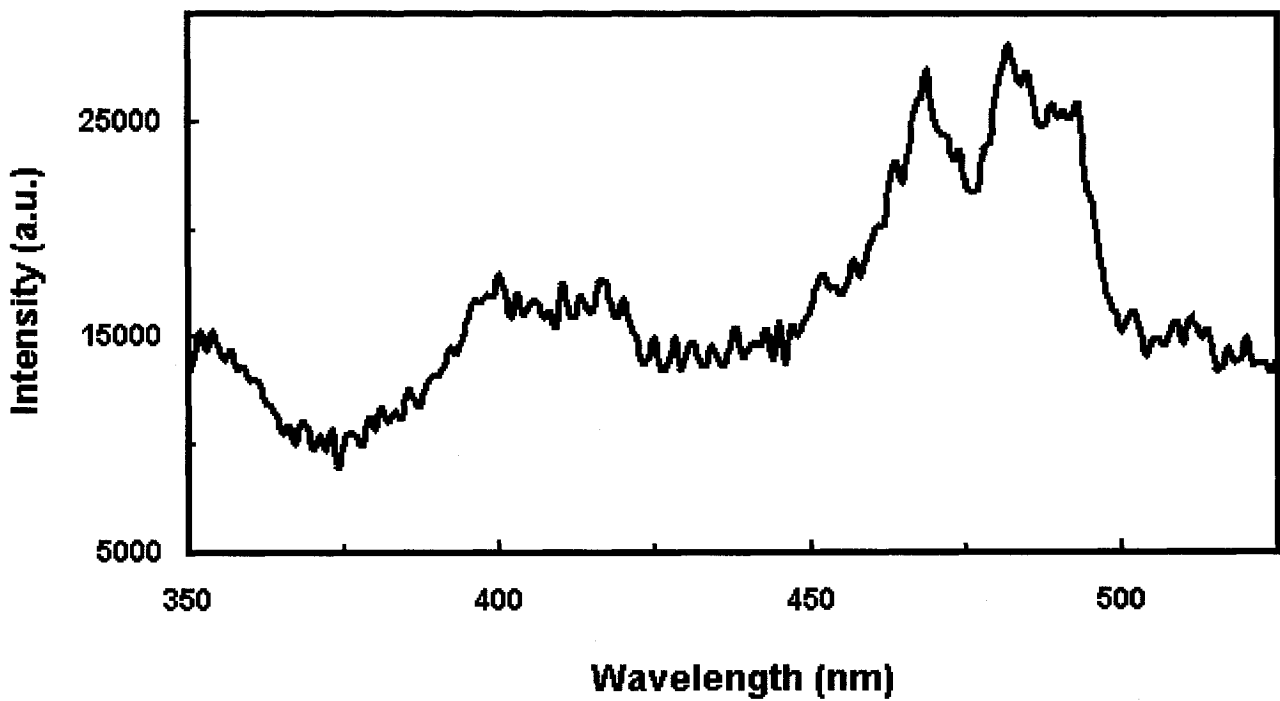


Figure 4.15 PL of sample 1: ZnO on glass - eight depositions - Excitation 285 nm

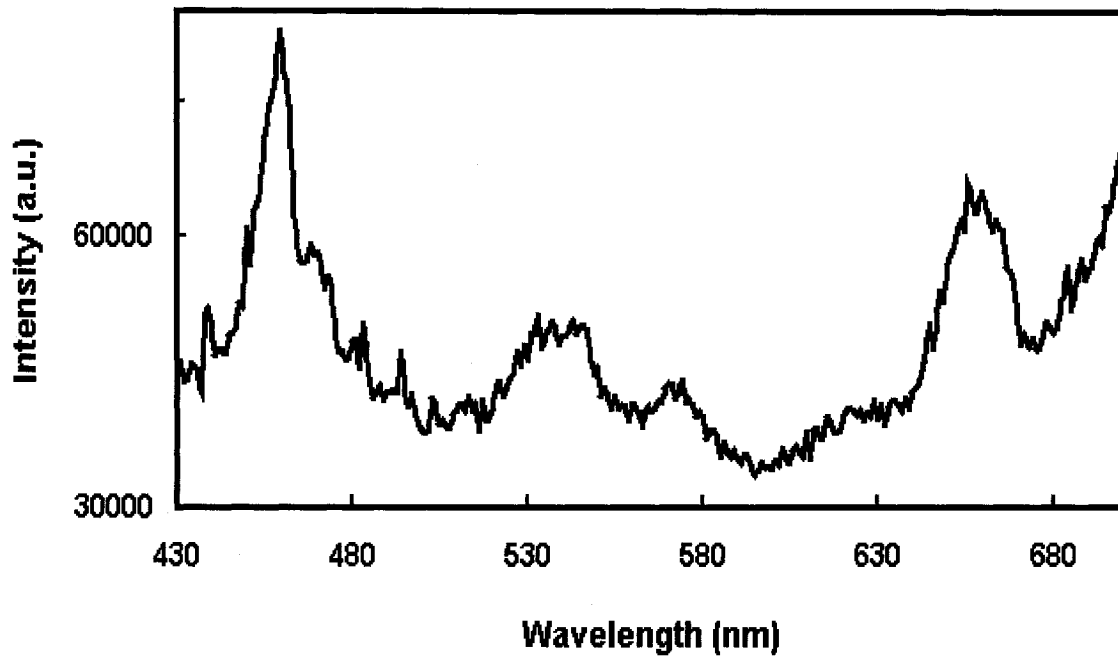


Figure 4.16 PL of sample 1: ZnO on glass - eight depositions - Excitation 369 nm

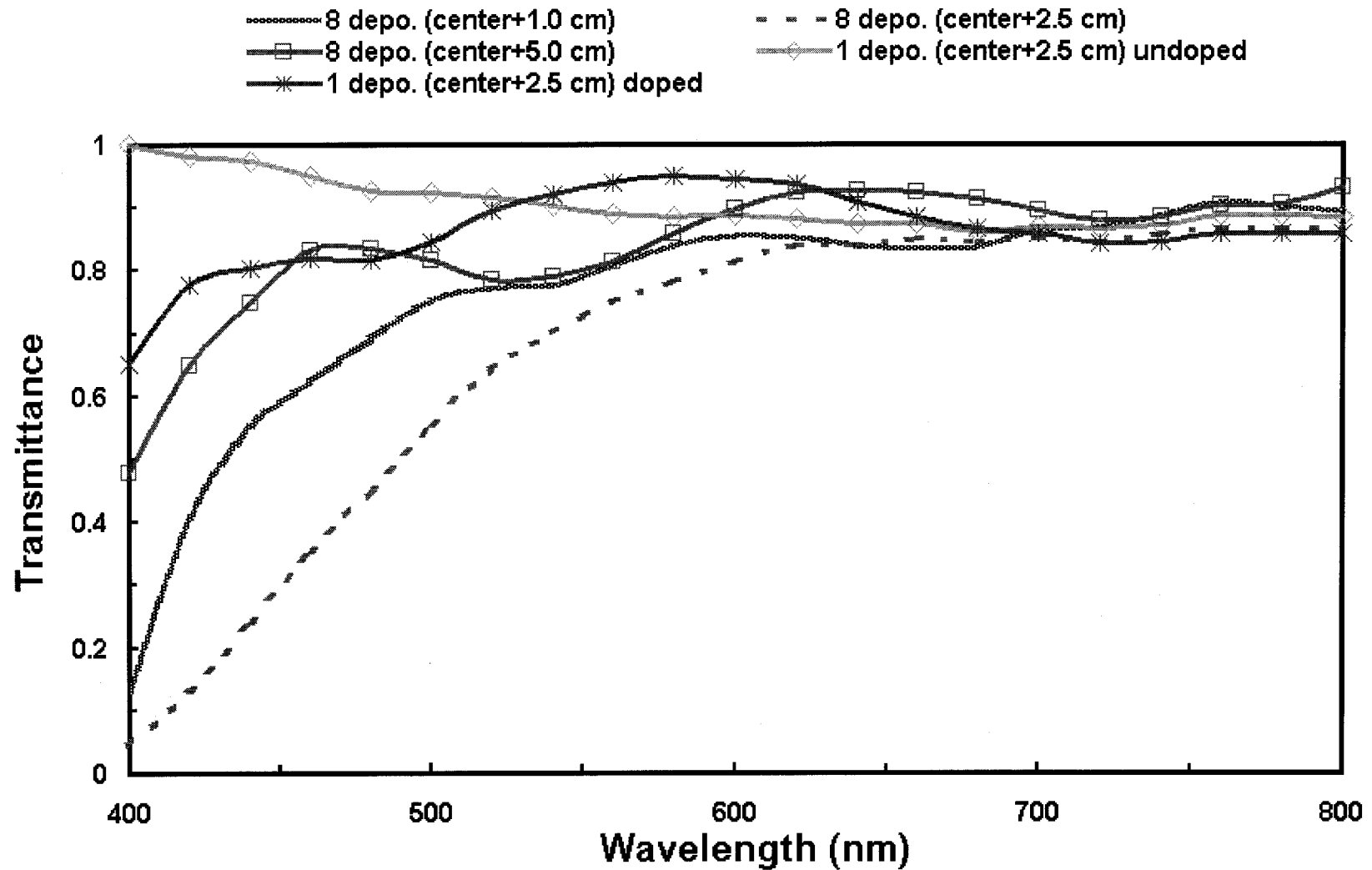


Figure 4.17 Optical transmission of ZnO after 8 depositions

4.4 Mapping of limited p-type ZnO film areas after eight depositions

4.4.1 Identification of limited p-type ZnO film area

After the eighth deposition, some layers of ZnO films near the center of the substrate peeled off, but the color of the remaining film is still uniform. The layers of ZnO films located far away from the center of the substrate have no visible damage and the fringes are still visible. In order to map the limited p-type film areas on the entire substrate, hot point probe measurements are performed with the probes kept as close as one millimeter. During the measurements, the temperature of the hot probe increases to about 150°C. The confined p-type areas on the samples are shown in Figures 4.18 and 4.19. Figure 4.18 is the shadow mask used during the deposition of ZnO for MIS diode. The minus sign indicate a deficiency of majority holes, which corresponds to a negative reading on the voltmeter during the measurement and vice-versa. Figure 4.19 shows the limited p-type ZnO film areas after eight depositions (first run reproduction) with broader substrate surface. The p-type ZnO films seem to be local and situated near the center and on the boundary of the regions where some layers of film peeled. The dimensions of the p-type ZnO films are in the order of about 5 mm and 2 mm at 1.0 cm and 2.5 cm from the center, respectively.

4.4.2 Explanation for formation of non-uniform sputtered films

Several previous experiments were performed for understanding the non-uniformity in sputtered ZnO. Song et al. studied aluminum doped ZnO sputtered on glass and noticed the films are laterally non-uniform [4.15]. By setting the deposition

conditions such as rf power, working gas pressure, substrate temperature and substrate-target distance fixed, they noticed that the thickness, resistivity, crystallinity and optical transmittance of the films are dependant on the positioning of the substrate with respect to the center of the substrate. Moreover, there is a report suggesting that a surface barrier created by chemisorption of oxygen onto the surface of crystallites can act as scattering and trapping centers, which can also reduce the effective mobility of the film [4.17].

Song et al. also observed the presence of inhomogeneous erosion of the target material where there is formation of circular erosion crater resulted from higher material consumption during sputtering. Figures 4.20 and 4.21 give the cross-sectional view of a model showing the formation of erosion crater in the target after deposition. The films formed right above the erosion crater ring tend to be thicker because as the deposition time increases, the material in the target is consumed more resulting in a deeper and wider erosion crater. Consequently, the lateral distribution of the plasma and the sputtering rate are different at different position in reference to the target; therefore, Song et al. believed that the thickness is maximal at the center of the substrate. The thickness of the sputtered films will differ and the properties of the films would differ with position causing non-uniformity.

Minami et al. performed X-ray diffraction analysis on their thin films and found that the crystalline structure of the film facing the erosion crater is different from the one not directly facing the erosion crater [4.16]. They believed that the thermal heating is higher at that region due to higher ion bombardment and could have altered the

crystalline structure. Thomann et al. suggested that the substrate surface during sputtering at low pressure is subject to high energetic species in the plasma and to UV irradiation. In their experiments, they believed that the flux is highest (about 10^{14} at/cm² s) and carry large energy ions in the order of 10s of eV near the center of the substrate, which can affect the growth of the material and may break the growing clusters [4.18]. Although not clearly understood, in our experiments, the peeling-off of the films near the erosion crater after eight depositions could also be due to high thermal heating and high energetic bombardment on thick layers of ZnO.

In our experiments, non-uniform conduction type of the ZnO films on the same glass substrate is noticed. The formation of p-type films seems to reside near the erosion crater where the deposition rate is faster resulting in higher thermal heating of the sputtered ZnO. Outside of the erosion crater, the films are n-type. In the following section, the electrical properties of the films obtained from Hall Effect measurements will be described.

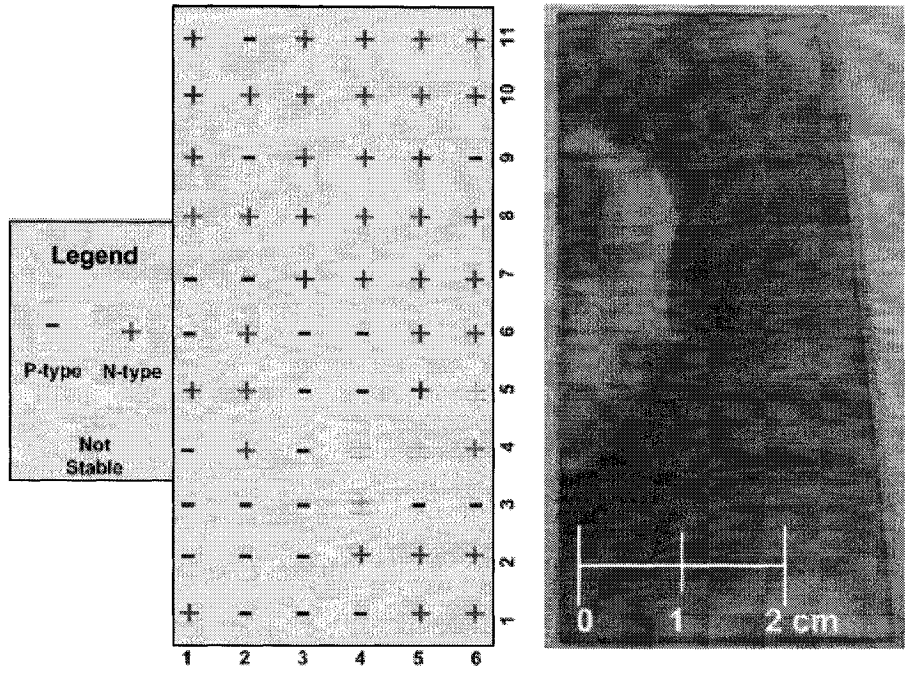


Figure 4.18 ZnO on a shadow mask after multiple depositions used in MIS experiment

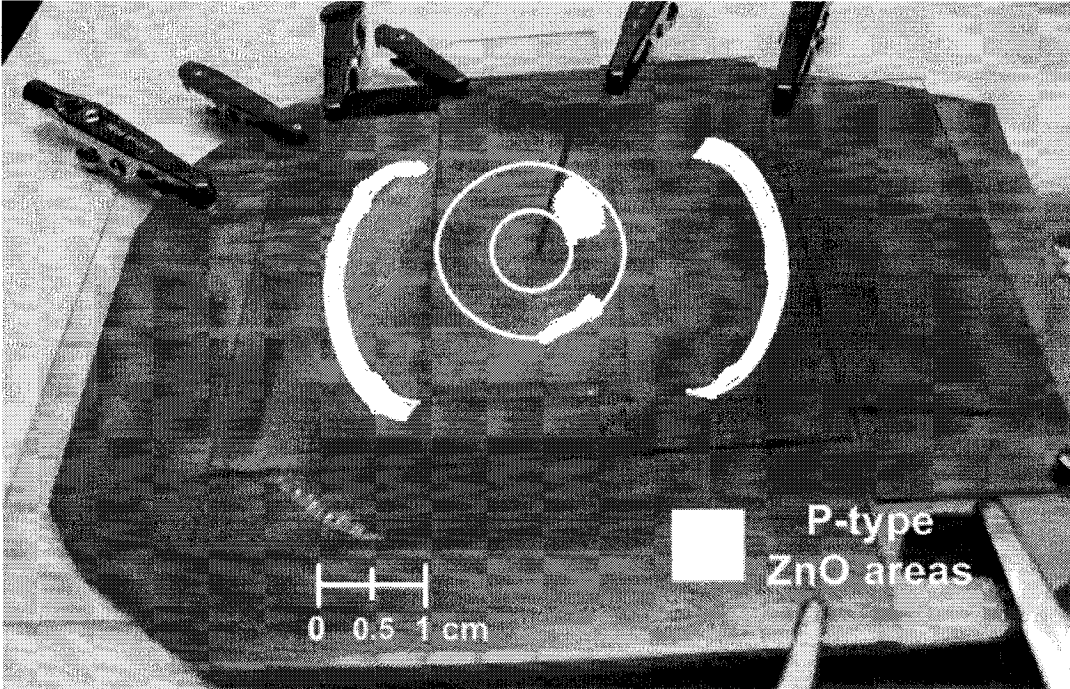


Figure 4.19 Samples on the substrate holder after 8 depositions. The white areas are p-type ZnO films mapped with hot probe measurements.

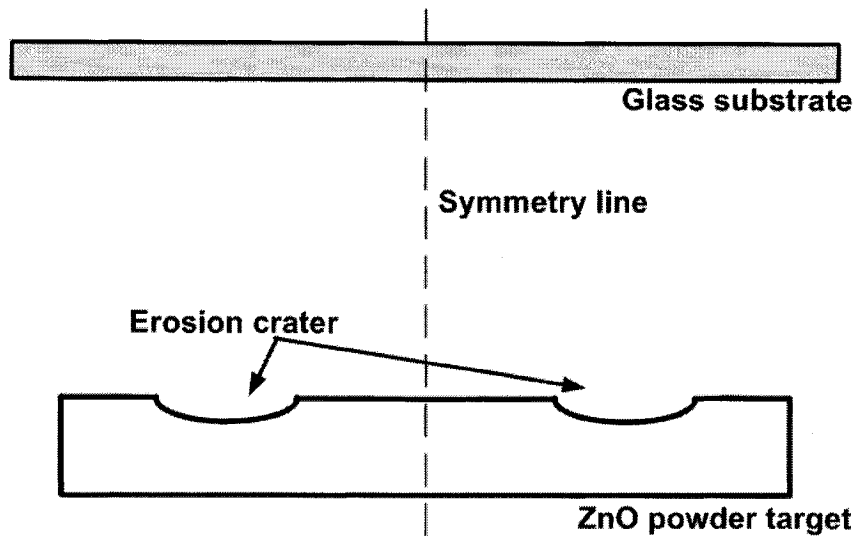


Figure 4.20 A schematic cross-section showing the ZnO powder target being more consumed in the erosion crater after deposition [15]

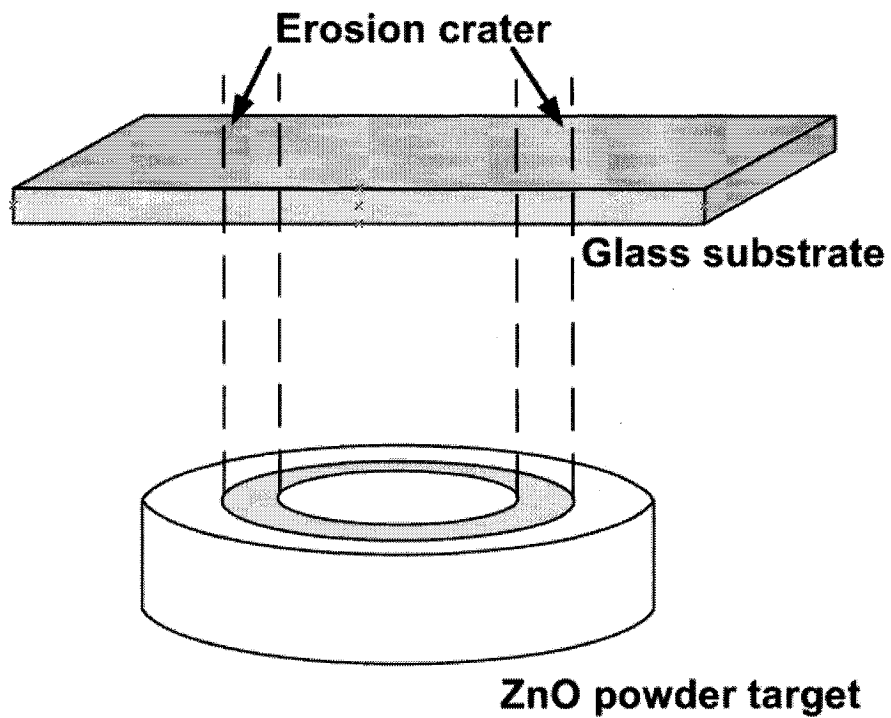


Figure 4.21 3-D view of the erosion crater in the ZnO target [16]

4.5 Electrical properties of ZnO films

For the first run, electrical measurements such as contact resistance, Hall effect and van der Pauw measurements were performed at room temperature for the samples No. P10, P11 and P12, which are located at positions 1.0, 2.5, and 5.0 cm from the center of the substrate respectively. For the second run, the p-type sample No. P13 was mapped with hot probe measurements and the electrical properties were calculated for comparison. The distance between the electrodes is in millimeter range. For contact resistance measurements, the longest distance between two electrodes is about 5 mm. For Hall effect measurements, the length of the region studied is kept to be about 5 mm and the width to be about 2.5 mm. For each sample, two sets of data are collected. Two measurements of the same sample with different contacts are performed. The contacts for the second measurement are about 1 mm away from the ones from the first measurement.

4.5.1 Metal contacts to ZnO films

ZnO is a wide bandgap energy semiconductor with electron affinity and bandgap energy about 4.35 and 3.37 eV respectively [4.19]. For n-type ZnO films, studies on Au/ZnO contacts reveal that they could be ohmic if the material surface is composed mostly of Zn [4.20]. In the case of p-type ZnO films, most of the studies on contacts are still in their infancy due to lack of p-type ZnO samples. However, it is believed that an alloy of titanium and platinum could achieve low contact resistance [4.21]. E-beam method is used for depositing the alloy due to its high melting point.

In our experiments, gold is used for both n-type and p-type ZnO films. Gold has a melting point of about 1065°C and a work function of 5.1 eV [4.22]. Circular gold contacts to ZnO samples are evaporated through holes with diameter about 0.5 mm on a shadow mask. The thickness of the metal is estimated to be about 7×10^{-8} m from the calculation shown in Figure 3.5 in chapter 3. Au contacts are created for ZnO films at 1.0, 2.5 and 5.0 cm from the center of the substrate. Copper wires are soldered on the contacts using Wood's metal.

4.5.2 Stabilization of contacts/material

Initially, no intentional treatment for improving the contacts was performed; as a result, the electric signals measured by the digital multimeter at room temperature are unstable for both p-type and n-type ZnO. The noise induced by the contacts and the non-uniformity of the films are too large for meaningful electrical characterization such as contact resistance and Hall effect measurements. Measuring the resistance across two contacts shows that the values fluctuate a lot with time. Furthermore, reverse-biasing the polarities of contacts indicates different resistance values. The difference in resistance readings could differ by as much as 25 %.

In order to improve the Au contacts to ZnO, a relatively large current (in mA range) was applied through the contacts for at least 30 seconds at room temperature. The same current was then reversed for at least 30 seconds. Afterwards, the resistance values were re-measured with both polarities and they were expected to decrease. If they differ by about 10 % or less, the contacts are considered stable and no additional current is

applied for improving the stability. On the other hand, if they still differ by much, the iteration continues until the resistances closely match. One hypothesis for explaining the phenomena is that application of high current across the samples generates joule heating of the contact and the material, which could improve the stability and reducing the contact resistances. For Hall effect measurements, high current passes through all four contacts and the order in which the current is applied is shown in Figure 4.22.

4.5.3 Contact resistance measurements

The contact resistance values measured at room temperature for samples P10, P11 and P12 are shown in Figures 4.23, 4.25 and 4.26, respectively. The extrapolations of the resistance versus the distance between the electrodes show that the contact resistances of gold on ZnO films are in the M Ω , K Ω and 10's K Ω range for samples P10, P11 and P12, respectively. It is noted that the contact resistance to p-type ZnO films is reduced by about half after the high current treatments as shown in Figures 4.23 and 4.24. The I-V curves of Au electrodes distanced by about 5 mm on ZnO films are shown in Figures 4.27, 4.28, 4.29 and 4.30.

4.5.4 Hall effect measurements

Hall effect measurements are performed for samples P10, P11, and P12. Hot probe measurement indicates that p-type ZnO should be located near 1.0 and 2.5 cm from the center of the substrate. Metal contacts are evaporated on sample P10 where p-type region is identified. Nevertheless, metal contacts are evaporated on the n-type region of sample P11 because the p-type region is too narrow at that location. Hall effect

measurements for all ZnO samples are carried out with a high magnetic field of 6560 Gauss (or 0.656 T) for increasing Hall voltage signals with respect to noise.

Figures 4.31, 4.32, 4.33 and 4.34 show the variation of Hall voltage with the applied current for Si and ZnO samples P10, P11, P12, respectively. For comparison, an n-type silicon sample (sample P_{silicon}) is measured for conduction type determination. A Hall voltage versus applied current plot for silicon bulk with two different magnetic field values, 0.656 T and 0.263 T, is shown in Figure 4.31. Keeping the same sign convention used in all Hall effect measurements, the Hall voltage values of n-type ZnO films (samples P11 and P12) and n-type Si have the same sign as shown in Figures 4.33 and 4.34. The variations of Hall voltage with applied current are also linear for all n-type samples. For sample P10, the measured Hall voltages have opposite sign comparing to the n-type samples. In the case of p-type samples, an average of three readings is taken for each point due to reading fluctuation.

The thickness, sheet resistance, Hall mobility, carrier concentration and the conduction type for samples P_{silicon}, P10, P11 and P12 are summarized in Tables 4.2, 4.3, 4.4 and 4.5. The thickness of ZnO samples at different location is determined by examining the cross-section of the samples in SEM. Sheet resistance is found by Van der Pauw method. * The average value of two sheet resistance values obtained in two different measurements is taken for calculating the Hall mobility in M1 and M2. ** For each measurement, the average of six carrier concentrations and Hall mobility values obtained from the Hall voltage data points is indicated in the table.

4.5.5 Discussion of results

The electrical properties of ZnO films after the eighth deposition on the same substrate are highly dependent on the positioning. Contact resistance and Hall effect measurements were performed on samples at three different positions, namely 1.0, 2.5 and 5.0 cm from the center of the substrate. Non-uniformity is clearly noticeable as the contact resistances at different position are different. The contact resistance of gold on n-type sample P11 is in $K\Omega$ range. Whereas the contact resistances of gold on p-type samples P10 and P13 are in $M\Omega$ range. From theoretical point-of-view, the electron affinity and bandgap energy of p-type ZnO is 4.35 and 3.37 eV, respectively. The work function of gold is 5.1 eV. High contact resistance could suggest that the energy bands of the semiconductor and metal are mismatched at the interface.

Hall effect measurements were performed not only to determine the electrical properties of the films, but also their conduction type. Measurements of n-type and p-type samples show that the Hall voltage values have different sign with the same measurement setup. In the case of n-type samples, the Hall voltages vary linearly with applied current. However, in the case of p-type samples, the variation is not entirely linear as shown in Figure 4.32. It appears that the curves in the first and third quadrants are linear but with different slope. Nevertheless, the carrier concentration and the mobility values are averaged. The results obtained are shown Table 4.6. For the p-type sample P10, the resistivity is $148.8 \Omega\text{-cm}$, the mobility is $0.0172 \text{ cm}^2/\text{V-sec}$ and the carrier concentration is $4.34 \times 10^{18}/\text{cm}^3$. The results are quite consistent to the ones presented in Table 2.5

(reference PLD2) in chapter 2 reported by Joseph et al. [4.24]. Using co-doping method, they reported p-type ZnO samples and the dopants were nitrogen and gallium.

Table 4.2 Electrical properties of silicon (sample Psilicon)

	Measurement 1 (M1)	Measurement 2 (M2)	Average
Metal contact	Wood's metal		-
Thickness of silicon	304.8 um		304.8 um
Sheet resistance *	117 Ω/□		117 Ω/□
Resistivity	3.57 Ω-cm	3.57 Ω-cm	3.57 Ω-cm
Magnetic field	0.656 T	0.263 T	-
Concentration **	2.04x10¹⁵/cm³	2.59x10¹⁵/cm³	2.32x10¹⁵/cm³
Hall mobility **	861 cm²/V-sec	678 cm²/V-sec	769 cm²/V-sec
Conduction type (by Hall effect)	n-type	n-type	-
Conduction type (by hot probe)	n-type	n-type	-

Table 4.3 Electrical properties of p-type ZnO (sample P10)

	Measurement 1 (M1)	Measurement 2 (M2)	Average
Metal contact	Au	Au	-
Contact resistance	0.72 MΩ	0.51 MΩ	0.62 MΩ
Thickness of ZnO	3.0 um		3.0 um
Sheet resistance*	3.98x10⁵ Ω/□	5.59x10⁵ Ω/□	4.79x10⁵ Ω/□
Resistivity	119.4 Ω-cm	178.2 Ω-cm	148.8 Ω-cm
Magnetic field	0.656 T	0.656 T	-
Concentration **	6.91x10¹⁸/cm³	1.76x10¹⁸/cm³	4.34x10¹⁸/cm³
Hall mobility **	9.50x10⁻³ cm²/V-sec	2.50x10⁻² cm²/V-sec	1.72x10⁻² cm²/V-sec
Conduction type (by Hall effect)	p-type	p-type	-
Conduction type (by hot probe)	p-type	p-type	-

* The average value of two sheet resistance values obtained in two different measurements is taken for calculating the Hall mobility in M1 and M2.

** For each measurement, the average of six carrier concentrations and Hall mobility values is indicated in the table.

Table 4.4 Electrical properties of n-type ZnO (sample P11)

	Measurement 1 (M1)	Measurement 2 (M2)	Average
Metal contact	Au	Au	-
Contact resistance	0.63 KΩ	0.57 KΩ	0.60 KΩ
Thickness of ZnO	5.0 μm		5.0 μm
Sheet resistance*	360 Ω/\square	710 Ω/\square	535 Ω/\square
Resistivity	0.18 $\Omega\text{-cm}$	0.36 $\Omega\text{-cm}$	0.27 $\Omega\text{-cm}$
Magnetic field	0.656 T	0.656 T	-
Concentration **	3.03x10¹⁷/cm³	1.12x10¹⁷/cm³	2.08x10¹⁷/cm³
Hall mobility **	77.2 cm²/V-sec	209 cm²/V-sec	143.1 cm²/V-sec
Conduction type (by Hall effect)	n-type	n-type	-
Conduction type (by hot probe)	n-type	n-type	-

Table 4.5 Electrical properties of n-type ZnO (sample P12)

	Measurement 1 (M1)	Measurement 2 (M2)	Average
Metal contact	Au	Au	-
Contact resistance	41.2 KΩ	17.3 KΩ	29.3 KΩ
Thickness of ZnO	1.5 μm		1.5 μm
Sheet resistance*	8850 Ω/\square	7860 Ω/\square	8355 Ω/\square
Resistivity	1.33 $\Omega\text{-cm}$	1.18 $\Omega\text{-cm}$	1.26 $\Omega\text{-cm}$
Magnetic field	0.656 T	0.656 T	-
Concentration **	2.75x10¹⁷/cm³	2.07x10¹⁷/cm³	2.41x10¹⁷/cm³
Hall mobility **	18.1 cm²/V-sec	24.2 cm²/V-sec	21.2 cm²/V-sec
Conduction type (by Hall effect)	n-type	n-type	-
Conduction type (by hot probe)	n-type	n-type	-

* The average value of two sheet resistance values obtained in two different measurements is taken for calculating the Hall mobility in M1 and M2.

** For each measurement, the average of six carrier concentrations and Hall mobility values is indicated in the table.

Table 4.6 Summary of the electrical properties of ZnO films

	Sample P10 (1st run)	Sample P11 (1st run)	Sample P12 (1st run)	Sample P13 (2nd run)
Metal contact	Au	Au	Au	Au
Contact resistance	0.62 MΩ	0.60 KΩ	29.3 KΩ	0.82 MΩ
Thickness of ZnO	3.0 μm	5.0 μm	1.5 μm	3.0 μm
Sheet resistance*	4.79x10⁵ Ω/\square	535 Ω/\square	8355 Ω/\square	6.68x10⁵ Ω/\square
Resistivity	148.8 $\Omega\text{-cm}$	0.27 $\Omega\text{-cm}$	1.26 $\Omega\text{-cm}$	200.6 $\Omega\text{-cm}$
Magnetic field	0.656 T	0.656 T	0.656 T	0.656 T
Concentration**	4.34x10¹⁸/cm³	2.08x10¹⁷/cm³	2.41x10¹⁷/cm³	4.82x10¹⁸/cm³
Hall mobility**	1.72x10⁻² cm²/V-sec	143.1 cm²/V-sec	21.2 cm²/V-sec	1.20x10⁻² cm²/V-sec
Conduction type (from Hall effect)	p-type	n-type	n-type	p-type
Conduction type (by hot probe)	p-type	n-type	n-type	p-type

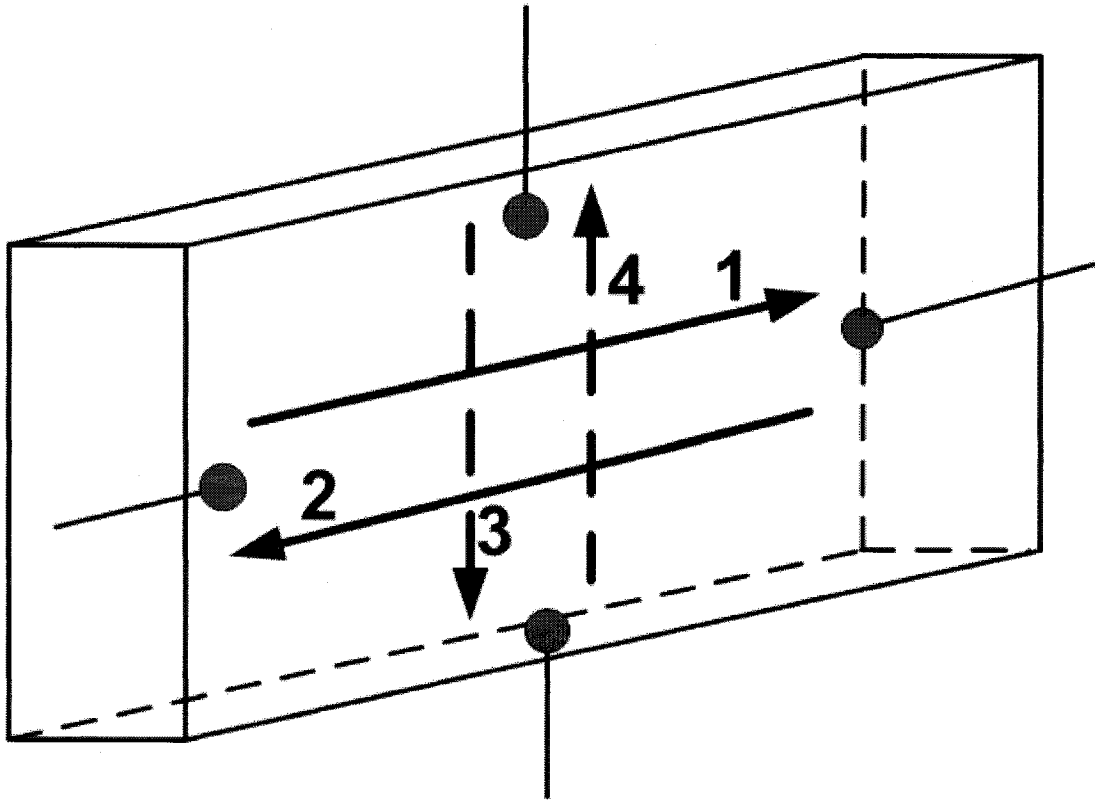


Figure 4.22 The order for high current treatment across a sample

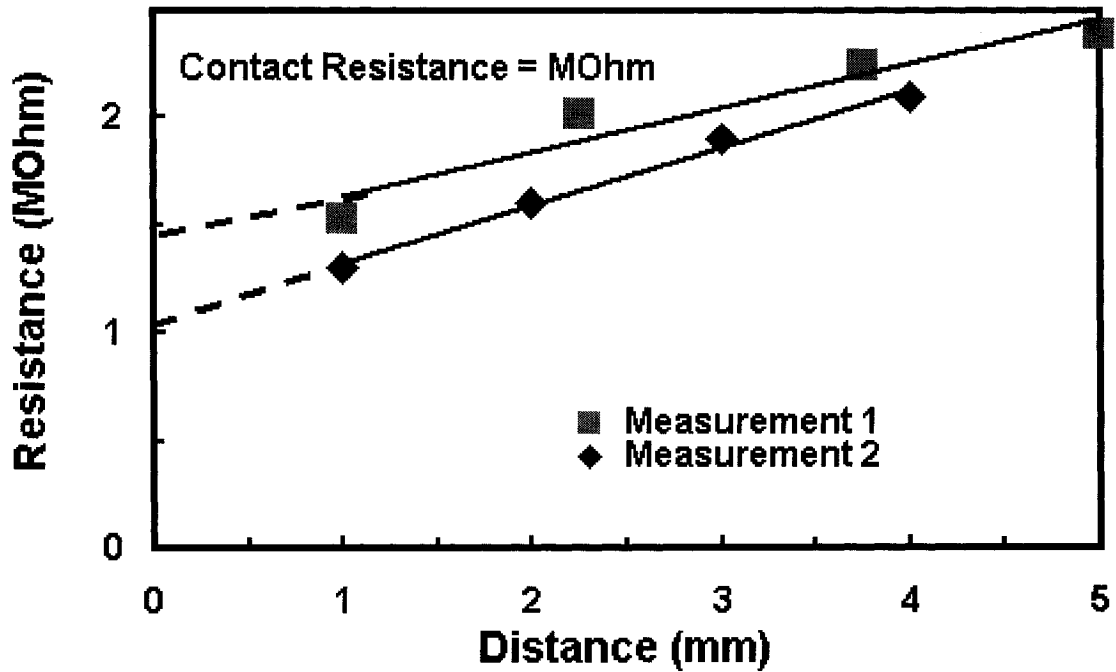


Figure 4.23 Sample P10 - Contact resistance of gold on ZnO films at 1.0 cm from the center of the substrate BEFORE high current treatment

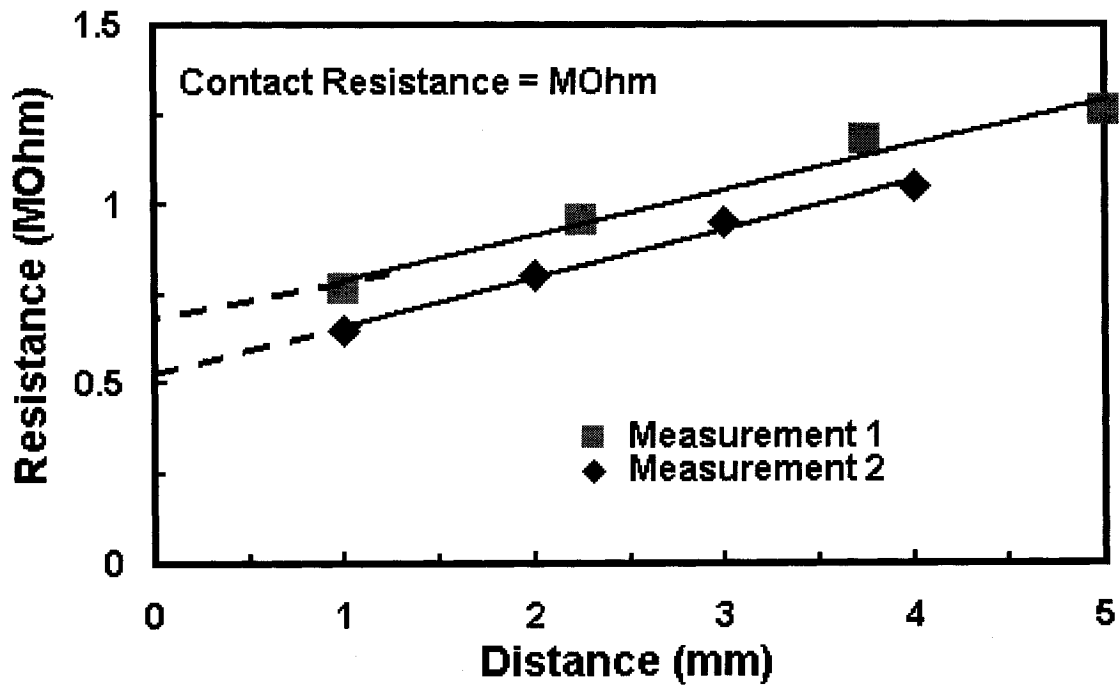


Figure 4.24 Sample P10 - Contact resistance of gold on ZnO films at 1.0 cm from the center of the substrate AFTER high current treatment

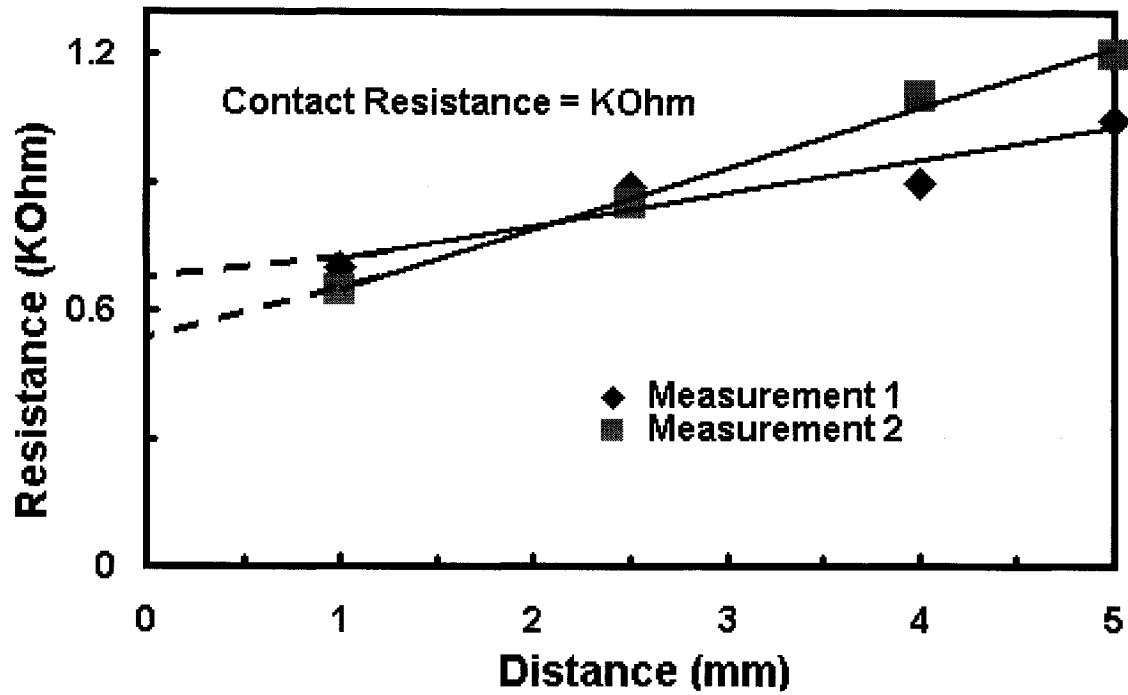


Figure 4.25 Sample P11 - Contact resistance of gold on ZnO films at 2.5 cm from the center of the substrate AFTER high current treatment

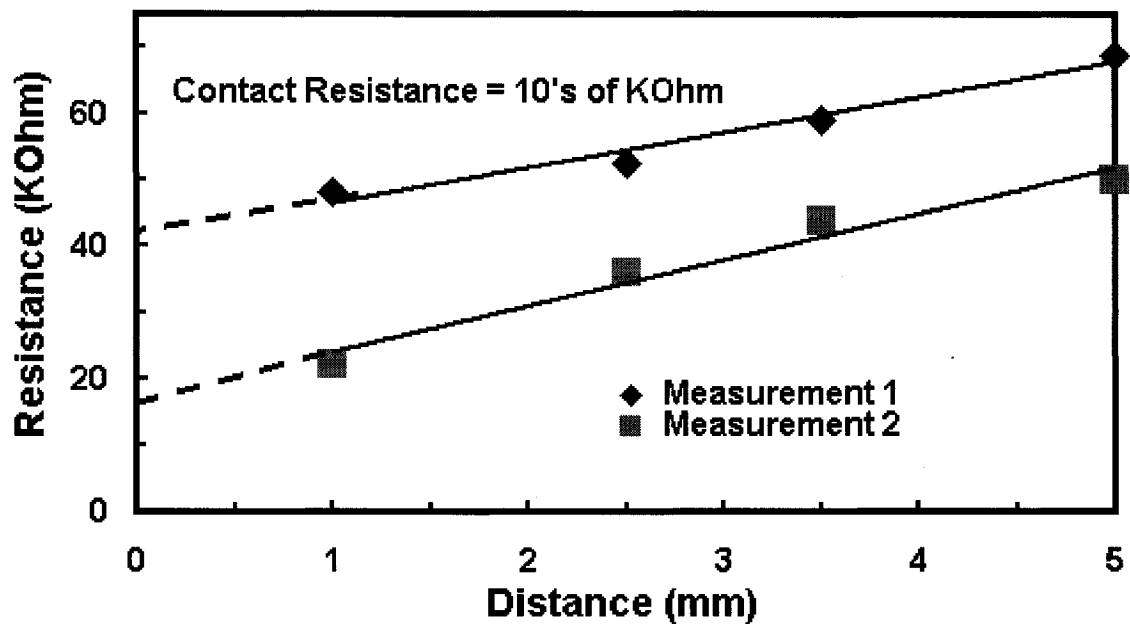


Figure 4.26 Sample P12 - Contact resistance of gold on ZnO films at 5.0 cm from the center of the substrate AFTER high current treatment

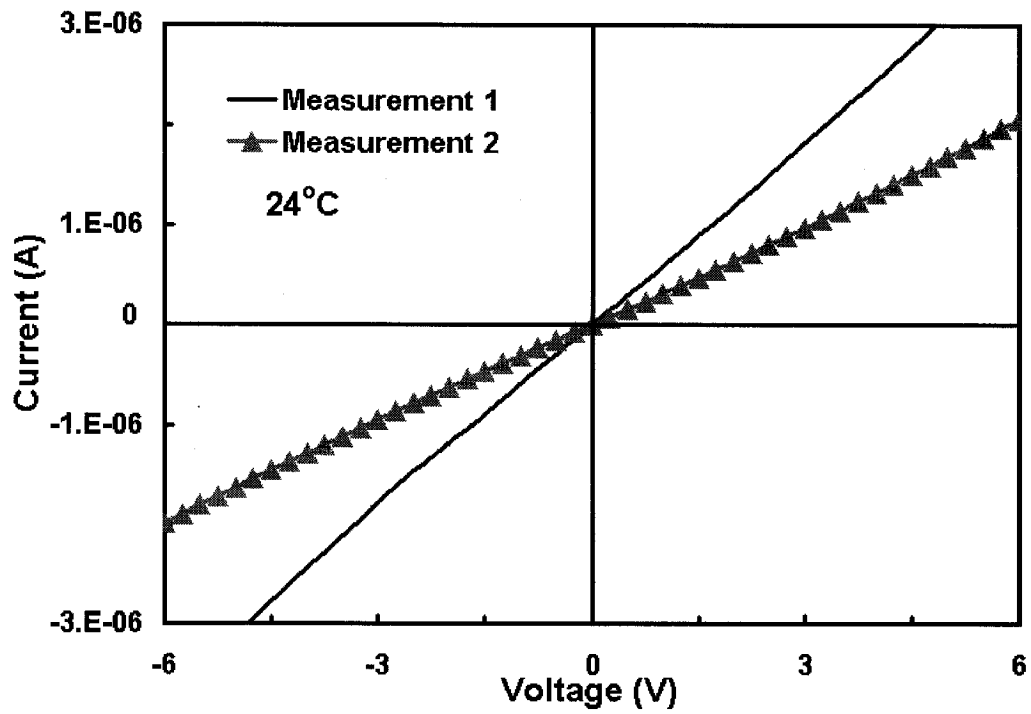


Figure 4.27 Sample P10 - I-V curves of gold contacts on ZnO at 1.0 cm from the center of the substrate BEFORE high current treatment

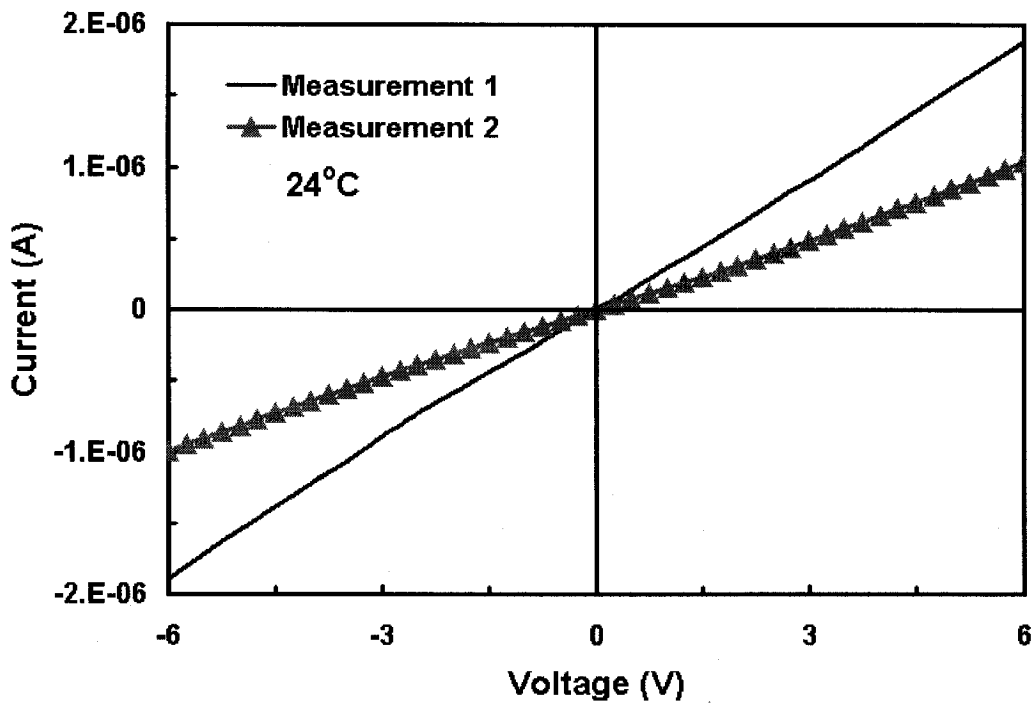


Figure 4.28 Sample P10 - I-V curves of gold contacts on ZnO at 1.0 cm from the center of the substrate AFTER high current treatment

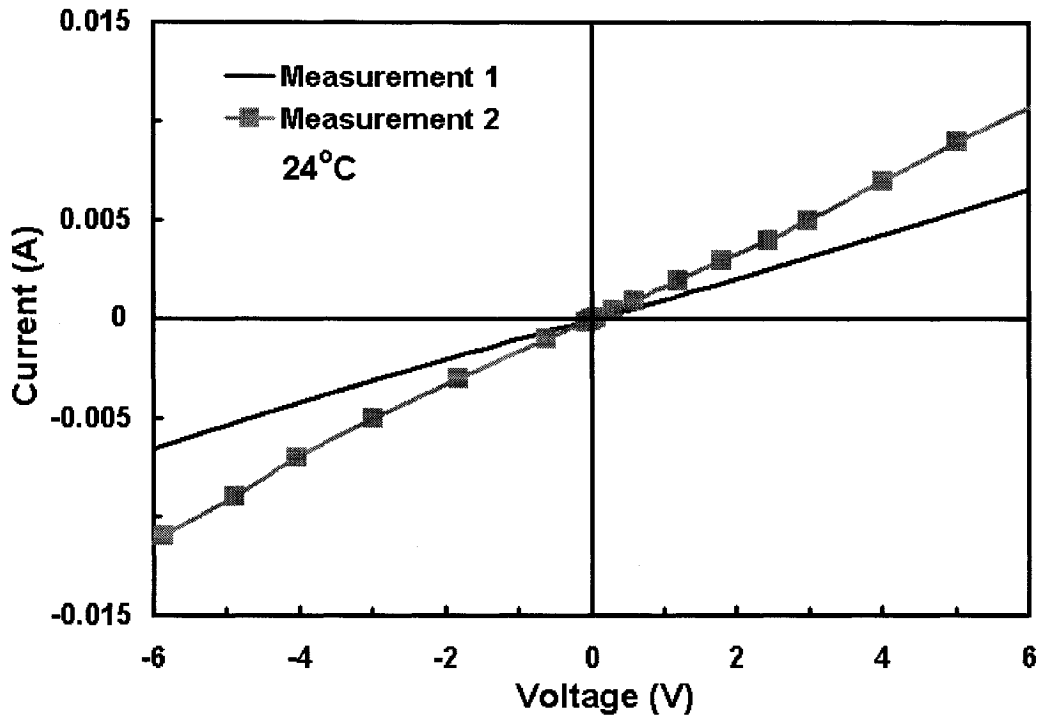


Figure 4.29 Sample P11 - I-V curves of gold contacts on ZnO at 2.5 cm from the center of the substrate AFTER high current treatment

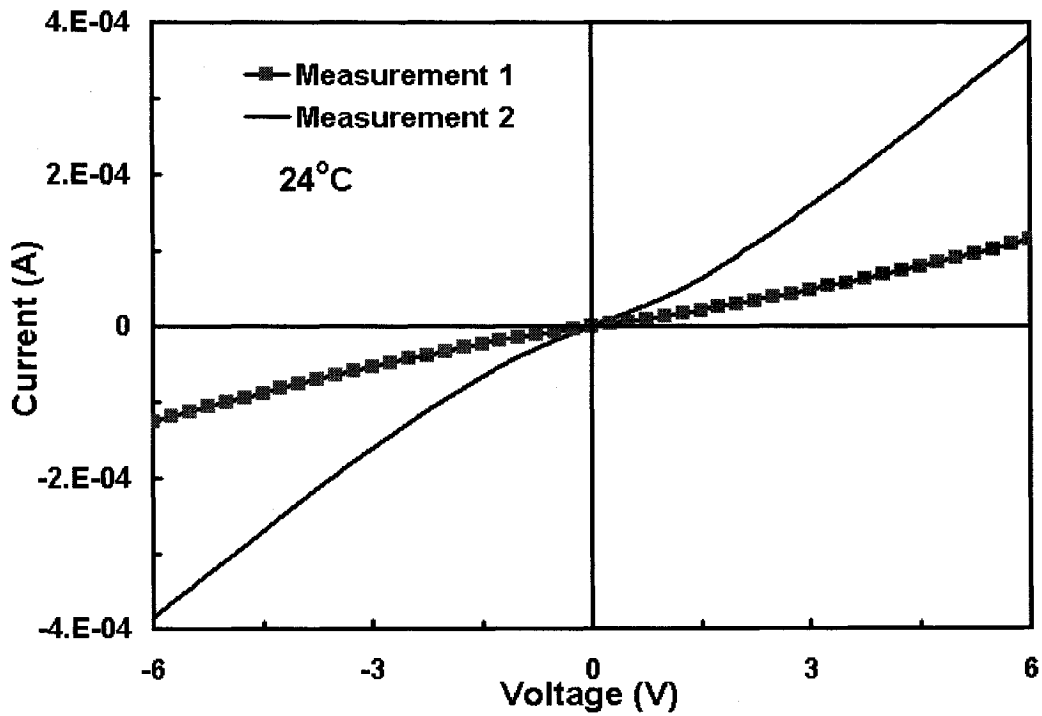


Figure 4.30 Sample P12 - I-V curves of gold contacts on ZnO at 5.0 cm from the center of the substrate AFTER high current treatment

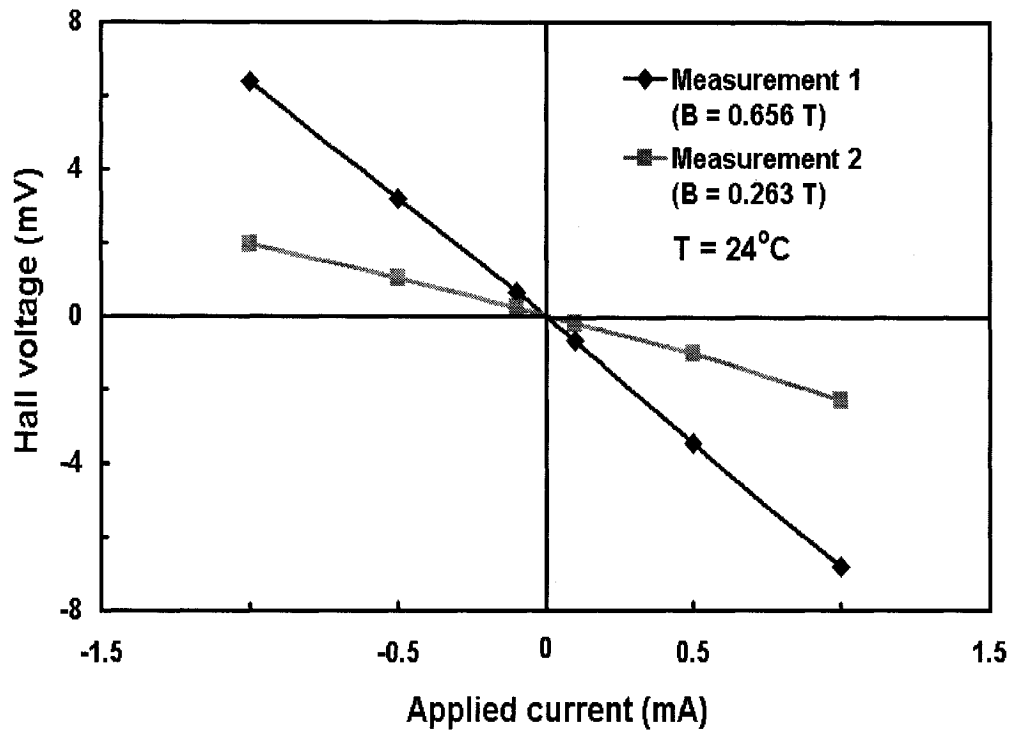


Figure 4.31 Sample Psilicon – Hall voltage versus applied current for a commercial n-type Si sample

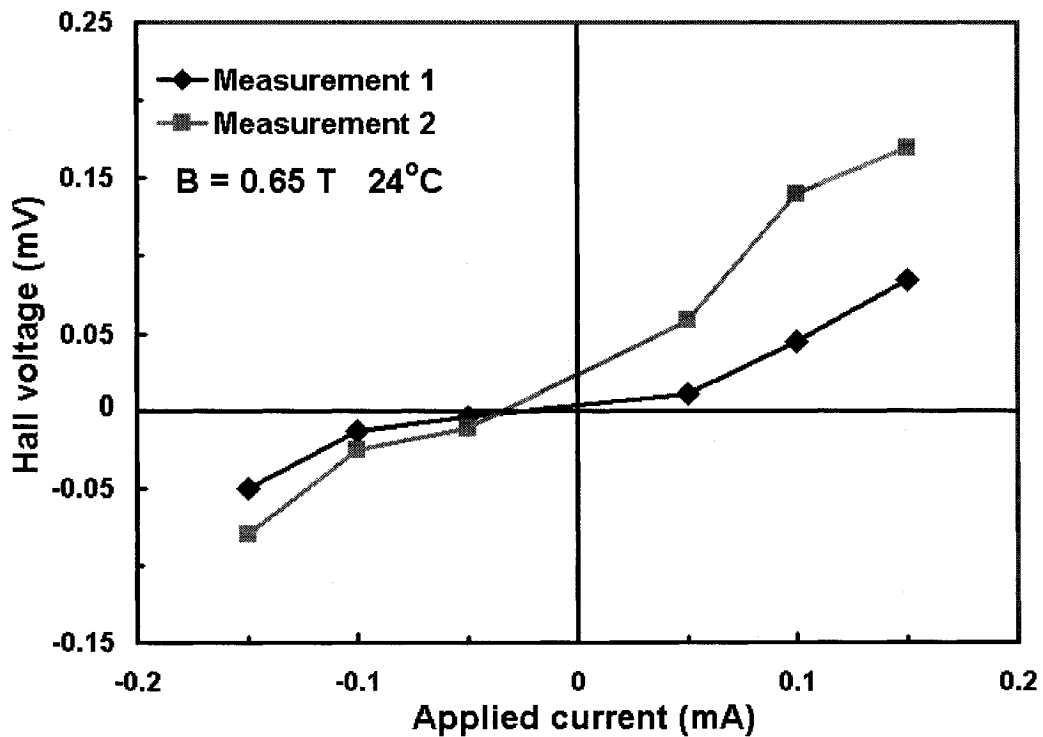


Figure 4.32 Sample P10 – Hall voltage versus applied current for p-type ZnO films located at 1.0 cm from the center of the substrate

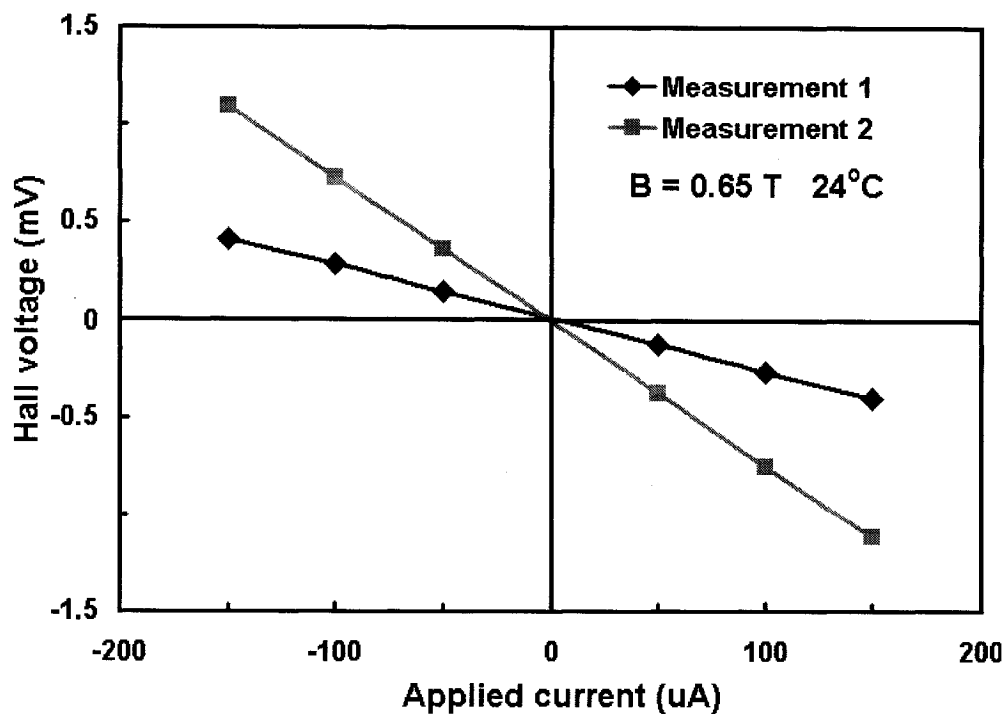


Figure 4.33 Sample P11 – Hall voltage versus applied current for n-type ZnO films located at 2.5 cm from the center of the substrate

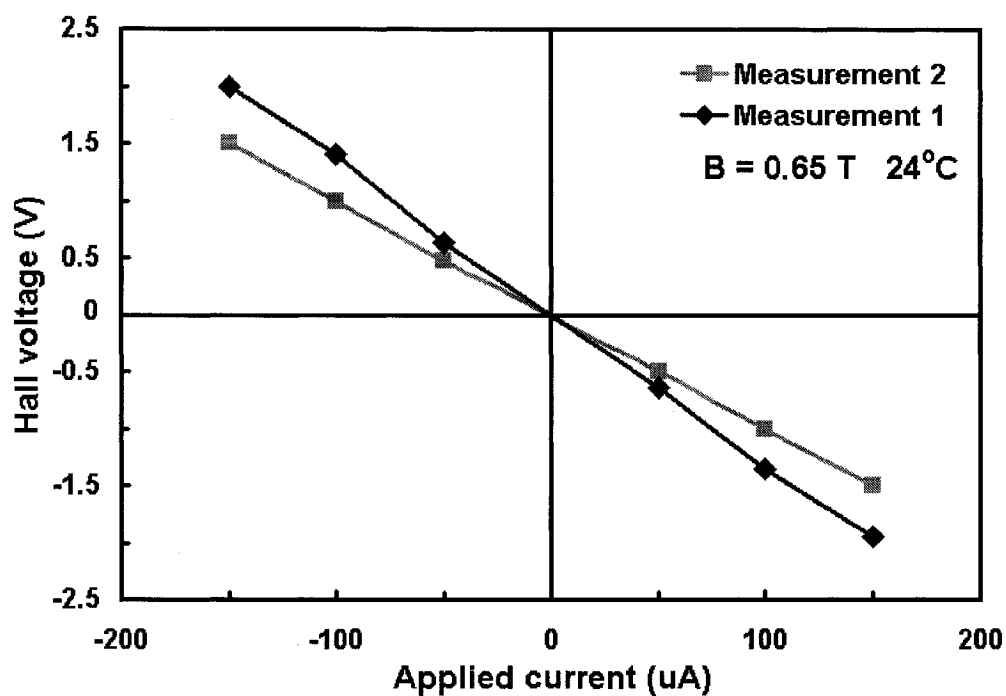


Figure 4.34 Sample P12 – Hall voltage versus applied current for n-type ZnO films located at 5.0 cm from the center of the substrate

4.6 Crystal structure of ZnO by X-ray diffraction analysis

X-ray diffraction (XRD) was performed on samples P10_xray1, P10_xray2, P11_xray and P12_xray for studying the preferred orientation of ZnO samples after the eighth deposition. Samples P10_xray1 and P10_xray2 were located at 1.0 cm from the center of substrate and both are p-type by hot probe measurements. Samples P11_xray and P12_xray were located at 2.5 cm and 5.0 cm from the center of substrate and both are n-type by hot probe measurements. XRD measurements were performed with an X-ray system having copper $K\alpha$ radiation and wavelength of the incident radiation is about 0.15405 nm.

The diffraction peaks of samples P10_xray1, P11_xray and P12_xray are shown in Figures 4.35, 4.36 and 4.37, respectively. It is seen that values of diffraction intensity at about 34° are the largest for samples P11_xray and P12_xray, indicating these to have (002) preferred orientation. This characteristic has been reported in most n-type ZnO films. Furthermore, there are minor peaks in both patterns and they are attributed to lattice mismatch of ZnO on glass substrate indicating a random orientation of the hexagonal crystallites in the polycrystalline films [4.9]. The preferred orientations are consistent with the results obtained by both Banerjee et al. and Ghosh et al. who studied on undoped ZnO on glass substrates [4.25, 4.9].

It is noticed that the diffraction peaks of both p-type ZnO samples are the same. However, for the sample P10_xray1 located closer to the projection of target center, the XRD patterns shown in Figures 4.35 show strong peaks at Y° and Z° , corresponding to

(100) and (101) orientations. These results are similar to the ones obtained by Zhang et al. who prepared nitrogen doped ZnO [4.26]. They reported that the values of (100) and (101) peaks became stronger as the atomic ratio of nitrogen dopant was increased. From the present XRD patterns, it is evident that the p-type ZnO samples prepared in this work are polycrystalline.

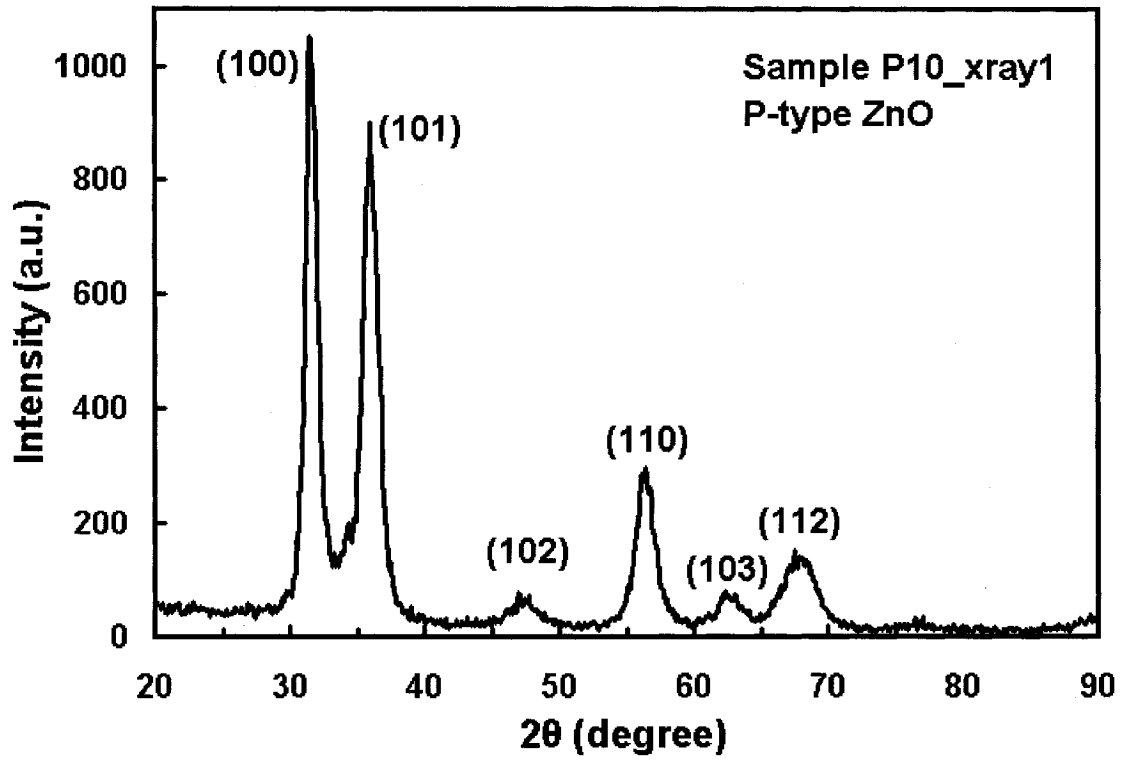


Figure 4.35 XRD pattern of p-type ZnO located at 1.0 cm from the projection of target center

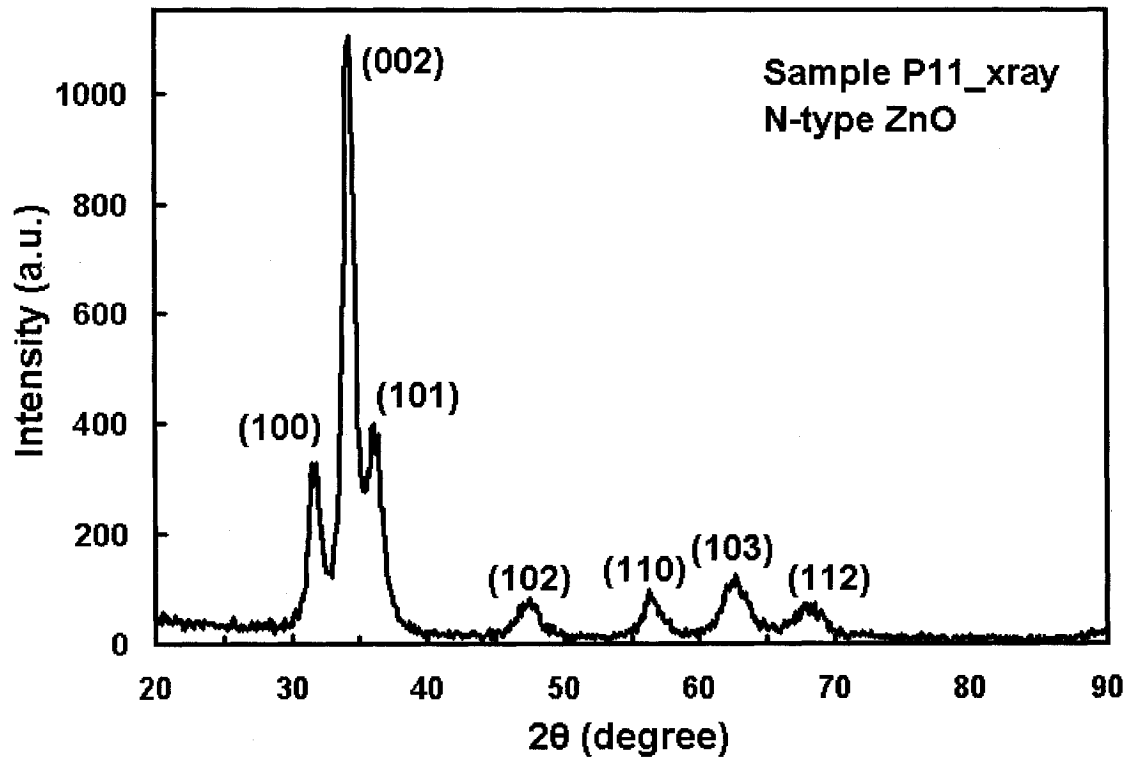


Figure 4.36 XRD pattern of n-type ZnO located at 2.5 cm from the projection of target center

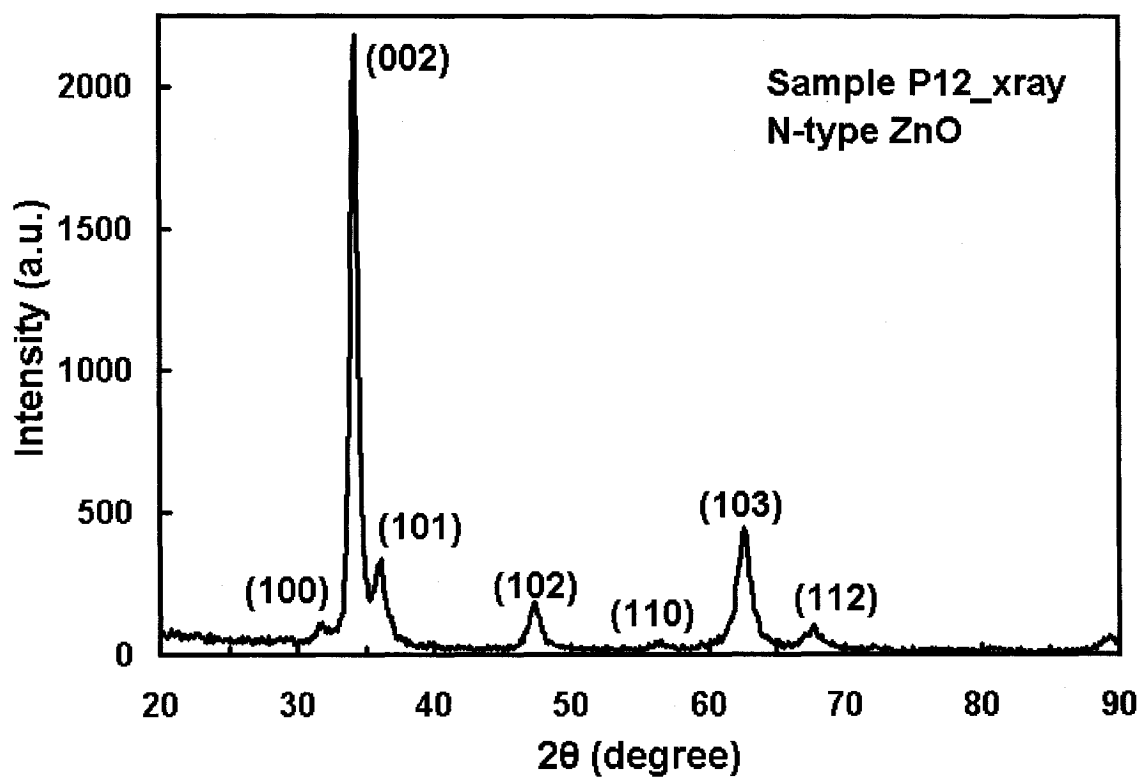


Figure 4.37 XRD pattern of n-type ZnO located at 5.0 cm from the projection of target center

CHAPTER 5 CONCLUSIONS

5.1 Summary of the study

N-type ZnO and its properties are well understood among researchers. Due to high concentration of native defects, intrinsic ZnO is naturally n-type. The native defects, such as zinc interstitial and oxygen vacancy, can act as compensating centers. As a result, p-type ZnO is difficult to fabricate and not clearly understood.

Theoreticians have been trying to find a model for explaining the difficulty in making p-type ZnO and specially chosen dopants for overcoming the problem. Yamamoto's codoping method is based on a model, which requires two dopants. One of the dopant plays the role of replacing another element in the material for making it electrically active. The other impurity is a by-player for making the incorporation of the other dopant easier in the material. In the case of ZnO, Yamamoto predicted that N-In could be a good co-dopant pair for successfully creating p-type ZnO.

The hexagonal wurtzite crystal structure of ZnO is also important. Sapphire substrate is expensive and it is believed to be able to reduce lattice mismatch near the interface of deposited ZnO. The deposition of ZnO thin films on an alternative low cost substrate, such as glass, is interesting. In the present work, it has been observed that thick layers of ZnO sputtered on glass substrate are required for reducing lattice mismatch.

In the initial phase of the work, ZnO thin films were deposited on silicon substrates and investigated. These as-deposit ZnO films have weak photoluminescence

response, which makes the analysis difficult due to background noise contribution. The PL responses of ZnO films on Si were much noticeable when they were annealed at elevated temperatures. Experimental results show that the energy peaks are the strongest when the films were annealed at 1100°C for one hour in oxygen. The strong peaks at 390, 460 and 500 nm correspond to free excitons of ZnO, zinc interstitials and oxygen defects, respectively. In particular, the peak intensity due to oxygen defects is reduced when annealed in oxygen compared to ZnO films annealed in air.

The non-uniformity of the films over the entire substrate surface was observed for ZnO films sputtered on glass substrates after eight depositions. The location of the samples with respect to the target has been found to affect greatly the properties of the films. In particular, deposition rate and unintentional substrate heating can have an effect on the properties of the ZnO films. As a result, p-type ZnO films were formed at locations near the target center and n-type ZnO films were created at locations further away from the target center.

After multiple depositions of ZnO material on the glass substrates, the photoluminescence spectra analysis revealed also many energy peaks. For ZnO films sputtered from the undoped target, the PL spectra were unnoticeable until the third deposition. After the fourth deposition, the peaks were sharper and stronger than the ones observed after the third deposition. Consequently, it is possible to conclude that the crystal structure is improved with multiple depositions. However, the native defects of ZnO are still present at 461 and 531 nm. For doped ZnO films, effects of incorporation of

dopants were confirmed by PL spectra analysis where additional peaks due to dopants were observed. The energy peaks due to nitrogen and indium dopants in ZnO were observed at 350 and 660 nm respectively. For the n-type ZnO films, PL spectra analysis revealed that there is no energy peak due to dopants.

X-ray diffraction patterns suggested that the sputtered ZnO is polycrystalline. For both p-type and n-type ZnO, it was found that there are more than one preferred orientations. On the same substrate, the preferred orientations of the p-type ZnO were (100) and (101). In the case of the n-type ZnO, the preferred orientation was (002).

Yamamoto's theoretical prediction suggested that if N-In co-dopants were incorporated in the films, the bandgap of the ZnO films should be reduced. This was verified by the optical transmission of samples. For the samples located at the proximity of the center of the substrate, short wavelength light is almost being blocked at 400 nm. For samples located further away from the center of the target, light is not blocked at 400 nm, but rather at a shorter wavelength.

For the present p-type ZnO films formed near the projection of the center of the substrate, the resistivity, hole concentration and mobility were found to be 148.8 Ω -cm, $4.34 \times 10^{18}/\text{cm}^3$ and $1.72 \times 10^{-2} \text{ cm}^2/\text{V-sec}$ respectively. N-type ZnO films were also obtained in the same deposition run, but these were located further away from the center of the substrate. In general, the resistivity of n-type ZnO was found to be much lower than p-type ZnO and the electron mobility much higher than its counterparts. The

thickness of ZnO films is in the order of micrometer. A summary of the results for ZnO thin films at different positions from the present work is given in the following table.

Table 5.1 Electrical properties of ZnO films at different locations

	Sample P10	Sample P11	Sample P12
Location (with respect to substrate center)	1.0 cm	2.5 cm	5.0 cm
Metal contact	Au	Au	Au
Contact resistance	0.62 MΩ	0.60 KΩ	29.3 KΩ
Thickness of ZnO	3.0 μm	5.0 μm	1.5 μm
Sheet resistance	4.79x10⁵ Ω/□	535 Ω/□	8355 Ω/□
Resistivity	149 Ω-cm	0.27 Ω-cm	1.26 Ω-cm
Magnetic field	0.656 T	0.656 T	0.656 T
Concentration	4.34x10¹⁸/cm³	2.08x10¹⁷/cm³	2.41x10¹⁷/cm³
Hall mobility	1.72x10⁻² cm²/V-sec	143 cm²/V- sec	21.2 cm²/V- sec
Conduction type (from Hall effect)	p-type	n-type	n-type
Conduction type (by hot probe)	p-type	n-type	n-type

5.2 Main contribution of this work

1) For ZnO films sputtered on silicon substrates and annealed at 1100°C in oxygen for one hour, the intensity peaks in photoluminescence spectra are sharper and stronger comparing to the ones annealed in air.

2) The lattice mismatch created near the interface of ZnO and glass substrate can be reduced when the thickness of the films is increased. The intensity peaks in PL spectra of ZnO deposited on glass is observed after the third deposition (roughly after 24 hours of deposition).

3) Dopants are incorporated in the films for the samples located at the proximity of the center of the substrate. The incorporation of dopants in the films is verified by the analysis of PL responses.

4) The optical transmission of samples located at the proximity of the center of the substrate show that short wavelength light is almost being blocked at 400 nm. The results suggest that the bandgap of the ZnO films is reduced and the N-In co-dopants are incorporated in the films, which coincides with Yamamoto's theoretical prediction.

5) The conduction types of ZnO films are confirmed by Hall effect measurements. On the same substrate, p-type ZnO is more likely to be located near the erosion crater with higher deposition rate and temperature compared to n-type films located further away from the crater.

5.3 Future work

Although reproducible p-type ZnO films have been obtained, there are many parameters to be improved and unknown to be solved. Specifically, the stability and stress of thick layers of ZnO need to be further studied. The metal contacts to p-type ZnO need to be investigated once p-type ZnO can be mass reproduced. The uniformity of thick ZnO at different positions needs to be examined. The electrical and optical properties of multi-layer ZnO at deposit at elevated substrate temperature (more than 1100°C) are also attractive.

REFERENCES

Chapter 1

- [1.1] E. F. Schubert. *Light-Emitting Diode*. Cambridge University Press (2003)
- [1.2] M. K. Hossain, S.C. Ghosh and Y. Boontongkong. *Growth of Zinc Oxide Nanowires and Nanobelts for Gas Sensing Applications*. Journal of Metastable and Nanocrystalline Materials Vol. **23**, p.27 (2005)
- [1.3] *Properties of the II-IV compound semiconductors*.
<<http://www.semiconductors.co.uk/propiiivi5410.htm>>, 24 April 2006
- [1.4] *Wide band gap ferromagnetic semiconductors and oxides*.
<http://www.mse.ufl.edu/~spear/recent_papers/WBGFerromag/WBGFerromag.htm>, 24 April 2006

Chapter 2

- [2.1] Y. I. Alivov, E. V. Kalinina, A. E. Cherenkov and D. C. Look. *Fabrication and characterization of n-ZnO/p-AlGaIn heterojunction light-emitting diodes on 6H-SiC substrates*. Applied Physics Letters, Vol. **83** Num. 23, p. 4719 (2003)
- [2.2] F. Tuomisto, K. Saarinen, D. C. Look and G. C. Farlow. *Introduction and recovery of point defects in electron-irradiated ZnO*. Physical Review B **72**, p. 085206-1 (2005)
- [2.3] A. Koboyashi, O. F. Sankey and J. D. Dow, Physical Review B **28**, p. 946 (1983)
- [2.4] L. G. Wang and A. Zunger. *Cluster-Doping Approach for Wide-Gap Semiconductors: The Case of p-Type ZnO*. Physical Review Letters Vol. **90** num. 25, p. 256401 (2003)
- [2.5] S. B. Zhang, S.-H. Wei and A. Zunger. *Intrinsic n-type versus p-type doping asymmetry and the defects of ZnO*. Physical Review B Vol. **63**, p. 075205 (2001)
- [2.6] C. H. Park, S. B. Zhang and S.-H. Wei. *Origin of p-type doping difficulty in ZnO*. Physical Review B Vol. **66**, p. 073202 (2002)
- [2.7] T. Yamamoto and H. Katayama-Yoshida. *Solution using a Codoping Method to Unipolarity for the Fabrication of p-type ZnO*. Jpn. J. Appl. Phys. Vol. **38**, p. L166 (1999)

- [2.8] T. Yamamoto. *Codoping for the fabrication of p-type ZnO*. Thin Solid Films Vol. **420**, p. 100 (2002)
- [2.9] *Phosphorous*.
<<http://www.webelements.com/webelements/elements/text/P/radii.html>>, 25 April 2006
- [2.10] D. C. Look and B. Clafin. P-type doping and devices based on ZnO. Phys. Stat. Sol. (b) **241** No. 3, p. 624 (2004)
- [2.11] D. C. Look, D.C.Reynolds, C. W. Litton, R. L. Jones, D. B. Eason and G. Cantwell, Appl. Phys. Lett. Vol. **80**, p. 1830 (2002)
- [2.12] C. Wang, J. Zhengu, L. Kun, Y. Xiang and Y. Zhizhen. *P-type ZnO thin films prepared by oxidation of Zn₃N₂ thin films deposited by DC magnetron sputtering*. J. of Crystal Growth **259**, p. 279 (2003) 279
- [2.13] J. Lu, Y. Zhang, Z. Ye, L. Wang, B. Zhao and J. Huang. *P-type ZnO films deposited by DC reactive magnetron sputtering at different ammonia concentrations*. Material Letters **57**, p. 3311 (2003) 3311
- [2.14] J. Lu, Y. Zhang, Z. Ye, L. Wang, B. Zhao, J. Huang and H. Chen. *Preparation and characteristics of p-type ZnO films by DC reactive magnetron sputtering*. J. of Crystal Growth **253**, p. 258 (2003)
- [2.15] G. Xiong, J. Wilkinson, S. Tuzemen, K. B. Ucer and R. T. Williams. *Towards a new ultraviolet diode laser: luminescence and p-n junctions in ZnO films*. Proceedings of SPIE - The International Society for Optical Engineering Vol. **4644**, p 256 (2002)
- [2.16] J. Huang, Z. Ye, H. Chen, B. Zhao and L. Wang. *Growth of N-doped p-type ZnO films using ammonia as dopant source gas*. Journal of Material Science Vol. **22**, p. 249 (2003)
- [2.17] K.-K. Kim, H.-S. Kim, D.-K. Huang, J.-H. Lim and S.-J. Park. *Realization of p-type ZnO thin films via phosphorus doping and thermal activation of the dopant*. Appl. Physics Letters Vol. **83** Num.1, p. 63 (2003)
- [2.18] S.-J. Park. *P-doping of zinc oxide using phosphorous oxide and thermal annealing*. IEEE TuA **3.2**, p. 116 (2003)
- [2.19] M. C. Jeong, D. K. Hwang, J. M. Myong, Y. D. Ko, M. S. Kim and I. Yun. *The Formation of p-type ZnO films by using a diffusion process*. Defect and Diffusion Forum Vols. **218-220**, p. 17(2003)
- [2.20] K.-H. Bang, D.-K. Hwang, M. C. Park, Y. D. Ko, I. Yun and J.-M. Myoung. *Formation of p-type ZnO film on InP substrate by phosphor doping*. Appl. Surface Science **210**, p. 177 (2003)

- [2.21] A. V. Singh, R. M. Mehra, A. Wakahara and A. Yoshida. P-type conduction in codoped ZnO thin films. *Journal of Applied Physics* Vol. **93** Num.1, p. 396 (2003)
- [2.22] M. Joseph, H. Tabata, H. Saeki, K. Ueda and T. Kawai. Fabrication of low-resistive p-type ZnO by co-doping method. *Physica B* Vol. **302-303**, p. 140 (2001)
- [2.23] M. Joseph, H. Tabata and T. Kawai. *P-type electrical conduction in ZnO thin films by Ga and N Codoping*. *Japn. J. Appl. Phys.* Vol. **38**, p. L1205 (1999)
- [2.24] T. Ohshima, T. Ikegami, K. Ebihara, J. Asmussen and R. Thareja. *Synthesis of p-type znO thin films using co-doping techniques based on KrF ecimer laser deposition*. *Thin Solid films* Vol. **435**, p. 49 (2003)
- [2.25] C-C Lin, S-Y Chen, S-Y Cheng and H-Y Lee. *Properties of nitrogen-implanted p-type ZnO films grown on Si₃N₄/Si by rf sputtering*. *Applied Physics Letters* Vol. **84** Num. 24, p. 5040 (2004)
- [2.26] J. M. Bian, X. M. Li, X. D. Gao, W. D. Yu and L. D. Chen. *Deposition and electrical properties of N-In codoped ZnO films by ultrasonic spray pyrolysis*. *Appl. Physics Letters* Vol. **84** Num. 4, p. 541 (2004)
- [2.27] J. M. Bian, X. M. Li, X. D. Gao, C. Y. Zhang and L. D. Chen. *Synthesis and characterization of two-layer-structure ZnO p-n homojunctions by ultrasonic spray pyrolysis*. *Appl. Physics Letters* Vol. **84** Num.19, p. 3783 (2004)
- [2.28] Z. Ji, C. Yang, K. Lin and Z. Ye. *Fabrication and characterization of p-type ZnO films by pyrolysis of zinc-acetate-ammonia solution*. *Journal of Crystal Growth* Vol. **253**, p. 239 (2003)
- [2.29] T. Yamamoto and H. Katayama-Yoshida. *Solution using a Codoping Method to Unipolarity for the Fabrication of p-type ZnO*. *Jpn. J. Appl. Phys.* Vol. **38**, p. L166 (1999)
- [2.30] T. Yamamoto. *Codoping for the fabrication of p-type ZnO*. *Thin Solid Films* Vol. **420**, p. 100 (2002)
- [2.31] Z. Yang and Y. Wang. *Blue luminescent center in ZnO films deposited on silicon substrates*. *Optical Materials* **26**, p. 239 (2004)
- [2.32] N.O. Korsunskaya and L.V. Borkovskaya. The influence of defect drift in external electric field on green luminescence of ZnO single crystals. *Journal of Luminescence* **102 - 103**, p. 733 (2003)

Chapter 3

- [3.1] A. Chambers, R. K. Fitch and B. S. Halliday. *Basic Vacuum Technology: 2nd Edition*. IOP Publishing Ltd, p.xii (1998)
- [3.2] L. G. Carpenter. *Vacuum Technology*. American Elsevier Publishing Company Inc, p. 16 (1970)
- [3.3] L. G. Carpenter, *Vacuum Technology*, American Elsevier Publishing Company Inc, p. 20 (1970)
- [3.4] A. Chambers, R. K. Fitch and B. S. Halliday. *Basic Vacuum Technology: 2nd Edition*. IOP Publishing Ltd, p.xiii (1998)
- [3.5] *Pirani Gauge Head*,
<http://www.vacgen.com/asp/catalogue.asp?url=http%3A//www.vacgen.com/catalogue/section-8/page08_03.htm&frame=1>, 09 Sept. 2005
- [3.6] C. R. Jaeger. *Introduction to Microelectronic Fabrication 2nd edition*. Addison-Wesley publishing company, p.136 (2002)
- [3.7] D. A. Neamen. *Semiconductor Physics & Devices 2nd edition*. Irwin, p. 156 (1997)

Chapter 4

- [4.1] M.-V. der Vorst, W. & V. Craeynest. *The Green Luminescence of ZnO*. Phys. Stat. Sol. **9**, p. 749 (1965)
- [4.2] D. Miller and L. Grigorjeva. *Luminescence of ZnO nanopowders*. Radiation Measurements **38**, p. 589 (2004)
- [4.3] Z. Yang and Y. Wang. *Blue luminescent center in ZnO films deposited on silicon substrates*. Optical Materials **26**, p. 239 (2004)
- [4.4] S. Kang, and K. Shin. *Optical and electrical properties of ZnO doped with nitrogen*. Phys. stat. sol. (b) **241**, No. 12, p. 2830 (2004)
- [4.5] H. J. Ko, and M.-S. Han. *Improvement of the quality of ZnO substrates by annealing*. Journal of Crystal Growth **269**, p. 493 (2004)
- [4.6] A. Toumiat and S. Achour. *Effect of nitrogen reactive gas on ZnO nanostructure development prepared by thermal oxidation of sputtered metallic zinc*. Nanotechnology **17**, p. 658 (2006)

- [4.7] P. Kumar, M. Ratheesh and C. Kartha. *On the properties of indium doped ZnO thin films*. *Semicond. Sci. Technol.* **20**, p. 120 (2005)
- [4.8] M. Jung, J. Lee, S. Park et al.. *Investigation of the annealing effects on the structural and optical properties of sputtered ZnO thin films*. *Journal of Crystal Growth* **283**, p. 384 (2005)
- [4.9] R. Ghosh, D. Basak, S. Fujihara. *Effect of substrate-induced strain on the structural, electrical, and optical properties of polycrystalline ZnO thin films*. *Journal of Applied Physics*, Vol. **96**, Num. 5, 2004
- [4.10] K. Prabakar, C. Kim and L. Chongmu Lee. *UV, violet and blue-green luminescence from RF sputter deposited ZnO:Al thin films*. *Cryst. Res. Technol.* **40**, No. 12, p. 1150 (2005)
- [4.11] J. J. Chen, Y. Gao, F. Zeng, D. M. Li and F. Pan. *Effect of sputtering oxygen partial pressures on structure and physical properties of high resistivity ZnO films*. *Applied Surface Science* **223**, p. 318 (2004)
- [4.12] E. M. Bachari, G. Baud, B. Amor and M. Jacquet. *Structural and optical properties of sputtered ZnO films*. *Thin Solid Films* **348**, p. 165 (1999)
- [4.13] T. Yamamoto and H. Katayama-Yoshida. *Solution using a Codoping Method to Unipolarity for the Fabrication of p-type ZnO*. *Jpn. J. Appl. Phys.* Vol. **38**, p. L166 (1999)
- [4.14] T. Yamamoto. *Codoping for the fabrication of p-type ZnO*. *Thin Solid Films* Vol. **420**, p. 100 (2002)
- [4.15] D. Song, P. Widenborg, W. Chin et al.. *Investigation of lateral parameter variations of Al-doped zinc oxide films prepared on glass substrates by rf magnetron sputtering*. *Solar Energy Materials & Solar Cells* **73**, p. 1 (2002)
- [4.16] T. Minami, H. Nanto, H. Sato and S. Takata. *Effect of applied external magnetic field on the relationship between the arrangement of the substrate and the resistivity of aluminum-doped ZnO thin films prepared by r.f. magnetron sputtering*. *Thin Solid Films* **164**, p. 275 (1988)
- [4.17] Y. Igasaki and H. Saito. *The effects of deposition rate on the structural and electrical properties of ZnO:Al films deposited on (1120) oriented sapphire substrates*. *J. Appl. Phys.*, **70** (7), p. 3613 (1991)
- [4.18] A. L. Thomann, J. P. Salvetat, Y. Breton et al.. *Thermal stability of metal nanoclusters formed by low-pressure plasma sputtering*. *Thin Solid Films* **428**, p. 242 (2003)

- [4.19] Y. I. Alivov, E. V. Kalinina. and A. E. Cherenkov. *Fabrication and characterization of n-ZnO/p-AlGaN heterojunction light-emitting diodes on 6H-SiC substrates*. Applied Physics Letters, Vol. **83** Num. 23, p. 4719 (2003)
- [4.20] N. Sakagamia, M. Yamashitaa, T. Sekiguchi et al.. *Variation of electrical properties on growth sectors of ZnO single crystals*. Journal of Crystal Growth **229**, p. 98 (2001)
- [4.21] K. Ip, G. T. Thaler and H. Yang. *Contacts to ZnO*. Journal of Crystal Growth **287**, p.149 (2006)
- [4.22] *Gold*, <<http://environmentalchemistry.com/yogi/periodic/Au.html>>, 12 April, 2006
- [4.23] F. Masanobu, Y. Katsuaki and T. Osamu. *Optical properties of zinc oxynitride thin films*. Thin Solid Films **317**, p. 322 (1998)
- [4.24] M. Joseph, H. Tabata, T. Kawai. *P-type electrical conduction in ZnO thin films by Ga and N Codoping*. Japn. J. Appl. Phys. Vol. **38**, p. L1205 (1999)
- [4.25] A. N. Banerjee, C. K. Ghosh, K. Chattopadhyay. *Low-temperature deposition of ZnO thin films on PET and glass substrates by DC-sputtering technique*. Thin Solid Films **496**, p. 112 (2006)
- [4.26] C. Zhang, X. Li and J. Bian. *Structural and electrical properties of nitrogen and aluminum codoped p-type ZnO films*. Solid State Communications **132**, p. 75 (2004)